공학박사학위논문

Rheological characterization of complex fluids under dynamic helical squeeze flow

동적 나선 유동 하에서 나타나는 복합 유체의 유변학적 특성에 대한 연구

2012년 8월

서울대학교 대학원

화학생물공학부

김 재 희

Abstract

Rheological characterization of complex fluids under dynamic helical squeeze flow

Jae Hee Kim
School of Chemical and Biological Engineering
The Graduate School
Seoul National University

The measurements of rheological properties are often carried out in the linear or nonlinear regime under simple shear flow. Even though these rheometric protocols provide useful information on the rheological properties of complex fluids, they are not enough in the sense that the flow fields are still too simple compared to real processes. It is necessary to take the rheological measurements with more complex flow than the simple viscometric flow. The measurement of rheological properties even under a little bit more complex flow field is not straightforward and still remains one of the challenging subjects of rheometry. The objective of this thesis is to investigate the

rheological behavior of complex fluids in both oscillatory squeeze flow (OSQ) and dynamic helical squeeze flow (DHSQ) and to provide a platform for the analysis of nonsymmetric stress signals.

In the oscillatory squeeze flow, the fluid experiences nonsymmetric stress history. This nonsymmetric stress response is a unique feature of oscillatory squeeze flow (OSQ), but has rarely been investigated. It was reported a robust framework for the analysis of nonlinear and nonsymmetric stress signals at larger strain amplitude under oscillatory squeeze flow, and the information obtainable from this approach is more rich and useful than that has been reported in the past. The normal stress was found to be nonsymmetric in both magnitude and shape at large strain amplitude, which leads to the appearance of even harmonics in Fourier transformation.

Dynamic helical squeeze flow of both oscillatory squeeze and oscillatory shear flow provides information for microstructural changes of material in superimposed flow field by means of mechanical spectroscopy. Although the realistic flow field is more complicated than dynamic helical squeeze flow, it is useful in understanding the flow behavior of complex fluids in well-defined complicated flow field, and enables to overcome the limitation of conventional rheometry, which has been confined mostly to

simple shear flow. The stress analysis of both stress shape and Lissajous plot showed dramatic change as the strain amplitude increases. Both shear and normal stress show nonsymmetric characteristics which mean the different response during compression and extension. In dynamic helical squeeze flow, the onset of material nonlinearity in the shear stress was faster than simple shear flow. This work was undertaken to further establish the use of dynamic helical squeeze flow in order to measure the rheological properties of complex fluids under more realistic flow circumstance.

Keywords: dynamic helical squeeze (DHSQ) flow, oscillatory squeeze (OSQ) flow, oscillatory shear (OS) flow, complex fluid, nonsymmetric stress curve, Lissajous plot, Fourier transform (FT)

Student Number: 2005-30274

Table of contents

List of Figures

List of Tables

Chapter 1. Introduction

1.1 Oscillatory shear (OS) flow

Oscillatory shear measurements are often carried out in the linear or nonlinear regime. The oscillatory shear test in linear regime, which is called small amplitude oscillatory shear (SAOS), has been widely used because it has sound mathematical background and is sensitive to the microstructural difference [Macosko, 1994]. Even though SAOS is a useful tool that enables us to correlate rheological properties with microstructure of the materials, it is valid only when deformation is either very small or slow enough to guarantee linear viscoelasticity. However the deformation is rapid and large in most industrial processes. Large amplitude oscillatory shear (LAOS) has been alternatively used to overcome the limitations of SAOS. LAOS is a useful flow because frequency and strain amplitude can be controlled individually allowing a widespread spectrum of conditions [Yosick *et al.*, 1997; Hyun *et al.*, 2011]. This nonlinear viscoelastic measurement provides useful information for material characterization under large deformation; however it is difficult to analyze the nonlinear stress signals with relevant theoretical background. Various methods have been developed and used to characterize the nonlinear stress signals obtained via LAOS test. Stress shape analysis is a

simple method to investigate the nonlinear stress response as a function of time. The Fourier-transform (FT) analysis is a sensitive method focusing on the relative higher harmonics to characterize the nonlinearity [Wilhelm *et al.*, 1998]. The stress decomposition (SD) method enables us to decompose stress signal into elastic and viscous components even in nonlinear regime [Cho *et al.*, 2005; Ewoldt *et al.*, 2008; Yu *et al.*, 2009]. All these methods provide useful information on the rheological response of complex fluids, but it is still restricted only to simple shear flow.

1.2 Oscillatory squeeze (OSQ) flow

Oscillatory squeeze flow (OSQ) has been studied for many years not only in experiment but also in simulation, though less attention has been paid than standard viscometric flow. This flow suffers from transient and inhomogeneous flow field due to the changing flow geometry during oscillation. Nevertheless oscillatory squeeze flow can be a useful tool to characterize the rheology of complex fluids: adhesives, printing inks, bone joints, biological materials, dental composites, etc [Kramer, 1974; Field *et al.*, 1996; Phan-Thien *et al.*, 2000; Jiang *et al.*, 2004; See and Nguyen, 2004]. Phan-Thien (1980) made theoretical approach for viscoelastic fluids at small

strain under oscillatory squeeze flow. Bell *et al.* (2006) derived a comprehensive theory considering fluid inertia for oscillatory squeeze flow. In experimental observation, the linear viscoelasticity of viscoelastic fluids was investigated under small amplitude oscillatory squeeze flow [Field *et al.*, 1996; See and Nguyen, 2004]. In the nonlinear regime, oscillatory squeeze flow was also analyzed with respect to the closed loop of [stress vs. strain] with a biological material and dental composite resin [Phan-Thien *et al.*, 2000; Jiang *et al.*, 2004]. The linear viscoelasticity of hard sphere suspension was studied with the oscillatory shear, oscillatory squeeze, and lubricated squeeze flow [Walberer and McHugh, 2001]. A numerical investigation for oscillatory squeeze flow was carried out by finite element method and simple model simulation [Phan-Thien, 2000; Debbaut and Thomas, 2004]. Even though these rheometric protocols provide useful information on the rheological properties of complex fluids, they are not enough in the sense that the flow fields are still too simple compared to real processes. Table 1-1 shows the summary of oscillatory squeeze flow in previous literatures.

Table 1-1 The summary of oscillatory squeeze flow in previous literatures.

Ref.	**System**	**Key points**
Phan-Thien (1980)	•Mathematical theory •Simple fluid	•Normal force of OSQ •Fluid inertia

Field *et al.* (1996)	•Newtonian oil •Hyaluronic acid •Human synovial fluid •Boger fluid	•Complex moduli
Phan-Thien *et al.* (2000)	•Pig kidney •Instrument: MFR[1]	•Nonlinear response •Large amplitude oscillatory flow •Model predictions
Walberer *et al.* (2001)	•Polydimethylsiloxane (PDMS) •Glass bead: 7μm •Instrument: CP20[2]	• G''/G' is a function of Mw. •The effect of filler
See *et al.* (2003)	•Araldite (methacrylate-based, epoxy resin adhesive) •Plasti-bond (styrene, benzoyl peroxide) •Instrument: MFR	•Application: to monitor the changes in viscoelastic properties.
Jing *et al.* (2003)	•Dental resin •Instrument: MFR	•Microstructural mechanism •Elastic and viscous contributions
Sakai (2004)	•Instrument: MFR	•Instrument compliance
Debbaut *et al.* (2004)	•Finite element simulation •A1 fluid (Polyisobutylene) •Instrument: CP20	•Strain limit •Multi-mode Giesekus model

[1] Micro-Fourier Rheometer, Commonwealth Scientific & Industrial Research Organization, Australia.
[2] Compressional Rheometer, TA Instruments, USA.

Bell *et al.* (2006)	•Silicone oil •A1 fluid (Polyisobutylene) •Polydimethyl sulfate •Polyacrylamide •Instrument: CP20	•BBW (Bell-Binding-Walters) theory •Fluid inertia

1.3 Dynamic helical squeeze (DHSQ) flow

The measurement of rheological properties even under a little bit more complex flow field is not straightforward and still remains one of the challenging subjects of rheometry. Nevertheless, the first investigation under more complex flow field was examined by Osaki *et al.* (1965), introducing parallel superposition of both steady shear and oscillatory shear flow in the same direction. Simmons (1966) reported rheological properties of polymer solutions using orthogonal superposition flow that the oscillatory motion is imposed into perpendicular direction of the main flow, steady shear. Similar measurements were carried out for other polymer solutions including aluminium dilaureate and ethylene-propylene copolymer [Booij, 1966; 1968], polyisolutylene-cetane solution [Tanner and Simmons, 1967; Simmons, 1968; Tanner, 1968; Kwon and Leonov, 1993], polyethylene melts [Kataoka and Ueda, 1969], polyisobutylene and monodisperse polystyrene [Macdonald,

1973], polystyrene and poly (ethylene oxide) [Powell and Schwarz, 1975], polyisobutylene and polyacrylamide solutions [De Cleyn and Mewis, 1987], polystyrene, poly (ethylene oxide) and ethylcellulose [Laufer *et al.*, 1975], polystyrene and ordered polystyrene latex [Zeegers *et al.*, 1995], alkali-swellable associative polymer [Tirtaatmadja *et al.*, 1997], human blood, polyacrylamide and Xanthan gum [Vlastos *et al.*, 1997], wormlike micellar solution [Anderson *et al.*, 2006], branched hydrophobic alkali-swellable emulsion [Mewis *et al.*, 2001], entangled polydisperse polymer melts [Somma *et al.*, 2007], entangled DNA and polybutadiene solutions [Boukany and Wang, 2009], soft glassy materials [Ovarlez *et al.*, 2010]. Vermant *et al.*(1997) designed a device making the two superposition modes of either parallel or orthogonal direction on a steady or oscillatory shear flow on a single instrument. Thereafter the parallel and orthogonal superposition measurements were investigated by means of comparative analysis for polyisobutene solution [Vermant *et al.*, 1998] and lyotropic liquid crystalline polymers [Walker *et al.*, 2000]. In recent the flow-induced anisotropy of rheological properties has been examined using two dimensional small amplitude oscillatory shear (2D-SAOS) achieved by synchronizing oscillatory motion in parallel and orthogonal to steady shear flow [Mobuchon *et al.*, 2009].

This study proposes a method to measure the rheological responses of complex fluids under dynamic helical squeeze flow (DHSQ) of both oscillatory shear and oscillatory squeeze. Although the realistic flow field is more complicated than the combination of these two flow types, e.g. both oscillatory shear and oscillatory squeeze, it may be regarded as a step forward to more realistic flows. It will be useful in understanding the flow behavior of complex fluids in a well-defined complicated flow field, and enables to overcome the limitation of conventional rheometry which has been confined mostly to shear flow. The objective of this study is to introduce an instrument which allows the rheological characterization of viscoelastic fluids under OSQ and DHSQ and to provide a platform for the analysis of experimental data. Thereby it is expected that the instrument bridges the gap between conventional rheometry and more complicated and practical real processes. Previous researches on the superimposed flows are summarized in Table 1-2.

Table 1-2 The summary on superimposed flow in previous literatures.

The type of flow	Ref.
Steady shear + Oscillatory shear	Anderson *et al*. (2006), Bernstein (1972), Booij *et al*. (1966, 1968), Boukany *et al*. (2009), De Cleyn *et al*. (1987), Dinser *et al*. (2007), Laufer *et al*. (1975), MacDonald *et al*. (1973), Osaki *et al*. (1965), Powell *et al*. (1975), Simmons (1968), Somma *et al*. (2007),

	Tanner (1968), Tanner *et al*. (1967), Tirtaatmadja *et al*. (1997), Vermant *et al*. (1998), Vlastos *et al*. (1997), Walker *et al*. (2000), Yamamoto (1971)
Steady shear + Oscillatory squeeze	Bernstein (1972), De Cleyn *et al*. (1987), Isayev *et al*. (1988), Mewis *et al*. (2001), Simmons *et al*. (1966), Tanner *et al*. (1967), Vermant *et al*. (1997), Vermant *et al*. (1998), Walker *et al*. (2000), Wong *et al*. (1989), Yamamoto (1971), Zeegers *et al*. (1995)
Oscillatory shear + Oscillatory squeeze	This study
Steady shear + Oscillatory shear + Oscillatory squeeze	Mobuchon *et al.* (2009)
Steady shear + Squeeze	Ovarlez *et al.* (2010)

1.4 Outline of the thesis

The study is organized as follows. In chapter 2, theoretical background of OS and OSQ will be presented in terms of linear viscoelasticity and nonlinear viscoelasticity. In the linear regime, based on the strain imposed and the stress response, storage and loss moduli are defined as ratio of stress and strain amplitude and phase angle. However, in the nonlinear regime, the stress wave becomes nonsinusoidal signal for most complex fluids which indicates nonlinear response. The nonlinear stress signal can no longer

describe in terms of storage and loss modulus due to higher harmonics. For the reason above, it is introduced how to characterize the nonlinear response under OS and OSQ.

In chapter 3, experimental and analysis method for OSQ and DHSQ are introduced. To develop the well-defined complicated flow, a combination of modified fixture and commercial rheometer was newly used: oscillatory squeeze flow and dynamic helical squeeze flow. In order to analyze the nonlinear stress data, graphical and discrete spectral method are given in detail: stress shape analysis and Fourier transform.

In chapter 4, it will be quantitatively analyzed the nonlinear responses of viscoelastic fluids at larger deformation under OSQ and provide a platform for the analysis of nonsymmetric stress signals. This study reports the characteristics of nonsymmetric normal stress signals under OSQ; the normal stress became nonsymmetric in terms of both magnitude and shape in positive and negative region of oscillation. This unique feature may be considered as the result of the microstructural change during compression and extension.

In chapter 5, the nonsymmetric stress responses under oscillatory squeeze flow is predicted via simple model simulation. Then it will be evaluated the predictability of the constitutive equations. First the theoretical

background used in this study including kinematics and constitutive equations will be introduced. Then, the stress curve, Lissajous plot, and Fourier transform of model predictions from UCM, Giesekus, and EPTT model will be compared with experimental data.

In chapter 6, it will be proposed a design and methodology to measure the rheological responses of complex fluids under dynamic helical squeeze flow (DHSQ). Although the realistic flow field is more complicated than the combination of these two flow types, it may be regarded as a step forward to more realistic flows. The section introduces an instrument which allows the characterization of complex fluids under DHSQ and provides a platform for the analysis of experimental data. Finally, the specific features for complex fluids encountered in dynamic helical squeeze flow (DHSQ) will be showed.

Interest in viscoelastic materials under a little bit more complicated flow is increasing across many disciplines. The contributions presented here provide the means to a better understanding of complex fluids under a complicated flow field.

Chapter 2. Theory

2.1 Oscillatory shear stress

2.1.1 Kinetics in shear flow

With one fixed plate and the other rotating at Ω, assuming no slip at the plates and neglecting inertial force, the velocity field can be obtained as follows:

$$v_\theta = \frac{zr\Omega}{H} \tag{2-1}$$

Eq. (2-1) is a velocity of the θ-direction in cylindrical coordinate (r,θ,z) on the fluid contained between two parallel plates separated by the distance H.

Deformation rate tensor of oscillatory shear flow in cylindrical coordinate (r,θ,z) is given by

$$\mathbf{D} = \frac{1}{2}\left[\nabla\mathbf{v} + (\nabla\mathbf{v})^T\right] = \begin{pmatrix} 0 & 0 & 0 \\ 0 & 0 & \frac{r\Omega}{2H} \\ 0 & \frac{r\Omega}{2H} & 0 \end{pmatrix} \tag{2-2}$$

where $\nabla\mathbf{v}$ is the velocity gradient, $(\nabla\mathbf{v})^T$ is the transpose of the velocity gradient, Ω is the angular velocity ($\Omega = \Omega_0 \sin\omega t$).

2.1.2 SAOS (Small Amplitude Oscillatory Shear) Flow

Oscillatory shear stress is obtained with dynamic shear test which is performed by applying a sinusoidal strain (or stress) and measures the stress (or strain) as a function of time. The shear stress in oscillatory shear test oscillates at applied frequency with respect to zero mean value of x-axis. When the strain amplitude is infinitesimal, the stress oscillates sinusoidally at the same frequency with a delay time. It is mathematically expressed as follows;

$$\sigma_{z\theta}(t) = \sigma_{z\theta 0} \sin(\omega t + \delta_\theta) \tag{2-3}$$

where $\sigma_{z\theta 0}$ is the magnitude and δ_θ is the phase angle of shear stress, respectively.

Eq. (2-3) can be decomposed into two waves of the same frequency as follows;

$$\sigma_{z\theta}(t) = \gamma_{\theta 0}[G' \sin \omega t + G'' \cos \omega t] \tag{2-4}$$

where, G' is called storage or elastic modulus meaning the mechanical energy storage, while G'' is called loss or viscous modulus representing the mechanical energy dissipation.

2.1.2 LAOS (Large Amplitude Oscillatory Shear) flow

On the other hand, if the strain amplitude is large, the stress wave

becomes nonsinusoidal signal for most complex fluids which indicates nonlinear response. The shape of non-sinusoidal shear stress manifests the structural change of complex fluids. The shear stress curve contains odd higher harmonics in LAOS as follows;

$$\sigma_{z\theta}(t) = \sum_{n=odd} \sigma_n \sin(n\omega t + \delta_n) \tag{2-5}$$

where the magnitude $\sigma_n(\omega, \gamma_{\theta 0})$ and the phase angle $\delta_n(\omega, \gamma_{\theta 0})$ depend on the strain amplitude and the frequency. This is why the linear viscoelasticity (G', G'') is not meaningful in LAOS. The nonlinear stress signal can no longer describe in terms of storage and loss modulus due to higher harmonics.

2.2 Oscillatory normal stress

2.2.1 Kinetics in squeeze flow

It is necessary to derive the velocity field and the normal force under squeeze flow from momentum equation. Since there is no rotation, $v_\theta = 0$ and $\partial/\partial\theta = 0$. The velocity field in cylindrical coordinate (r, θ, z) is assumed to be that of a Newtonian and incompressible fluid as follows:

$$v_z = f(z, t) \tag{2-6}$$

$$v_r = -\frac{1}{2} r f'(z,t) \tag{2-7}$$

where $f = -3\dot{h}\left[\left(\frac{z}{H}\right)^2 - \frac{2}{3}\left(\frac{z}{H}\right)^3\right]$, $H(t) = H_0 + a\sin\omega t$;

$\dot{h} = dH/dt = a\omega\cos\omega t$ is the axial velocity of the dynamic motion and dot denotes differentiation with respect to t , and a is the deformation amplitude in vertical direction. With lubrication approximation, $H(t)$ can be replaced by H_0 when $H_0 >> a$.

Deformation rate tensor of oscillatory squeeze flow in cylindrical coordinate (r,θ,z) is given by

$$\mathbf{D} = \frac{1}{2}\left[\nabla\mathbf{v} + (\nabla\mathbf{v})^T\right] = \begin{pmatrix} 3\dot{h}\frac{z}{H_0^2}\left(1-\frac{z}{H_0}\right) & 0 & \frac{3}{2}\dot{h}\frac{r}{H_0^2}\left(1-2\frac{z}{H_0}\right) \\ 0 & 3\dot{h}\frac{z}{H_0^2}\left(1-\frac{z}{H_0}\right) & 0 \\ \frac{3}{2}\dot{h}\frac{r}{H_0^2}\left(1-2\frac{z}{H_0}\right) & 0 & -6\dot{h}\frac{z}{H_0^2}\left(1-\frac{z}{H_0}\right) \end{pmatrix}$$

$$= \dot{\gamma}_z \begin{pmatrix} 3\frac{z}{H_0}\left(1-\frac{z}{H_0}\right) & 0 & \frac{3}{2}\frac{r}{H_0}\left(1-2\frac{z}{H_0}\right) \\ 0 & 3\frac{z}{H_0}\left(1-\frac{z}{H_0}\right) & 0 \\ \frac{3}{2}\frac{r}{H_0}\left(1-2\frac{z}{H_0}\right) & 0 & -6\frac{z}{H_0}\left(1-\frac{z}{H_0}\right) \end{pmatrix}, \tag{2-8}$$

showing the presence of both shear and extensional terms, where $\nabla\mathbf{v}$ is the velocity gradient, $(\nabla\mathbf{v})^T$ is the transpose of the velocity gradient, $\dot{h}$ is the

velocity in vertical direction ($\dot{h} = a\omega\cos\omega t$) and $\dot{\gamma}_z = \gamma_{z0}\omega\cos\omega t$.

The normal force *F* that the fluid exerts on the upper plate is obtained by

$$F = \frac{3\pi\eta V R^4}{2H^3}, \tag{2-9}$$

where η is the constant viscosity, V is the constant velocity.

This normal force was calculated based on the assumptions: the fluid is assumed to be isothermal and incompressible; inertia, gravity and surface force are assumed to be unimportant; there is no-slip on the plates; the radius of plate (R) is significantly larger than the initial gap height (H_0).

In dynamic mode for viscoelastic fluids, the normal force in Eq. (2-9) can be rewritten as follows:

$$F = \frac{3\pi\eta^* \dot{h} R^4}{2H_0^3}, \tag{2-10}$$

where η^* is the complex viscosity, $\dot{h}$ is the axial velocity of the dynamic motion, *R* is the radius of the upper plate, H_0 is the initial gap height [Phan-Thien, 1980]. Eq. (2-10) is similar to the Stefan's equation with viscosity η replaced by complex viscosity η^* ; a substitution generally accepted for small strain amplitude in dynamic mode. Note if small strain amplitude ($H >> a$)

is imposed, $H(t)$ is equivalent to the initial gap height H_0. Actually when the deformation becomes large, $H(t)$ is not equivalent to the H_0. However it was assumed that Eq. (2-10) can be apparently used to derive material functions even under large deformation.

2.2.2 SAOSQ (Small Amplitude Oscillatory Squeeze) Flow

In small strain amplitude, the normal stress oscillates sinusoidally at the same frequency but with a phase angle (δ_z),

$$\sigma_{zz}(t) = \sigma_{zz0} \sin(\omega t + \delta_z) \tag{2-11}$$

where ω is the applied frequency, σ_{zz0} is the magnitude of the normal stress. The storage (E') and loss (E'') modulus for the normal stress component in OSQ can be determined by

$$E' = \frac{2H_0^2}{3R^2}\frac{\sigma_{zz}}{\gamma_{z0}}\cos\delta_z, E'' = \frac{2H_0^2}{3R^2}\frac{\sigma_{zz}}{\gamma_{z0}}\sin\delta_z \tag{2-12}$$

where δ_z is the phase angle of the normal stress [Bell *et al.*, 2006]. E' and E'' are known as the storage and loss modulus of OSQ. In this study, the inertial effect is not significant due to high viscosity of the samples and narrow initial gap.

The complex viscosity in OSQ is defined by [Debbaut and Thomas, 2004].

$$\eta_z^* = \frac{1}{\omega}\sqrt{(E')^2 + (E'')^2} \ . \qquad (2\text{-}13)$$

2.2.3 LAOSQ (Large Amplitude Oscillatory Squeeze) flow

As the strain amplitude increases, the normal stress curve becomes nonlinear as well as nonsymmetric. The normal stress curve contains odd and even higher harmonics in LAOSQ as follows;

$$\sigma_{zz}(t) = \sum_{n=odd,even} \sigma_n \sin(n\omega t + \delta_n) \qquad (2\text{-}14)$$

where the magnitude $\sigma_n(\omega, \gamma_{z0})$ and the phase angle $\delta_n(\omega, \gamma_{z0})$ depend on the strain amplitude and the frequency. Likewise oscillatory shear flow, the linear viscoelastic theory is insufficient to demonstrate the nonlinear response under large strain amplitude. Furthermore, the nonsymmetric normal stress displays the difference in magnitude at both maximum and minimum, and the difference increases with the strain amplitude. The difference is small at low strain amplitude, but becomes pronounced at large strain amplitude. For this reason, it is needed to calculate the moduli by the internal area of closed loop, [stress vs. strain] or [stress vs. strain rate]. By the internal area of the loop, the moduli from normal stress can be calculated as follows [Cho *et al*., 2005; Bell *et al*., 2006];

$$E' = \frac{2H_0^2}{3R^2}\frac{1}{\pi\gamma_{z0}^2}\left|\oint \sigma_{zz} d\left(\dot{\gamma}_z / \omega\right)\right| \tag{2-15}$$

$$E'' = \frac{2H_0^2}{3R^2}\frac{1}{\pi\gamma_{z0}^2}\left|\oint \sigma_{zz} d\left(\gamma_z\right)\right| \tag{2-16}$$

2.3 Kinetics in DHSQ (dynamic helical squeeze) flow

In cylindrical coordinate (r,θ,z), the velocity fields in dynamic helical squeeze flow (DHSQ) is assumed to be that of a Newtonian and incompressible fluid as follows, respectively:

$$v_r = -\frac{1}{2} rf'(z,t) \tag{2-17}$$

$$v_\theta = \frac{zr\Omega}{H} \tag{2-18}$$

$$v_z = f(z,t) \tag{2-19}$$

where $f = -3\dot{h}\left[\left(\frac{z}{H}\right)^2 - \frac{2}{3}\left(\frac{z}{H}\right)^3\right]$, $H(t) = H_0 + a\sin\omega t$; $\dot{h}$ is the dynamic axial velocity of DHSQ. With lubrication approximation, $H(t)$ can be replaced by H_0 when $H_0 >> a$.

Deformation rate tensor of dynamic helical squeeze flow is given by

$$\mathbf{D}=\frac{1}{2}\left[\nabla\mathbf{v}+(\nabla\mathbf{v})^{T}\right]=\begin{pmatrix} 3\dot{h}\frac{z}{H_0^2}\left(1-\frac{z}{H_0}\right) & 0 & \frac{3}{2}\dot{h}\frac{r}{H_0^2}\left(1-2\frac{z}{H_0}\right) \\ 0 & 3\dot{h}\frac{z}{H_0^2}\left(1-\frac{z}{H_0}\right) & \frac{r\Omega}{2H} \\ \frac{3}{2}\dot{h}\frac{r}{H_0^2}\left(1-2\frac{z}{H_0}\right) & \frac{r\Omega}{2H} & -6\dot{h}\frac{z}{H_0^2}\left(1-\frac{z}{H_0}\right) \end{pmatrix} \tag{2-20}$$

where $\nabla\mathbf{v}$ is the velocity gradient, $(\nabla\mathbf{v})^{T}$ is the transpose of the velocity gradient. Here, it is clear that the deformation rate of DHSQ can be denoted by the simple summation with those of oscillatory shear and oscillatory squeeze flow. It has not been made clear material properties for DHSQ with large deformation and non-Newtonian fluid. The theoretical analysis in DHSQ leads to considerable complexity despite using even standard constitutive models. Thus, any robust theoretical presentation for DHSQ is yet to be worked out. For this reason, it was assumed that the normal and shear stresses in DHSQ are apparently used as those by obtained in oscillatory squeeze and oscillatory shear flow, respectively.

2.4 Basic assumptions

Here it was estimated the effect of inertia relative to the normal force. The inertial force of oscillatory squeeze flow is given by [Debbaut and

Thomas, 2004]

$$F_{inertia} = \frac{3\pi a R^4}{2H_0^3} \frac{\omega^2 \rho H_0^2}{10}, \tag{2-21}$$

where ρ is the density of PEO solution (1130 kg/m^3) and the deformation amplitude a is 0.42 mm.

The ratio of inertial force to normal force is given by

$$\frac{F_{inertia}}{F} = \frac{a\omega^2 \rho H_0^2}{10\eta^* \dot{h}_{\max}} \sim O(10^{-6}) \tag{2-22}$$

where $\dot{h}_{\max}$ is the axial velocity at zero strain ($\dot{h}_{\max} = a\omega$).

Thus the inertial effect can be neglected in this experiment unless the frequency is not too high.

It was also checked the surface force at the rim of the sample. The surface force is given by

$$F_{sur} \sim \Gamma\left(\frac{1}{R_{c,1}} + \frac{1}{R_{c,2}}\right) \times 2\pi R H_0 \tag{2-23}$$

where $R_{c,1}$ and $R_{c,2}$ are the radius of curvature of the sample in $r\theta$ and rz plane, R is the radius of upper plate; surface tension of PEO solution Γ =0.043 N/m at 25℃ [Roe, 1968]. Even though the radius of curvature changes during the dynamic test, it can be assumed as follows: $R_{c,1} \cong R$,

$H_0/2 \le R_{c,2} \le \infty$.

Employing Eq. (2-10) and (2-23), the ratio of surface force to normal force is given by

$$\frac{F_{sur}}{F} = \frac{4\Gamma H_0^4}{3\eta^* \dot{h}_{\max} R^3}\left(\frac{1}{R_{c,1}} + \frac{1}{R_{c,2}}\right) \tag{2-24}$$

which depends on the radius of curvature, $R_{c,1}$ and $R_{c,2}$.

The ratio is maximum for $R_{c,1} \cong R$ and $R_{c,2} = H_0/2$, and $F_{sur}/F \sim O(10^{-5})$. Thus the surface force is negligible compared to the normal force in the oscillatory squeeze flow.

2.5 Compressibility

In fluid mechanics, compressibility is a measure of the relative volume change of a material according to an applied pressure. The compressibility β can be given by

$$\beta = -\frac{1}{V}\frac{\partial V}{\partial P} \tag{2-25}$$

where V is the volume of fluid and P is the imposed pressure under deformation. The fluid was repeatedly compressed or extended during oscillatory squeeze or dynamic helical squeeze flow. Generally speaking,

compressibility of polymers becomes significant only when rather large pressures are employed, say, above 3×10^{8} Pa [Haward, 1969]. The value was $4.5\times10^{-11}Pa^{-1}$ for polymer solutions and $4.6\times10^{-10}Pa^{-1}$ for water [Haward, 1969]. Thus, the compressibility can be obviously neglected in this study.

Chapter 3. Experiment and analysis

3.1 Measurements

3.1.1 Data acquisition

For raw data acquisition, a 16bit ADC card (PCI-6052E; National Instruments) with sampling rate up to 333 kHz was used. This ADC card was plugged into a personal computer equipped with home written LabView software (National Instruments) and connected to the rheometer (RMS800, TA Instruments) through BNC (Bayonet Neill Concelman) cables. Thus, during the strain sweep test at fixed frequency, the stresses (torque and normal) and strain (displacement) data were obtained simultaneously by the ADC card. Overall diagram for experimental setup displays in Fig. 3-1.

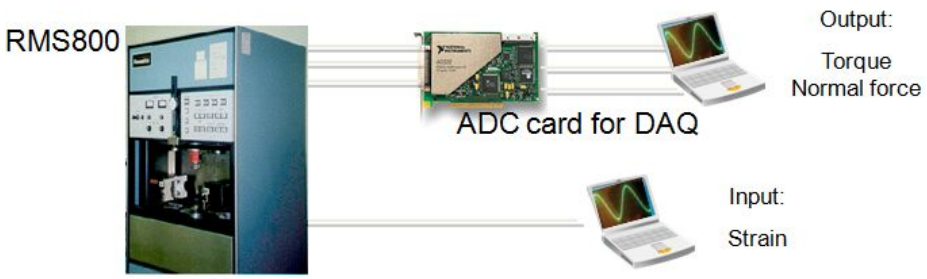

Fig. 3-1 Experimental setup for data acquisition in OSQ and DHSQ. The strain-controlled type rheometer RMS800 was used.

3.1.2 Shear and normal stresses

In a torsionally driven parallel plate geometry, the governing equations for the measured shear stress ($\sigma_{z\theta}$) and imposed shear strain ($\gamma_{\theta 0}$) that are used for most rheometer are given by Eqs. (3-1) and (3-2),

$$\sigma_{z\theta} = \frac{T}{2\pi R^2}\left[3 + \frac{d\ln T}{d\ln \dot{\gamma}_R}\right] \tag{3-1}$$

$$\gamma_{\theta 0} = \frac{R\theta}{H_0} \tag{3-2}$$

where H_0 is the initial gap height, R is the radius of plate, θ is the angular displacement, T is the torque.

In a squeezing geometry, the governing equations for the measured normal stress (σ_{zz}) and imposed normal strain (γ_{z0}) are given by Eqs. (3-3) and (3-4),

$$\sigma_{zz} = \frac{F}{\pi R^2} \tag{3-3}$$

$$\gamma_{z0} = \frac{a}{H_0} \tag{3-4}$$

where F is the measured normal force, H_0 is the initial gap height, R is the radius of plate, a is the deformation amplitude in vertical direction.

3.2 Modified fixture

The modified fixture was designed to develop a well-defined

complicated flow: oscillatory squeeze flow and dynamic helical squeeze flow [Kim *et al.*, 2008]. The fixture can impose the dynamic motion into axial deformation or helical deformation. This device is mounted on the RMS800 (TA Instruments) as shown in Fig. 3-2. Fig. 3-3 displays lower fixtures for OSQ and DHSQ. Four different kinds of inclined angle (α =45°, 50°, 55°, 60°) were designed to make the dynamic helical squeeze flow. The ball screw of the modified fixture allows dynamic vertical displacement when acted upon by motor (see in Fig. 3-4(a)). Guide holder was used to support the lower fixture and ball screw (see in Fig. 3-4(b)). A detailed driving procedure will be demonstrated in next section.

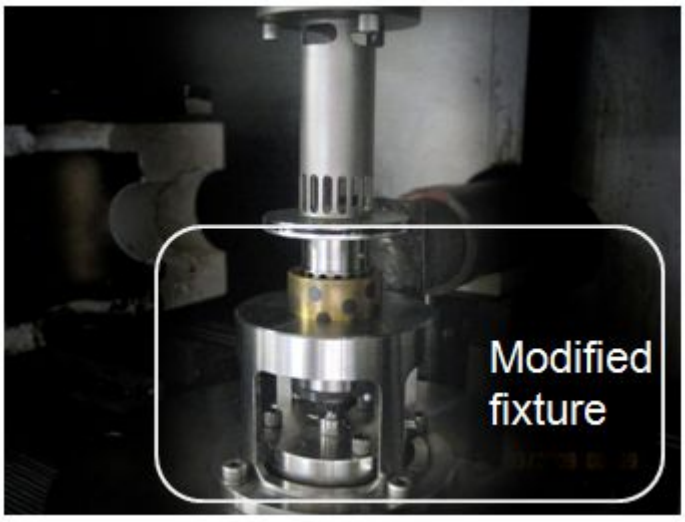

Fig. 3-2 Real image of the modified fixture for OSQ and DHSQ. The device is mounted on RMS800.

Fig. 3-3 Lower fixtures of the modified fixture for OSQ and DHSQ. There are four different kinds of inclined angle α : 45°, 50°, 55° and 60°.

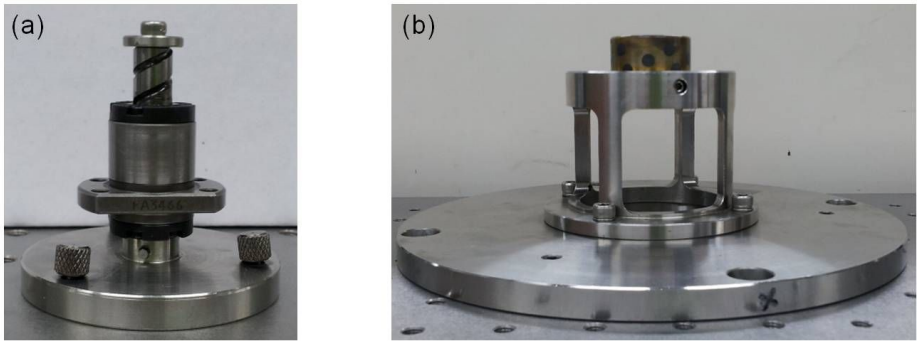

Fig. 3-4 (a) Ball screw and (b) guide holder of the modified fixture.

3.3 Oscillatory squeeze (OSQ) flow

For the oscillatory squeeze experiments, a new setup was built on a conventional rheometer (RMS800, TA Instruments) by introducing a modified fixture. The schematic diagram of the modified fixture is shown in Fig. 3-5. It was designed to apply the dynamic squeeze motion into axial direction only. The ball screw of the modified fixture allows dynamic vertical displacement when acted upon by the motor. In the oscillatory squeeze flow mode, the test material is contained between two parallel-plates, the top of which is stationary. The bottom plate is subjected to dynamic squeeze motion in vertical direction only. The procedure for sample loading is similar to that of parallel plate rotational rheometry. The normal stress developed during the test was measured by a transducer connected to the upper fixture, and recorded by an on-line computer. The experiments were performed on dynamic test mode with a plate-plate fixture (diameter: upper plate 40mm and lower plate 50mm; gap: 1mm for simple shear flow and 1.5mm for oscillatory squeeze flow). Silicone oil was used to prevent evaporation of PEO aqueous solutions at the edge disclosed to the air. All measurements were taken at room temperature.

The upper plate is fixed, while the lower plate is given a dynamic displacement of vertical motion as shown in Fig. 3-5. The strain amplitude in

axial displacement is defined by

$$\gamma_{z0} = \frac{a}{H_0}, \tag{3-6}$$

where H_0 is the initial gap height, a is the deformation amplitude in vertical direction.

The oscillatory motion is imposed by,

$$\gamma_z = \gamma_{z0} \sin \omega t , \tag{3-7}$$

where ω is the applied frequency, γ_{z0} is the strain amplitude in vertical direction. The normal stress oscillates sinusoidally at the same frequency but with a phase lag with respect to the applied strain,

$$\sigma_{zz} = \sigma_{zz0} \sin\left(\omega t + \delta_z\right) \tag{3-8}$$

where ω is the applied frequency, σ_{zz0} is the magnitude of the normal stress.

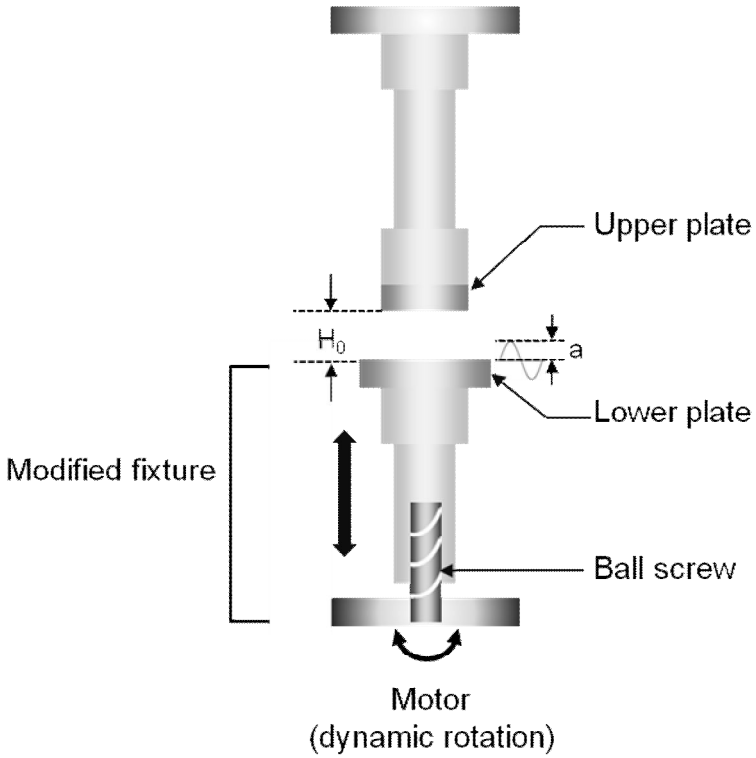

Fig. 3-5 Schematic diagram of the modified fixture for oscillatory squeeze flow.

3.4 Dynamic helical squeeze (DHSQ) flow

The schematic diagram of the modified fixture for dynamic helical squeeze flow is shown in Fig. 3-6. The modified fixture (lower fixture) was designed to apply the dynamic helical squeeze motion of both oscillatory shear and oscillatory squeeze. The ball screw plays an important role to transfer rotational movement to helical movement when the motor is operated. Parallel-plate geometry of radius 12.5 and 20 mm was used for all measurements. In the DHSQ mode, the top plate is fixed in the same way, and the bottom plate is allowed to helical squeeze movement. The dynamic helical squeeze was conducted on RMS800 (TA Instruments) with the modified fixture with a gap of 1.5mm. The normal and shear stress developed during the test was measured by normal and shear transducer connected to the upper fixture, and recorded by an on-line computer. All measurements were taken at room temperature.

As the fluid is deformed in two directions in DHSQ, at least two strain amplitudes need to be defined. The strain amplitude in angular and axial displacement are defined respectively by

$$\gamma_{\theta 0} = \frac{R\theta}{H_0}, \tag{3-9}$$

$$\gamma_{z0} = \frac{a}{H_0}, \tag{3-10}$$

where R is the radius of the plate, θ is the angular displacement, H_o is the initial gap between the plates, and a is the deformation amplitude in vertical direction. The inclined angle determines the ratio of γ_{z0} and $\gamma_{\theta 0}$. When the inclined angle is zero or 90°, the oscillatory deformation becomes unidirectional. In this study, the inclined angle, $\alpha = \tan^{-1}\left(\gamma_{z0} / \gamma_{\theta 0}\right)$, was fixed at 60°, which implies the bi-directional deformation. The two oscillatory motions are operated at the same frequency;

$$\gamma_\theta = \gamma_{\theta 0} \sin \omega t, \tag{3-11}$$

$$\gamma_z = \gamma_{z0} \sin \omega t, \tag{3-12}$$

where ω is the applied frequency, $\gamma_{\theta 0}$ and γ_{z0} are the strain amplitudes of angular and vertical direction, respectively. The shear and normal stresses oscillate sinusoidally at the same frequency but are delayed by the phase lags, δ_θ and δ_z, with respect to the applied strains.

$$\sigma_{z\theta} = \sigma_{z\theta 0} \sin\left(\omega t + \delta_\theta\right) \tag{3-13}$$

$$\sigma_{zz} = \sigma_{zz0} \sin\left(\omega t + \delta_z\right) \tag{3-14}$$

where ω is the applied frequency, $\sigma_{z\theta 0}$ and σ_{zz0} are the stress amplitudes of angular and vertical direction, respectively.

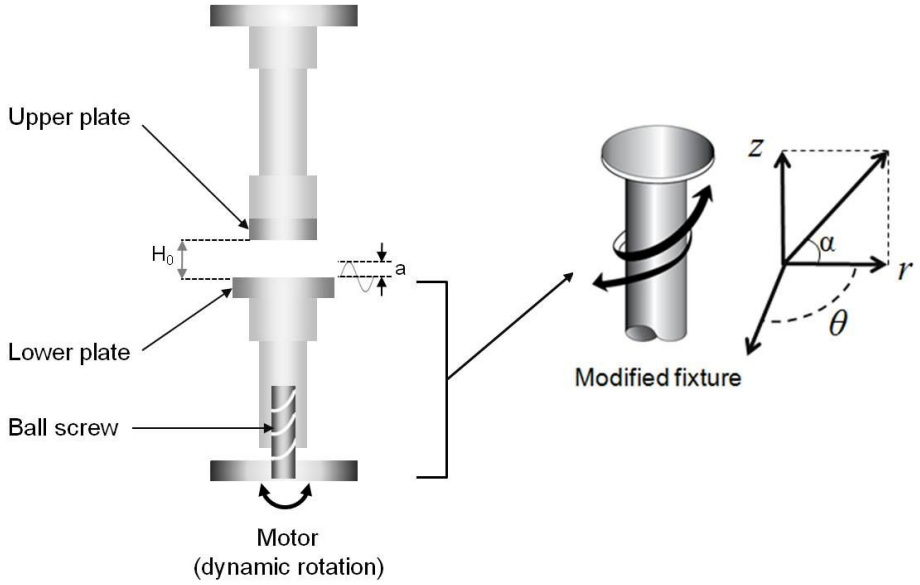

Fig. 3-6 Schematic diagram of the modified fixture for dynamic helical squeeze flow.

3.5 Materials and sample preparation

Table 3-1 Characteristics of the samples. Zero-shear viscosity (η_0) was calculated by fitting the complex viscosity data to the Carreau model*. The relaxation time (λ) is the reciprocal of the cross-over frequency [ω_c, frequency at G′(ω)= G″(ω) in the frequency sweep test].

Sample	Molecular weight [g/mol]	Concentration (wt%)	η_0^* [Pa·s]	λ (=1/ω_c) [s]
PB	920		20	-
PEO4m2.5	4×10^6	2.5	114	1.1
PEO4m3	4×10^6	3	297	2
PEO4m4	4×10^6	4	1307	5.5
PEO4m5	4×10^6	5	3430	8.3

*Carreau model: $\eta/\eta_0 = \left[1+(a\dot{\gamma})^b\right]^{(n-1)/b}$

Polybutene (PB, Sigma-Aldrich) was used as a Newtonian fluid and polyethylene oxide solution (PEO, Sigma-Aldrich) as a non-Newtonian fluid that is highly shear-thinning. The molecular weight is 920 g/mol for PB and 4×10^6 g/mol for PEO according to the supplier. 2.5, 3, 4, 5 wt% of PEO aqueous solutions were prepared by rotating the magnetic bar in a sealed glass bottle at 60 rpm for 6 days at room temperature. The polymer concentration was much higher than the overlap concentration at which the polymer

molecules start to entangle with each other. The overlap concentration (c^*) was 0.076 wt%, given the radius of gyration (R_g), molecular weight (M_w) and Avogadro's number (N_A) [$c^*=3M_w/4N_A\pi R_g^3$] [Dasgupta *et al.*, 2002]. The storage (G') and loss moduli (G'') and complex viscosity (η^*) are presented as a function of frequency in Fig. 3-7. All of PEO solutions exhibited strong shear-thinning behavior and G' exceeds G'' indicating dominant elastic nature over the cross-over frequency ω_c. Table 3-1 lists the molecular characteristics of the samples used in this work.

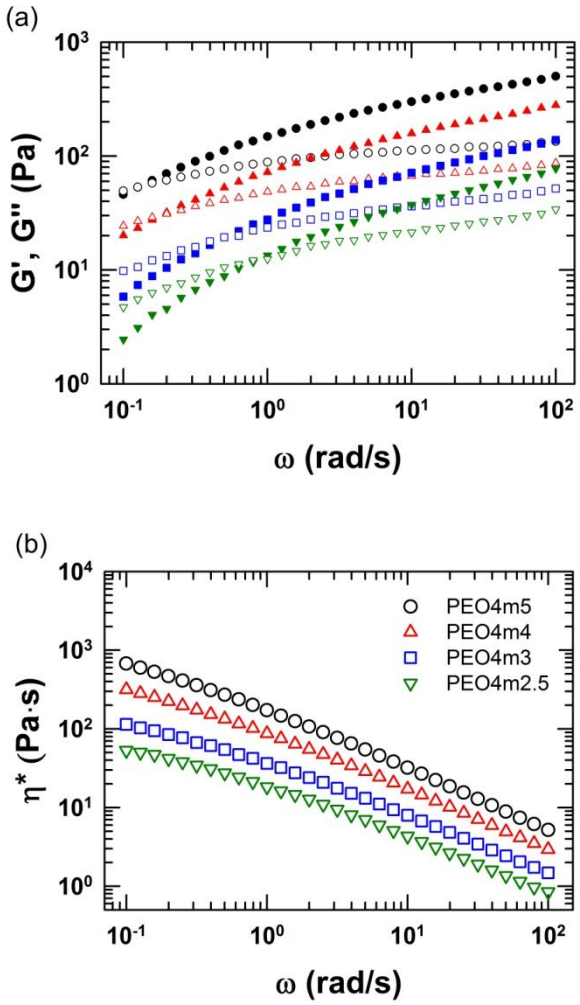

Fig. 3-7 (a) Storage (closed symbols) and loss(open symbols) moduli, G' and G'', for 5wt%(●, ○), 4wt%(▲, △), 3wt%(■, □), 2.5wt%(▼, ▽). (b) Complex viscosity η^* of PEO solutions as a function of frequency ω at room temperature.

Table 3-2 Description of the samples used in this study. Zero-shear viscosity was calculated by fitting data from complex viscosity curve to the Carreau model*. The relaxation time (λ) is the reciprocal of the cross-over frequency [ω_c, frequency at G′(ω)= G″(ω) in the frequency sweep test].

Sample	Concentration (wt%)		η_0^*	λ (=1/ω_c)
	PVA	Borate	(Pa·s)	(s)
P15	15	-	103	-
P15_B0.08	15	0.08	200	-
P15_B0.16	15	0.16	427	0.03
P2_B1	2	1	86	0.45

*Carreau model: $\eta/\eta_0 = \left[1+(a\dot{\gamma})^b\right]^{(n-1)/b}$

Polyvinyl alcohol (PVA) is a water-soluble synthetic polymer. Polyvinyl alcohol has excellent film forming, emulsifying and adhesive properties, and is also resistant to oil, grease and solvents. It has high tensile strength and flexibility, as well as high oxygen and aroma barrier properties. However these properties are dependent on humidity, in other words, with higher humidity more water is absorbed. PVA was purchased from Sigma-Aldrich, Inc., and the molecular weight of it was 124,000–186,000 g/mol with

98-99% hydrolyzed. Borax is the common name for sodium borate ($Na_2B_4O_7 \cdot 10H_2O$). A small amount of sodium borate produces a remarkable increase in viscosity of PVA aqueous solutions. This is due to the formation of a complex between hydroxyl groups and borate anions, which plays a role as a temporary crosslinking among PVA chains. The 15 wt% PVA with 0.08 or 0.16 wt% Borax was dissolved in dust-free purified water, and then the solution was rotated at 300 rpm for about 4 h at 85 ℃. All materials were used for the tests within 1 day. The complex viscosity as a function of frequency was plotted in Fig. 3-8. The aqueous solutions both PVA and PVA Borax show shear thinning behavior as the frequency increases, but they will display constant viscosity irrespective of the applied frequency at lower frequency region. Table 3-2 shows the molecular characteristics of the PVA and PVA borate used in this work.

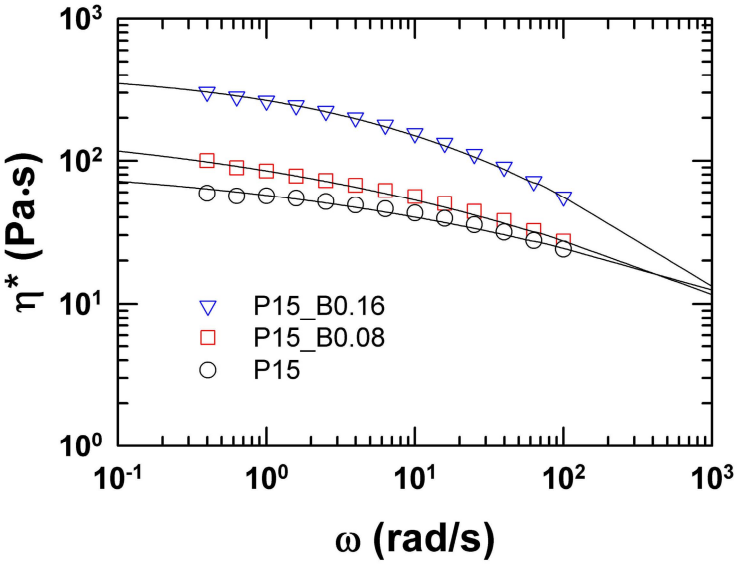

Fig. 3-8 The complex viscosity as a function of frequency; ▽ (PVA 15 wt%, Sodium Borate 0.16 wt%), □ (PVA 15 wt%, Sodium Borate 0.08 wt%), ○ (PVA 15 wt%) at strain amplitude 0.3 and room temperature. The solid line is the fitted result with the Carreau viscosity model.

Table 3-3 Medium and particles used to prepare for non-colloidal suspension.

Medium	**Molecular weight [g/mol]**	**Density [g/cm^3]**	η_0 **[Pa·s]**
PB	920	0.84	20
Particles	**Average diameter a[μm]**	**Density [g/cm^3]**	
PMMA20	20	1.19	
PMMA50	50	1.19	

Polybutene (PB, Sigma-Aldrich) was used as a suspending fluid which is non-volatile and hydrophobic. More detailed properties are provided in Table 3-3. As a non-colloidal hard sphere, poly-disperse poly(methylmethacrylate-co-ethyleneglycol dimethacrylate) [PMMA-EGDMA or PMMA, Sigma-Aldrich] particles were used with average diameter of 20 and 50 μm. The PMMA could be regarded as hard sphere. The concentrated suspensions were prepared by three-roll milling after hand-mixing. A three roll mill is an instrument which uses drag force created by means of three horizontally positioned rolls rotating to opposite directions. A vacuum oven was used to remove the bubbles in the non-colloidal suspension.

In suspension of non-colloidal hard spheres, Brownian motion and interparticle forces can often be ignored. The effect of sedimentation in concentrated suspensions does not play an important role during the rheological measurement because of the state of high volume fraction. Fig. 3-9 shows complex moduli of PMMA20 suspended in PB as a function of frequency with strain amplitude 0.004. The elastic and viscous moduli show a gentle slope with increasing volume fraction at lower frequency region.

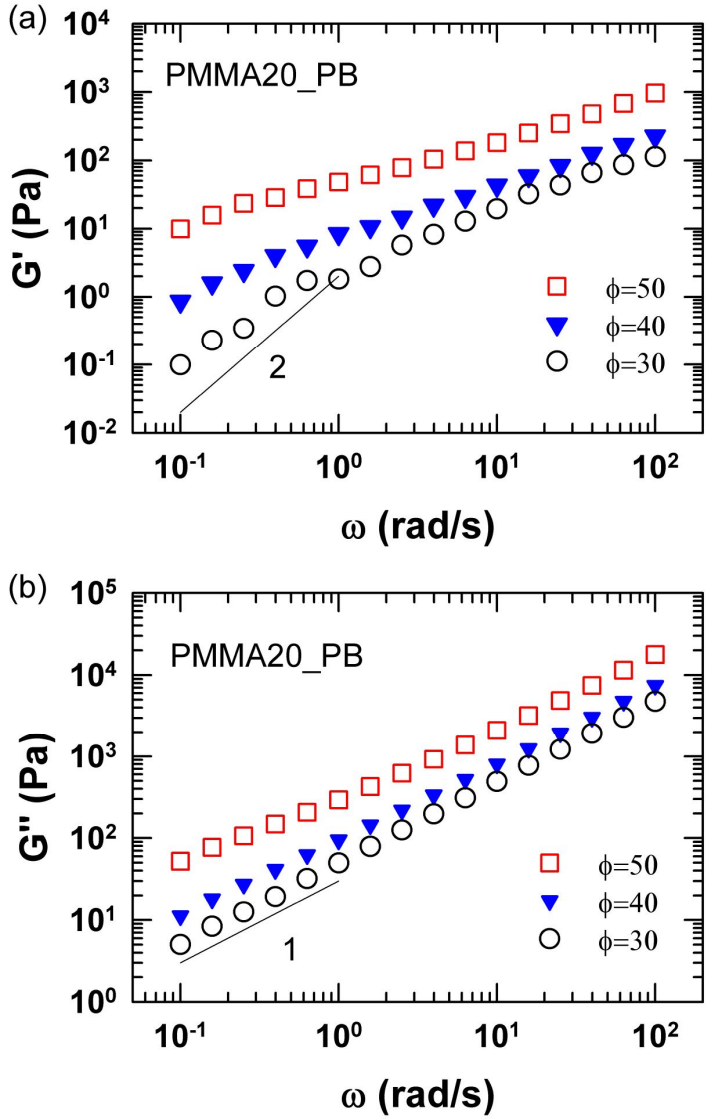

Fig. 3-9 Complex moduli of PMMA20_PB as a function of frequency at strain amplitude 0.004 and room temperature.

3.6 Preliminary test

3.6.1 Oscillatory squeeze test

To validate the performance of the equipment, a coil spring and polybutene (PB) were used as elastic and viscous materials, respectively. The spring constant of coil spring was calculated from the normal force which was proportional to strain amplitude (spring constant: 88.6 N/m). The coil spring can be considered as purely elastic material and PB as a viscous fluid. The phase angle of normal stress under dynamic squeeze deformation was measured. Fig. 3-10(a) shows the phase angle of normal stress as a function of strain amplitude for both coil spring and PB. The phase angle of coil spring was nearly zero degree regardless of strain amplitude within the measurable range. This result shows that the instrument responds to the elastic object very well. However the phase angle of PB was less than 90°, which seems to be caused by inertia or weak elastic nature of PB. Complex viscosity was also measured under oscillatory squeeze flow. Fig. 3-10(b) shows the complex viscosity (η^*) calculated from the normal stress signals as a function of strain amplitude at frequency 1rad/s. The complex viscosity of PB was about 20 Pa·s. The complex viscosity obtained from the equipment coincides well with the one measured from a conventional rheometer (RMS800, TA instruments) under simple shear flow. As there is a good agreement between the complex

viscosities measured from both oscillatory shear flow and oscillatory squeeze flow [Debbaut and Thomas, 2004; Bell *et al.*, 2006], it can be confirmed that the equipment measures the viscoelastic properties reasonably well though not very precise quantitatively. This slight difference will be corrected after adjusting the inertia and stiffness of the moving fixture.

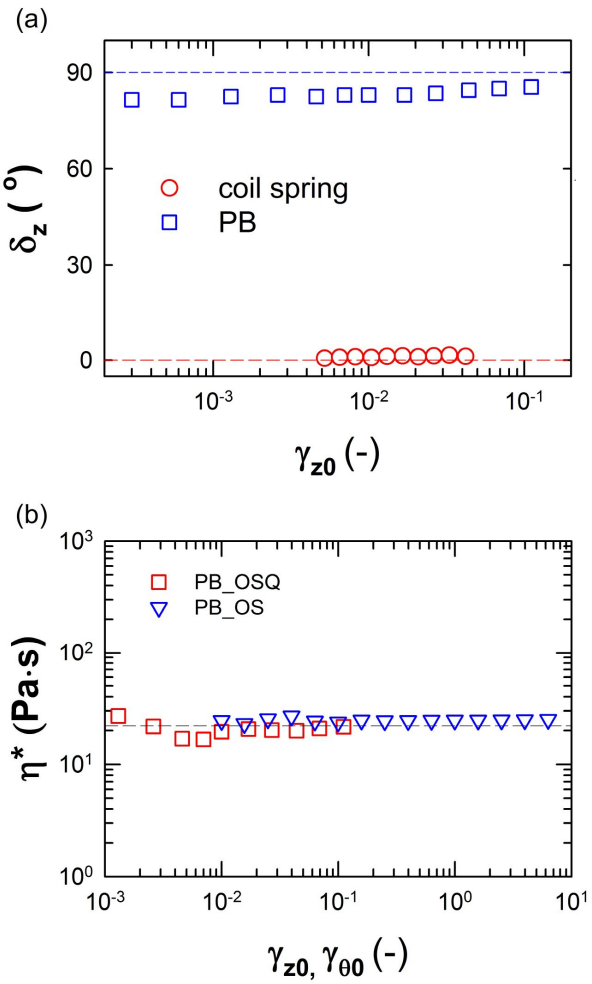

Fig. 3-10 (a) Phase angle (δ_z) of coil spring and PB as a function of strain amplitude, γ_{z0}. (b) Complex viscosity (η^*) of PB as a function of strain amplitudes, γ_{z0} in oscillatory squeeze mode and $\gamma_{\theta 0}$ in oscillatory shear mode at frequency 1rad/s. All measurements were made at room temperature.

3.6.2 Dynamic helical squeeze test

Fig. 3-11 shows the complex viscosity of PB solution as a function of strain amplitude under DHSQ. The complex viscosities, η_z^* and η_θ^*, from normal (σ_{zz}) and shear stress ($\sigma_{z\theta}$) of DHSQ, were calculated respectively: $\eta_z^* = 2H_0^2\sigma_{zz}/3R^2\omega\gamma_{z0}$, $\eta_\theta^* = \sigma_{z\theta}/\omega\gamma_{\theta 0}$ [Macosko, 1994; Debbaut and Thomas, 2004]. All of the complex viscosities of PB solution shows nearly 20 Pa·s at room temperature. The complex viscosities obtained from the equipment agree with the values determined in shear flow with standard rheometry (RMS800, TA instruments). From the preliminary test, it was confirmed that the equipment measures the viscoelastic property reasonably well though not very precise quantitatively.

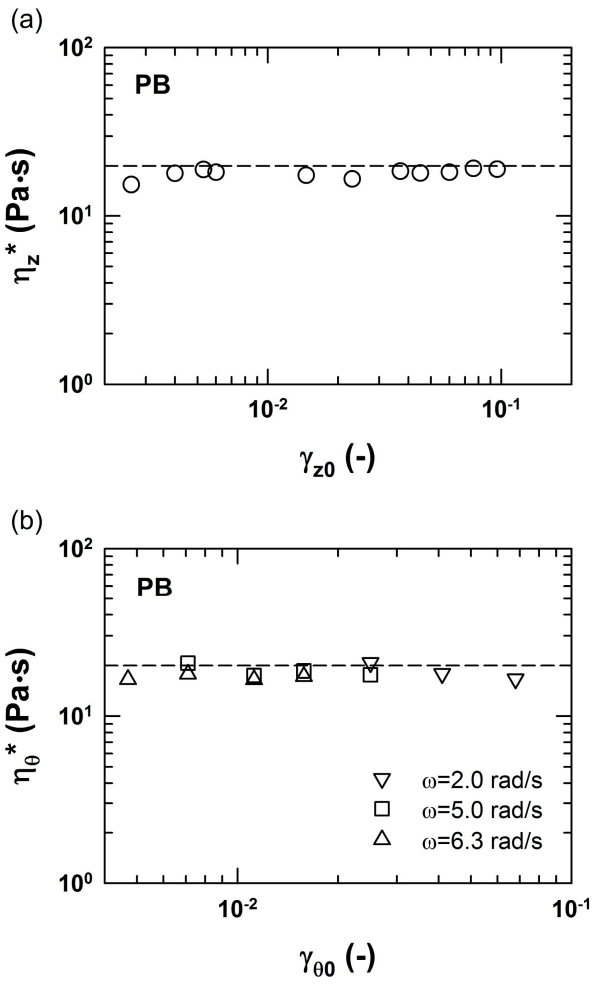

Fig. 3-11 The complex viscosities of PB under DHSQ; (a) complex viscosity ($\eta_z^* = 2H_0^2\sigma_{zz}/3R^2\omega\gamma_{z0}$) of normal stress component as a function of strain amplitude, γ_{z0} at frequency 1 rad/s; (b) complex viscosity ($\eta_\theta^* = \sigma_{z\theta}/\omega\gamma_{\theta 0}$) for shear stress component as a function of strain amplitude, $\gamma_{\theta 0}$ at frequencies 2, 5 and 6.28 rad/s, at room temperature.

3.7 Analysis of nonlinear stress

For large amplitude dynamic test, the stress output is not purely sinusoidal and the behavior can no longer be fully described in terms of a storage modulus and loss modulus due to the presence of higher harmonics. The viscoelastic nonlinearity can be analyzed into two ways: stress shape analysis, Fourier transform (FT) and nonlinear regression.

3.7.1 Stress shape analysis

Stress curve

The stress curve provides insightful and visual information during structural changes of the material when the deformation becomes large. The stress curve is sinusoidal in linear region, while it becomes distorted in nonlinear region. The nonlinear stress waveform displays different shapes depending on polymer solutions or polymer melts. The linear PP melt shows a "forward tilted stress" shape, while the branched PP melt displays a "backward tilted stress" shape [Hyun *et al.*, 2003]. This forward tilted shape was observed in polymer melt and solution with a linear chain structure, but the backward tilted shape was observed in suspension and polymer melts with branched chain. The stress shape analysis can also be used to understand the difference among polymer solutions [Hyun *et al.*, 2003]. There are

distinctively different shapes: “saw tooth shape” of Xanthan gum (XG) with highly extended and disordered backbone, “rectangular shape” of poly(ethylene oxide)-poly(propylene oxide)-poly(ethylene oxide) (PEO-PPO-PEO) of hard gel with a close-packed array of micelles. These materials reveal the same generic behavior in terms of the linear viscoelastic moduli, while the nonlinear stress waveform take completely different shapes. From these examples, it is clear that the stress shape analysis provides more insightful information than simple linear viscoelasticity.

Lissajous plot

The Lissajous plot, examples of stress-strain variation, is useful in describing the alteration of nonlinear responses and is plotted as stress vs. strain or stress vs. strain rate. It changes over different phase shifts. The loop is in phase for elastic materials leading to a straight line on [stress vs. strain] plot, in case of linear elastic materials. On the other hand, the loop is out of phase ($\pi/2$) for viscous materials. This behavior is represented as a circle in the plot, if the fluid is viscous or Newtonian. For a viscoelastic material, with a phase lag $0 < \delta < \pi/2$, the stress strain curve is elliptical. Lissajous plot of the shear stress of viscoelastic fluids is ellipse at the linear region, while the loop becomes distorted at the nonlinear region. In the case of normal stress

difference, the loop showed one-fold symmetry to the strain or strain rate due to even harmonics [Nam *et al.*, 2010]. Under oscillatory squeeze flow, the loop of [stress vs. strain] or [stress vs. strain rate] represented nonsymmetry with respect to zero mean value of x-axis [Phan-Thien, 2000; Phan-Thien *et al.*, 2000].

3.7.2 Fourier transform (FT)

Fourier transform (FT) analysis can effectively explain the nonlinear behavior by separation of the contributions from higher order harmonics. FT has widely been used to quantify the nonlinearity with high sensitivity. By Euler's formula, the Fourier transform of a time domain results in the frequency domain as follows;

$$S(\omega) = \int_{-\infty}^{\infty} s(t) e^{-i\omega t} dt \qquad (3\text{-}15)$$

FT filters the inherent periodic contributions from a time dependent signal and displays the amplitude and phase as a function of frequency [Wilhelm, 2002]. In oscillatory shear test, the shear stress shows only odd higher harmonic contribution which means the degree of distortion from sinusoidal curve [Hyun *et al.*, 2011]. On the other hand, the normal stress difference shows even harmonics growing with an even power of the strain amplitude at small and intermediate strain amplitude [Nam *et al.*, 2008; 2010].

In the case of oscillatory squeeze flow, the normal stress represents all higher harmonics. Appearance of both odd and even harmonics is one of the distinct features of nonsymmetric stress response. The higher order harmonic intensity relative to the fundamental intensity, I_n/I_1, is plotted as a function of strain amplitude ($I_n \propto \gamma_{z0}^n$, n=1,2,3$\cdots$) [Debbaut and Thomas, 2004].

3.7.3 Polynomial regression

The polynomial regression is among regression analysis in which experimental data are fitted by a function, using a linear combination of the model parameters. The basic idea of linear regression is to relate a response to a predictor variable. For instance, the nonlinear data F can be fitted by a trigonometric polynomial as follows;

$$F = A_0 + \sum_{n=odd}\left(A_n^1 \sin n\omega t + A_n^2 \cos n\omega t\right) + \sum_{n=even}\left(B_n^1 \sin n\omega t + B_n^2 \cos n\omega t\right) \tag{3-16}$$

where A_0 is an intercept, $A_n = \sqrt{\left(A_n^1\right)^2 + \left(A_n^2\right)^2}$ and $B_n = \sqrt{\left(B_n^1\right)^2 + \left(B_n^2\right)^2}$. The trigonometric polynomial is a linear combination of functions $\sin(nx)$ and $\cos(nx)$ with finite n numbers. The degree of nonlinearity for given data can be estimated by the coefficients, A_n and B_n.

Chapter 4. Nonlinear behavior of polymer solutions under oscillatory squeeze flow

4.1 Nonlinear response

In this study, the rheological measurements were carried out on a controlled strain type rheometer (RMS800, TA Instruments) with the modified fixture. Fig. 4-1(a) shows an example of raw data; normal force of PEO4m2.5 in the strain range γ_{z0}=0.027~0.28 at a frequency of ω=1 rad/s. The amplitude increased with strain amplitude, and the stress reached steady value very quickly upon the increase of strain amplitude. In Fig. 4-1(b), the strain and the normal stress are plotted altogether. The normal stress curve shows different shape in both positive and negative region, which represents different material response when the sample is compressed and extended. The nonsymmetric stress response was also reported in the first normal stress difference under large amplitude oscillatory shear flow [Nam *et al*., 2010]. The nonsymmetric stress signal in LAOS looks similar in terms of shape, but differs in higher harmonics in Fourier transform rheology. The normal stress oscillates with both even and odd harmonics in OSQ, while the first normal stress difference oscillates with even harmonics only in LAOS. The details will be discussed later.

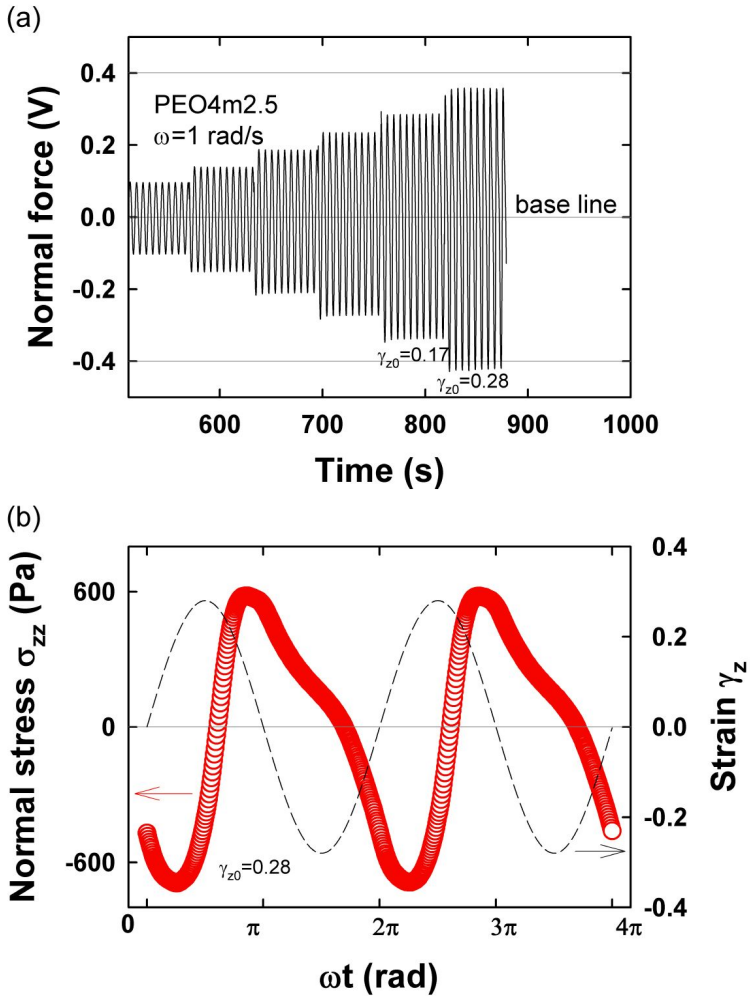

Fig. 4-1 (a) Normal force signal of PEO4m2.5 during the strain sweep from γ_{z0}=0.027 to 0.28 at a fixed frequency of 1 rad/s. (b) Strain γ_z and normal stress σ_{zz} at the strain amplitude of 0.28.

4.2 Strain sweep test

Previous researches focused on OSQ at small strain amplitude only, and the nonlinear regime has rarely been investigated. For this reason, it is needed to explore the nonlinear regime under OSQ at larger deformation. Fig. 4-2 shows the storage and loss modulus as a function of strain amplitude under OSQ and OS. At small strain amplitude, the storage and loss modulus are constant regardless of strain amplitude under both OS and OSQ though there exists a slight variation in OSQ due to low intensity stress signals. In the nonlinear regime at large deformation, however, the storage and loss modulus decrease with strain amplitude. The storage and loss modulus under OS and OSQ shows strain thinning behavior which is commonly observed in polymer solutions and melts. The origin of strain thinning will be similar to that leading to shear thinning in steady shear flow. Even though both OSQ and OS show strain thinning behavior after the linear regime, they have different critical strain amplitude at which the modulus starts to decrease. Note that the strain amplitudes, γ_{z0} and $\gamma_{\theta 0}$, are not equivalent to each other. The oscillatory squeeze flow shows the onset of nonlinear regime at lower strain amplitude than oscillatory shear flow. The nonlinear behavior under LAOS has been studied for decades. There are various analysis tools to interpret the

nonlinear behavior such as the stress shape analysis, Lissajous plot, Fourier transformation (FT), and so on. In this study, it was employed the analysis methods developed primarily to understand the nonlinear behavior of LAOS to investigate the nonlinear characteristics under LAOSQ.

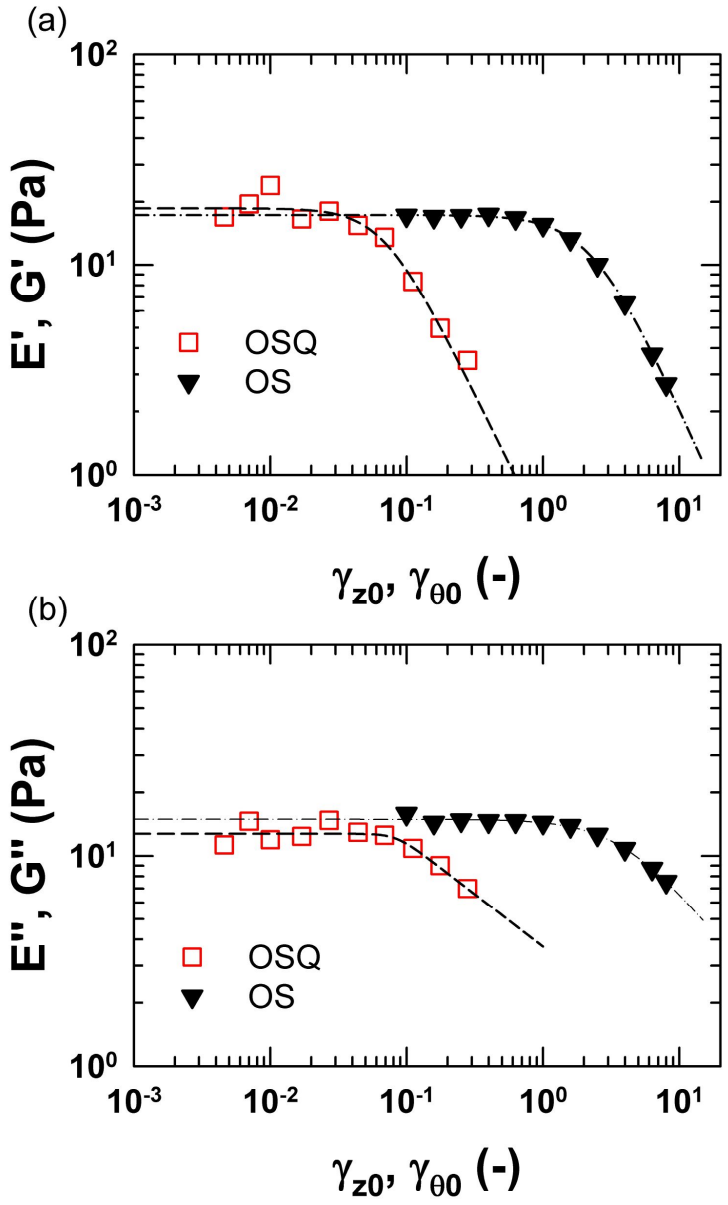

Fig. 4-2 The storage modulus (E', G') and loss modulus (E'', G'') as a function of strain amplitude under OSQ and OS at frequency 1 rad/s. The dotted lines are the fitted results with the Carreau viscosity model.

4.3 Nonsymmetric normal stress

In order to quantify the nonlinear response of a viscoelastic fluid when subjected to dynamic squeeze flow, the stress curve was analyzed with the help of Lissajous plot. The stress curve provides insightful and visual information during structural changes of the material when the deformation becomes large. The stress curve is sinusoidal in linear region, while it becomes distorted in nonlinear region. The Lissajous plot is useful in describing the alteration of nonlinear responses and is plotted as stress vs. strain or stress vs. strain rate.

Fig. 4-3 shows typical wave curves of normal stress at frequency 1rad/s, at different strain amplitudes from linear to nonlinear region. At low strain amplitude, the normal stress is sinusoidal and symmetric in both positive and negative region. However as the strain amplitude increases, this sinusoidal and symmetric response cannot be maintained any more. The normal stress becomes distorted and nonsymmetric; both magnitude and shape are different in positive and negative region. This nonsymmetry is a unique feature of normal stress. The shear stress in simple shear flow is symmetric with respect to the direction of deformation even at very large strain amplitude [Hyun *et al*., 2003; Nam *et al*., 2008]. In terms of stress

shape, the normal stress exhibits forward-tilted shape that is related with strain-thinning behavior of the material. The forward-tilted stress shape was also observed in linear polymer solutions and melts under large amplitude oscillatory shear flow [Hyun *et al.*, 2003; 2006]. The difference of normal stress at maximum and minimum increases with strain amplitude, which may be considered as the result of the microstructural change as the viscoelastic fluid is compressed and extended.

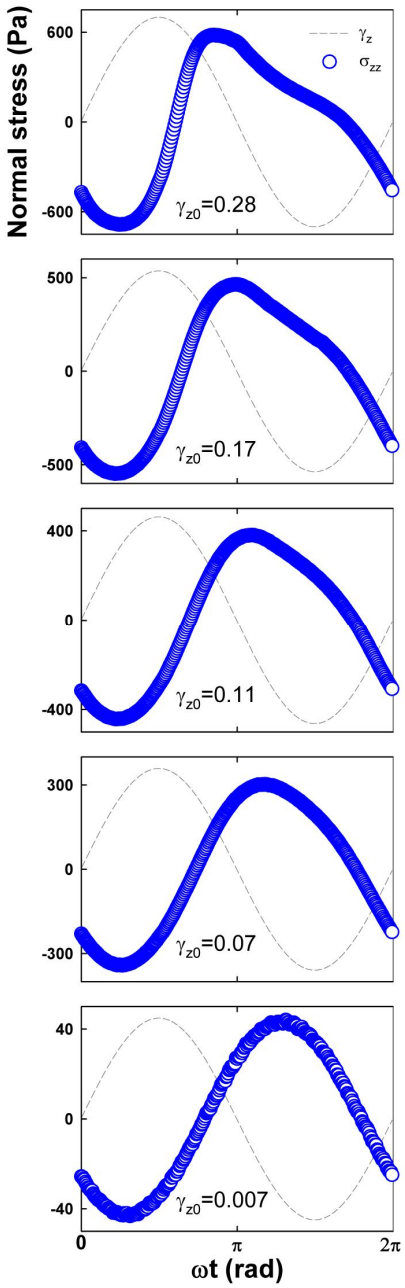

Fig. 4-3 The strain (dashed line) and the stress (solid line) signals of PEO4m2.5 at frequency ω =1rad/s.

The trigonometric polynomial was employed to decompose the normal force into odd and even contribution. This polynomial can be considered a periodic function with period some multiple of 2π. The torque of OS only shows odd contributions, but the normal force of OSQ includes not only odd but also even contribution. This result was observed in Fourier transform which can separate nonlinear behavior to the higher order harmonics. Fig. 4-4(a) display the normal force at strain amplitude 0.28 and its regression curve. The regression curve was plotted by the eq. (3-16) up to n=5. Note, higher order coefficients $n \geq 3$ can be neglected because the magnitude was very small compared to $n \leq 2$. Polynomial coefficients (A_1, B_2) as a function of strain amplitude were plotted with linear-linear scale in Fig. 4-4(b). Coefficient A_1 represents odd function and B_2 displays even function. The coefficient A_1 was higher than B_2, and also agreed with the normal force except large strain amplitude. But, the coefficient B_2 shows an exponential increase as the strain amplitude increases. From this analysis, it was confirmed that the normal force of OSQ becomes more nonsymmetric by the even contributions, not the odd contributions, with increasing strain amplitude.

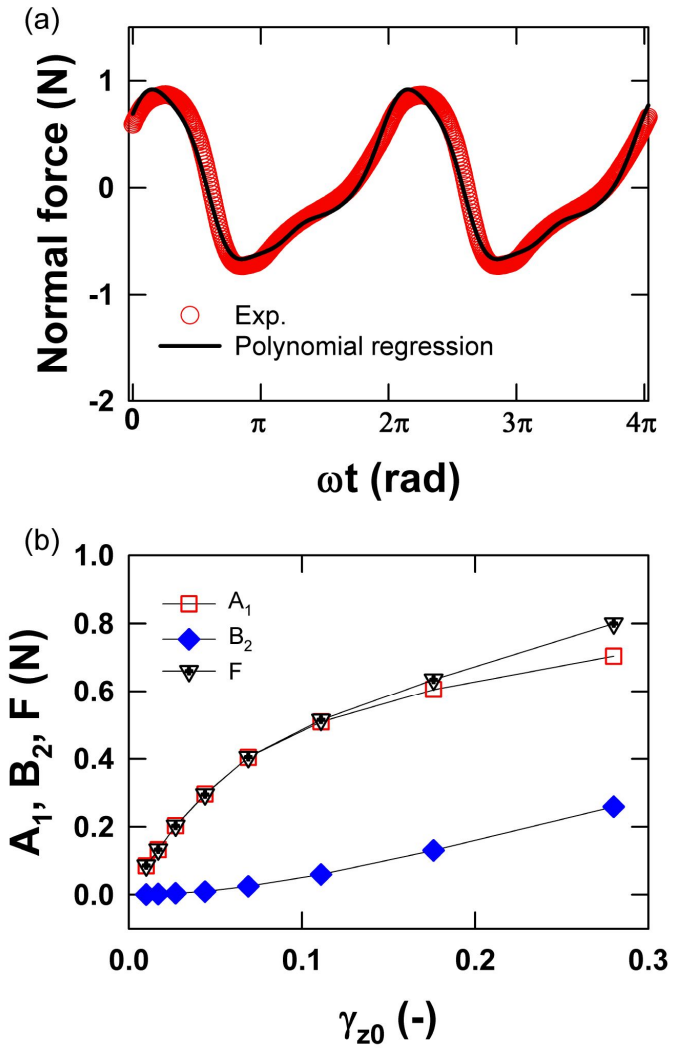

Fig. 4-4 (a) The normal force and its regression curve and (b) polynomial coefficients (A_1 , B_2) as a function of strain amplitude. The coefficients were obtained from the normal force signal using polynomial regression.

The response of normal stress under dynamic squeeze flow typically shows nonsymmetric curve at large strain amplitude as shown in Fig. 4-3. This nonsymmetric stress signal shows distinct features compared with shear stress of simple shear flow via not only the stress shape analysis, but also the difference of compressive and extensional stresses. In this section, it was concentrated on the peak region of compression and extension of normal stress. Generally, the shear stress of dynamic shear flow exactly shows symmetric amplitude on the basis of zero mean value, while the normal stress of dynamic squeeze flow exhibits nonsymmetric amplitude. Fig. 4-5(a) shows the difference (σ_{zz}^{c} - σ_{zz}^{e}) of compression (σ_{zz}^{c}) and extension (σ_{zz}^{e}) peak of normal stress of PEO solutions as a function of strain amplitude. The difference (σ_{zz}^{c} - σ_{zz}^{e}) increases exponentially as the strain amplitude increases without a plateau in log-linear plot within the investigated region. Over the critical strain amplitude as can be seen in Fig. 4-5(a), the normal stress is larger in the compressive region than in extensional region, and then the difference increases up to large strain amplitude more and more. Fig. 4-5(b) shows the difference as a function of dimensionless relaxation time of PEO aqueous solutions at various strain amplitude and fixed frequency. It is clear that the slope of difference is 1 for various strain amplitudes according to

dimensionless relaxation time. This result means the difference of compressive and extensional stresses increases linearly as relaxation time over entangled concentration for PEO aqueous solutions. From these examinations, it was confirmed that the difference of compressive and extensional stresses can be related to the nonsymmetric response of the materials under two different deformations of compression and extension. Fig. 4-6 shows the average normal stress and the scaling relationship of the difference ($\sigma_{zz}^{c} - \sigma_{zz}^{e}$) of compressive (σ_{zz}^{c}) and extensional (σ_{zz}^{e}) normal stresses as a function of strain amplitude for PEO4m2.5. In the scaling, the slope of the difference was 2 at lower strain amplitude, but was less than 2 at higher strain amplitude.

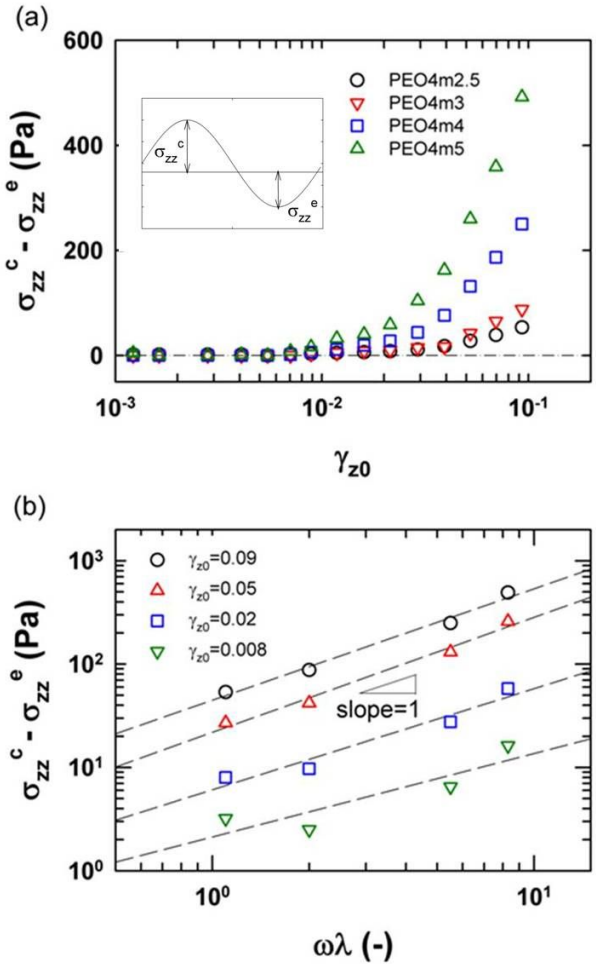

Fig. 4-5 (a) The difference (σ_{zz}^{c} - σ_{zz}^{e}) of compressive (σ_{zz}^{c}) and extensional (σ_{zz}^{e}) normal stresses of PEO solutions as a concentration 2.5, 3, 4, 5 wt% and a function of strain amplitude, (b) The difference as a function of dimensionless relaxation time ($\omega\lambda$) at various strain amplitudes. The inset in the figure defines both compressive and extensional stresses.

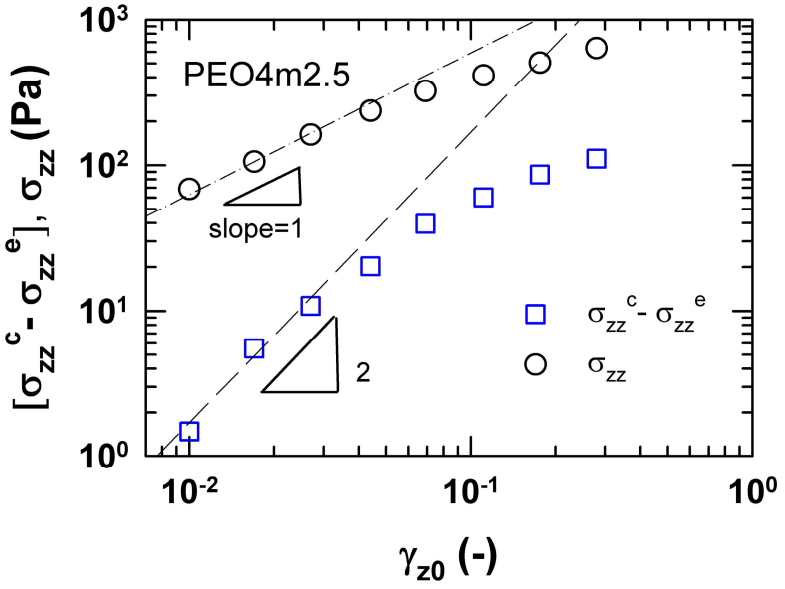

Fig. 4-6 Scaling relationship of the normal stress and the difference (σ_{zz}^{c} - σ_{zz}^{e}) of compressive (σ_{zz}^{c}) and extensional (σ_{zz}^{e}) stresses as a function of strain amplitude of PEO4m2.5.

4.4 Lissajous plot

The Lissajous plots - normal stress vs. strain and normal stress vs. strain rate - are shown in Fig. 4-7. At strain 0.007, the [$\sigma_{zz}(t)$ vs. $\gamma_z(t)$] plot shows an ellipsoidal loop meaning the linear viscoelastic regime. On the other hand, at the same strain amplitude, the plot [$\sigma_{zz}(t)$ vs. $\dot{\gamma}_z(t)$] looks more rounded, which is commonly observed with viscous fluids. As the strain amplitude increases, the normal stress becomes more and more non-sinusoidal and nonsymmetric. The Lissajous plots also become more distorted as the strain amplitude increases. Above strain amplitude 0.07, both Lissajous plots clearly show nonsymmetric pattern with respect to zero mean value. This has never been reported under large amplitude oscillatory shear (LAOS) which has symmetric curvilinear loop for both elastic and viscous stresses [Ewoldt *et al.*, 2008; Cho *et al.*, 2010; Renou *et al.*, 2010].

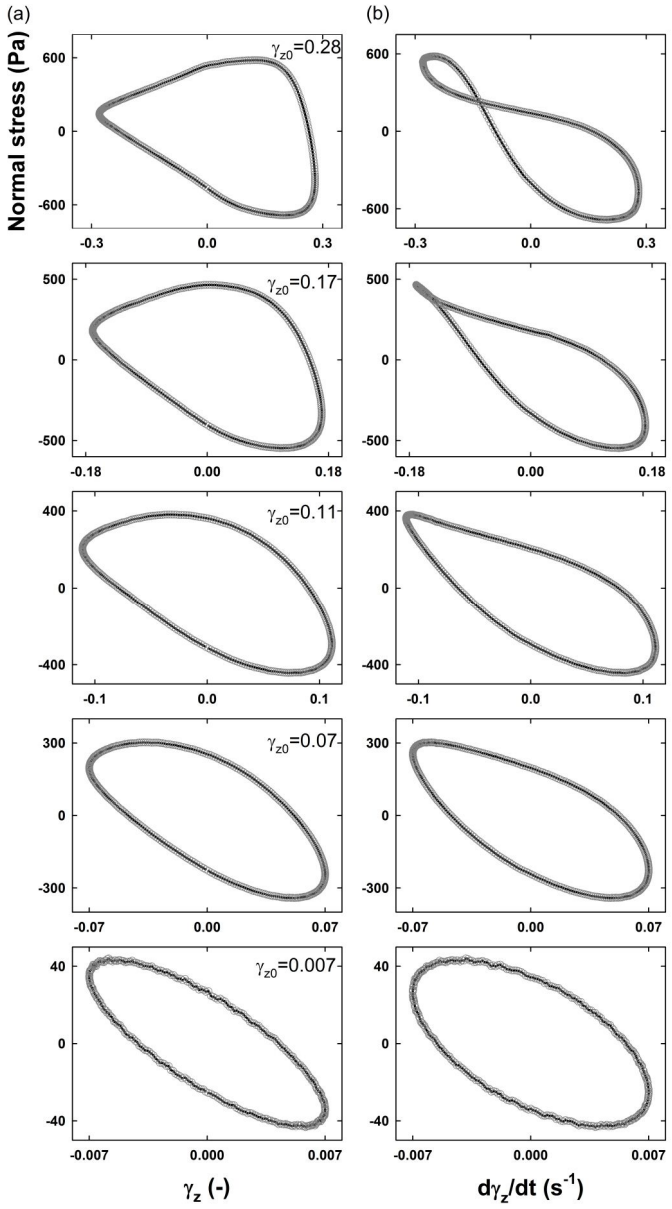

Fig. 4-7 (a) Closed loops are normal stress vs. strain, [$\sigma_{zz}(t)$ vs. $\gamma_z(t)$]. (b) Closed loops are normal stress vs. strain rate, [$\sigma_{zz}(t)$ vs. $\dot{\gamma}_z(t)$] for PEO4m2.5 at frequency 1rad/s.

4.5 Trace of pathway

To further understand the nonsymmetric nature of the normal stresses, the pathway of the Lissajous plot, $\sigma_{zz}(t)$ vs. $\gamma_z(t)$ and $\sigma_{zz}(t)$ vs. $\dot{\gamma}_z(t)$, was traced during compression and extension at strain amplitude 0.28. The extensional part of stress curve follows pathway 1 and 2, the compressive part follows pathway 3 and 4, respectively (Fig. 4-8). In the plot of $\sigma_{zz}(t)$ vs. $\gamma_z(t)$, the trace follows quite different path with respect to zero mean value. This implies that the nonsymmetric Lissajous plot is caused by different response of the fluid depending on whether the sample is compressed or extended. The Lissajous plot of $\sigma_{zz}(t)$ vs. $\dot{\gamma}_z(t)$ shows a secondary loop when the sample is extended, but not during compression. This secondary loop was also reported in both experiment and model simulation under large amplitude oscillatory shear [Ewoldt *et al*., 2008]. However, little is known about its origin, and more research will be necessary to understand the physical meaning of the secondary loop.

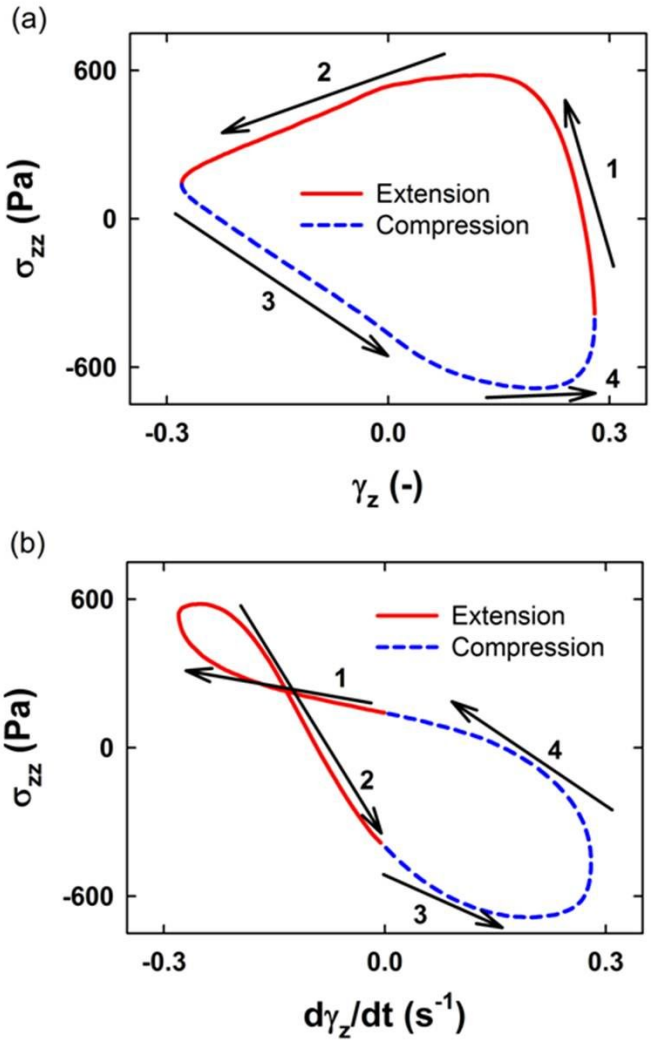

Fig. 4-8 (a) Lissajous plot of normal stress vs. strain and (b) Lissajous plot of normal stress vs. strain rate of PEO4m2.5 at frequency 1rad/s and strain amplitude 0.28. The extensional part of stress signal follows pathways 1 and 2, the compressive part of stress signal follows pathway 3 and 4.

The Lissajous plot of normal stress vs. strain rate exhibits a one-fold loop which is a distinctive feature of OSQ under large deformation. In order to further investigate the origin of one-fold loop, it was plotted the Lissajous loop of a Newtonian fluid; the normal force vs. dH/dt as calculated with a constant viscosity using Eq. (2-10). At small strain amplitude 0.001, the Lissajous loop of viscous fluid shows a straight line, which represents the linear regime as shown in Fig. 4-9(a). On the other hand, at large strain amplitude 0.28, the Lissajous loop becomes nonlinear and one-fold symmetric as shown in Fig. 4-9(b). The one-fold symmetric loop of viscous fluid implies the same response during compression and extension. However viscoelastic fluid shows nonsymmetric one-fold loop which indicates different energy storage when the sample is compressed or extended.

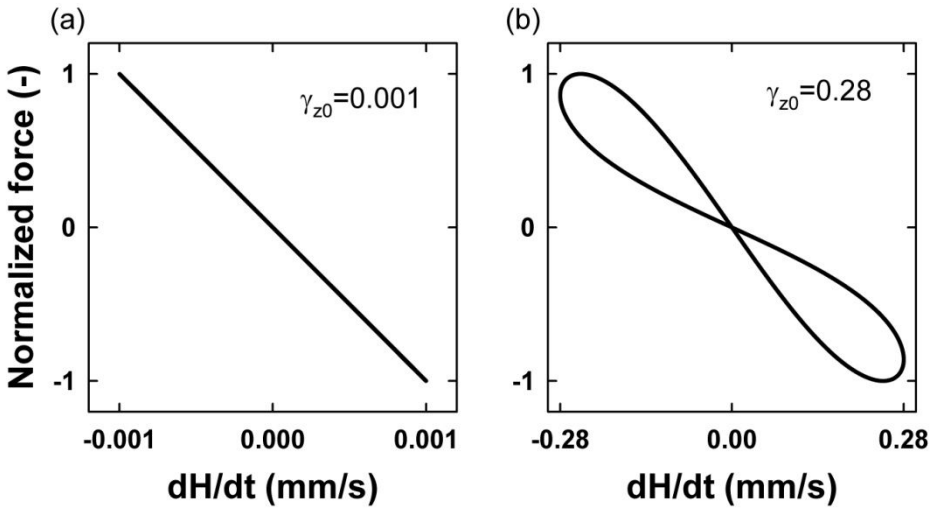

Fig. 4-9 Lissajous plot of normalized normal force vs. dH/dt for a Newtonian fluid at frequency 1 rad/s: (a) strain amplitude=0.001, (b) strain amplitude=0.28.

4.6 Lissajous plot with squared strain

Fig. 4-10 shows the normal stress and squared strain as a function of time, and the Lissajous curves plotted as normal stress vs. squared strain. The squared strain shows doubled-frequency dependence of the applied frequency. If the strain oscillates at a frequency ω, the squared strain oscillates at a doubled frequency 2ω. Fig. 4-10(a) shows stress responses, extensional (σ_{zz}^{e}) and compressive (σ_{zz}^{c}) stresses, together with the squared strain as a function of time. At small strain amplitude, the normal stress curve is sinusoidal. As the strain amplitude increases, the sinusoidal stress curve becomes distorted, especially in positive region where the extensional deformation takes place. When the Lissajous pattern is plotted as normal stress vs. squared strain, the loop becomes one-fold symmetric. The Lissajous pattern changes dramatically from one-fold symmetry to two-fold nonsymmetry as the strain amplitude increases. At strain amplitude 0.007, the Lissajous curve shows one-fold symmetry which belongs to linear viscoelasticity. The symmetric loop with respect to the mean value indicates the same magnitude in both compressive (σ_{zz}^{c}) and extensional (σ_{zz}^{e}) stress at maximum and minimum of sinusoidal wave. As the strain amplitude increases, the symmetric loop becomes distorted, and the loop displays more pronounced nonsymmetry. This nonsymmetric loop is formed because of

different pathway during extension and compression with increasing strain amplitude as shown in Fig. 4-10(b). From this stress shape analysis with squared strain, it can be known that the nonlinear-and-nonsymmetric normal stress can be effectively probed even by visual inspection; decomposed normal stress curves (σ_{zz}^{c} and σ_{zz}^{e}) and Lissajous pattern.

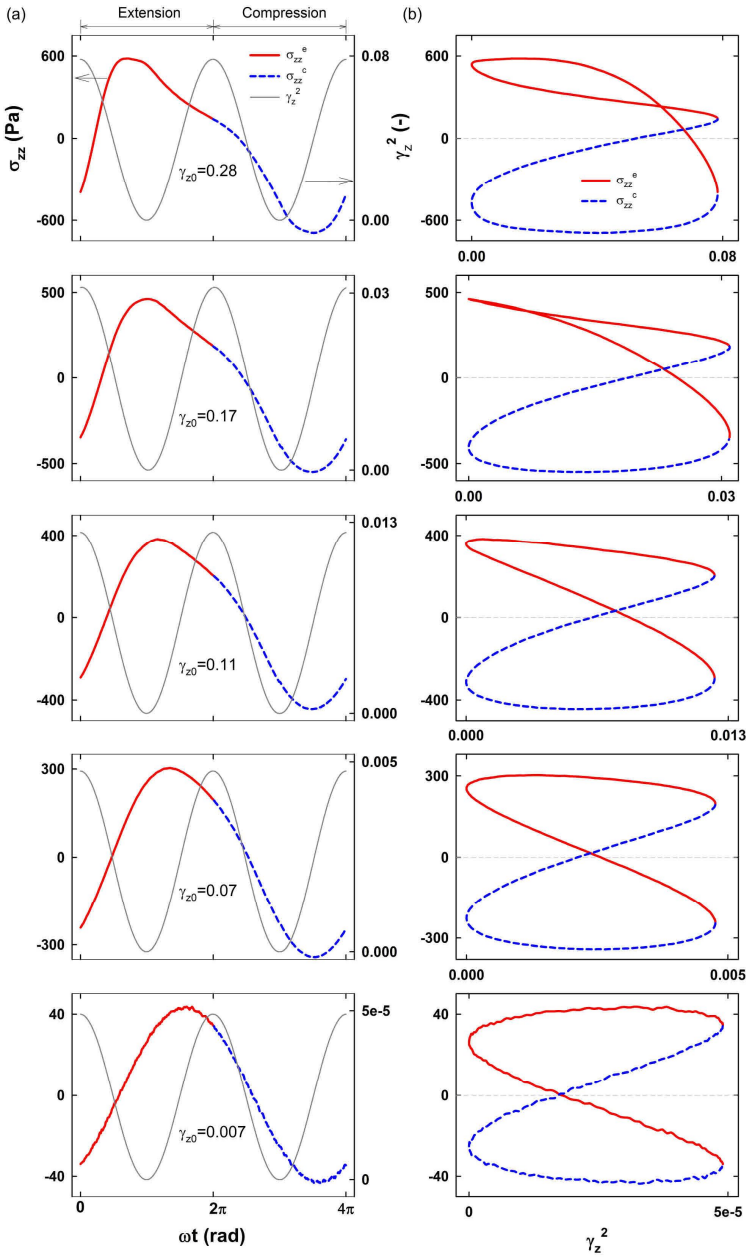

Fig. 4-10 (a) The normal stress and squared strain as a function of time; solid line represents extensional part, dashed line compressive part; PEO4m2.5 at

frequency 1rad/s. (b) The Lissajous plot of the normal stress vs. squared strain, [$\sigma_{zz}(t)$ vs $\gamma_z^2(t)$]; solid line represents extensional part and dashed line indicates the compressive part of the normal stress.

4.7 Fourier transform (FT)

The nonlinear behavior can be effectively described by Fourier transform (FT) analysis that separates the contribution from higher order harmonics. FT is widely used to quantify the nonlinearity with high sensitivity. FT filters the inherent periodic contributions from a time dependent signal and displays the amplitude and phase as a function of frequency [Wilhelm, 2002]. The FT intensities of PEO4m2.5 are plotted in terms of the harmonics in Fig. 4-11(a). The Fourier intensity increases and higher order harmonics start to appear with increasing strain amplitude. Here, the normal stress shows both odd and even harmonics, while the shear stress exhibits only odd harmonics. Appearance of both odd and even harmonics is one of the distinct features of nonsymmetric stress response. The intensity of all higher harmonics increases without plateau in the measurable region. The higher order harmonic intensity relative to the fundamental intensity, I_n/I_1, is plotted as a function of strain amplitude in Fig. 4-11(b). In the linear regime, below γ_{z0}=0.01, the higher

order harmonics are rarely observed. In the nonlinear regime, over γ_{z0}=0.01, the higher harmonic contribution, I_n/I_1, becomes more pronounced because of the strong nonlinearity of the normal stress. In particular, the second harmonic undergoes a rapid growth, while all the other harmonics show rather slow development. In Fig. 4-12, the reduced intensity I_n/I_1 is plotted as a function of strain amplitude, and there exists a scaling relationship at medium strain amplitude.

$$\log(I_n/I_1) = a + b\log\gamma_{z0} \tag{4-1}$$

Eq. (4-1) predicts the scaling behavior between I_n/I_1 and the strain amplitude with an intercept *a* and slope *b*. In this figure, the slope b is almost constant regardless of excitation frequencies. The I_2/I_1 is proportional to the strain amplitude, and the others I_n/I_1 are almost proportional to the (n-1)th power of strain amplitude at medium strain amplitude. This coincides with the result of LAOS, but the slope seems to be a little bit less than (n-1). To understand the origin of even harmonics, it was intentionally generated symmetric and nonsymmetric curves, according to Eq. (4-2) and (4-3), respectively.

$$\sigma(t) \propto \sin(\omega t) + 0.05\sin(3\omega t + \phi_3) \tag{4-2}$$

$$\sigma(t) \propto \sin(\omega t) + 0.1\sin(2\omega t + \phi_2) + 0.05\sin(3\omega t + \phi_3) \tag{4-3}$$

Let us assume that the second and third harmonics are 10% and 5% of the first

harmonic, and the harmonics higher than three are negligible. Also the phase angles, ϕ_2 and ϕ_3, were fixed at 270°. As shown in Fig. 4-13, the nonsymmetric curve results in both even and odd harmonics, while the symmetric curve shows odd harmonics only. By this simple calculation, it is clear that the appearance of even harmonics originates from the nonsymmetric stress signals.

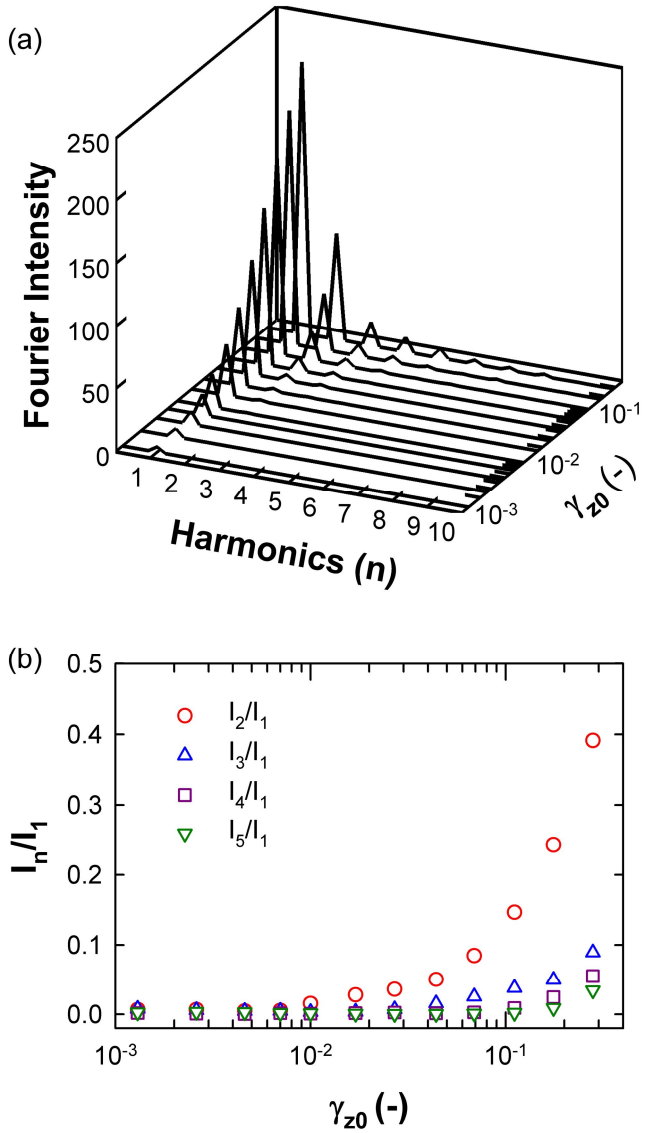

Fig. 4-11 (a) The Fourier intensity as a function of strain amplitude and spectrum harmonics (n) at frequency 1rad/s, and (b) relative intensity (I_n/I_1) as a function of strain amplitude for PEO4m2.5.

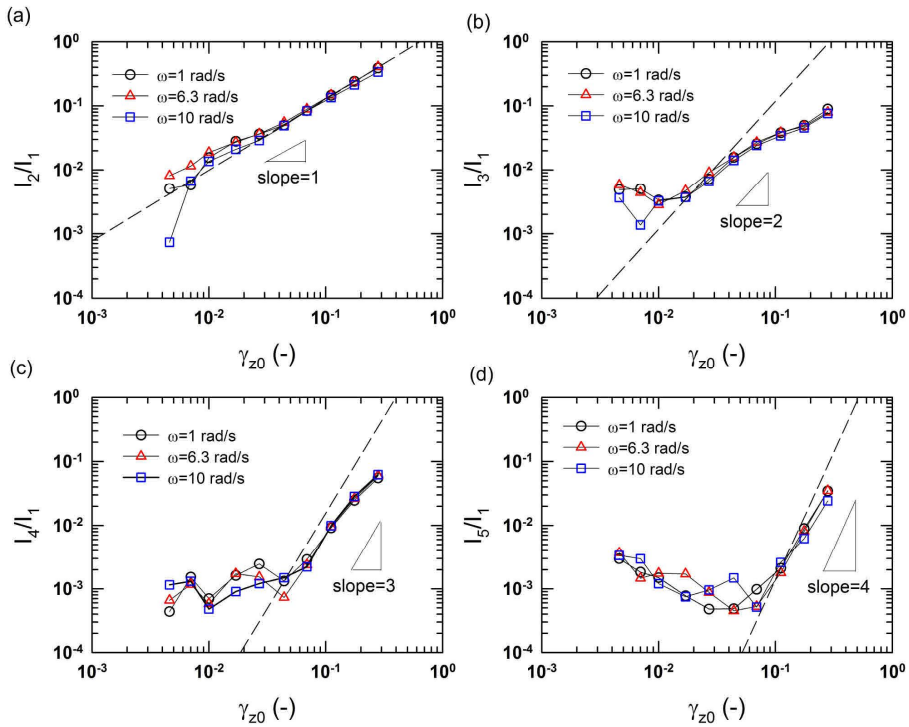

Fig. 4-12 Relative intensity I_2/I_1 (a), I_3/I_1 (b), I_4/I_1 (c), and I_5/I_1 (d) as a function of strain amplitude for PEO4m2.5 at various frequencies.

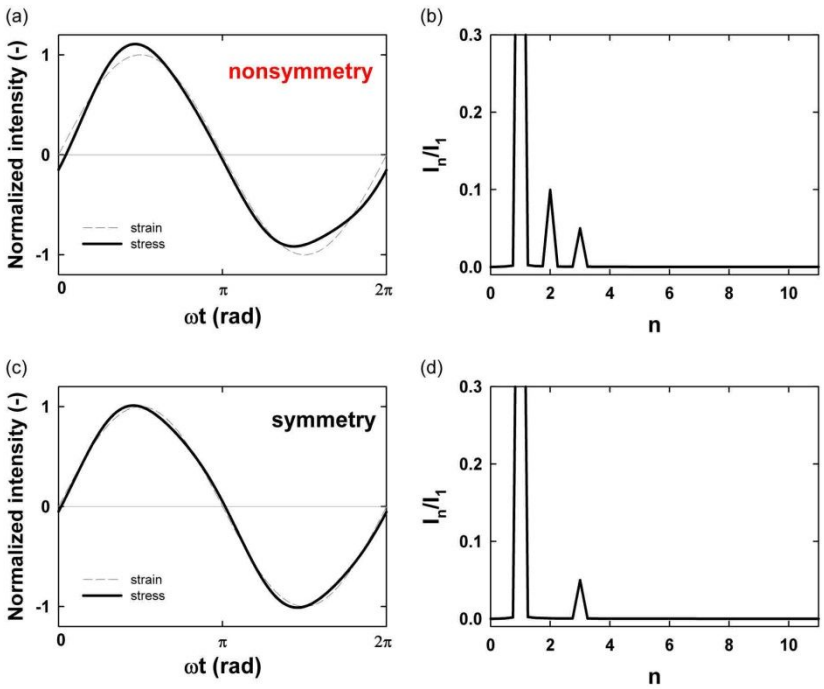

Fig. 4-13 (a) Nonsymmetric curve generated by $[\sigma(t) \propto \sin(\omega t)+0.1\sin(2\omega t+ \phi_2)+0.05\sin(3\omega t+ \phi_3)]$ at phase angle $\phi_2 = \phi_3 = 270°$; (b) relative intensity as a function of harmonics for nonsymmetric curve generated in (a). (c) Symmetric curve $[\sigma(t) \propto \sin(\omega t)+0.05\sin(3\omega t+ \phi_3)]$ at phase angle $\phi_3 = 270°$; (d) relative intensity as a function of harmonics for symmetric curve generated in (c). Frequency was fixed at 1 rad/s.

4.8 Strain hardening behavior

The strain hardening behavior of cross-linked polymer was investigated under OSQ and OS. The OS test has been performed to compare with the OSQ test. Frequency sweep test takes linear viscoelastic measurements at selectable frequencies while holding a constant strain and temperature. Ideally, the selected strain should be within the linear viscoelastic region of the sample. Fig. 4-14 shows storage (G') and loss (G'') moduli as a function of frequency of P15, P15_B0.08, and P15_B0.16. P15 (without Borax) sample showed $G'' > G'$ at overall frequency region and no occurrence of crossover frequency ($G' = G''$). The crossover frequency can be used to estimate viscoelastic property of the material. The reciprocal of the crossover frequency means the relaxation time of the fluid. The transition from viscous to elastic behavior occurs, at the crossover frequency $\omega_c = 1/\lambda$, with λ a characteristic time of the material. P15_B0.08 and P15_B0.16 has higher moduli than P15 as shown in Fig. 4-14. As the borate is added, the polymer chains develop a complex formation. Therefore polymer chain has a strong resistance to the flow direction as strain is increased, and the moduli increase [Hyun *et al.*, 2002].

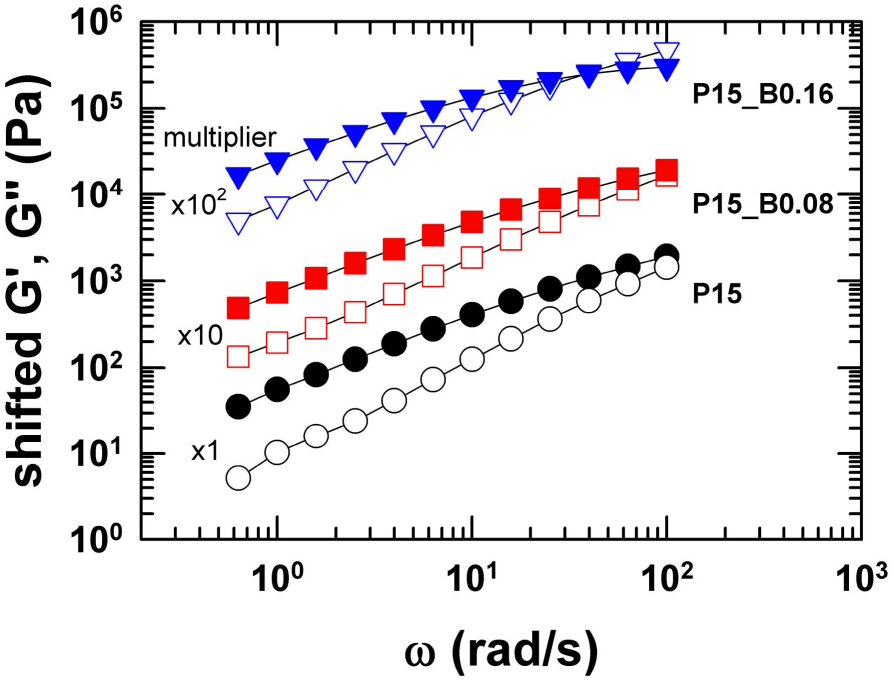

Fig. 4-14 Storage modulus (G' , open symbols) and loss modulus (G'' , filled symbols) as a function of frequency from OS measurement at fixed strain amplitude 0.3. Note that curves have been shifted vertically by the multiplier indicated by the ordinate.

The linear viscoelastic moduli were measured with OSQ test as shown in Fig. 4-15. The relaxation time was 0.05s for P15, 0.09s for P15_B0.08, 0.28s for P15_B0.16. As the sodium borate was added, the relaxation time increased under OSQ flow. All samples have crossover frequency unlike OS test. The result indicates that the onset of transition occurs faster in OSQ than in OS as given in Fig. 4-16. It means that the crossover frequency under OSQ is moved toward lower region than under OS. The strong secondary bonding effects between PVA and borate was more pronounced in OSQ than in OS.

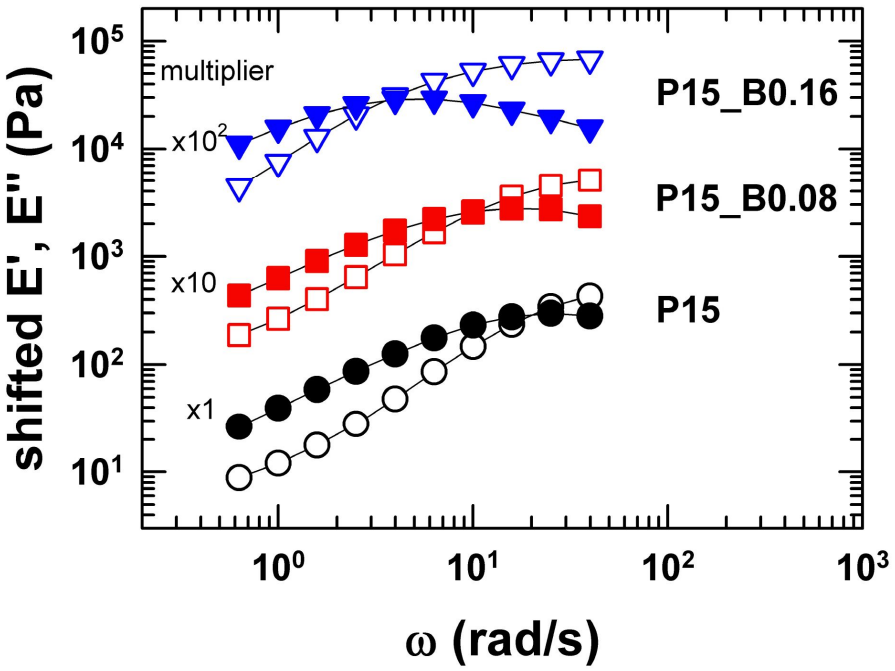

Fig. 4-15 Storage modulus (E', open symbols) and loss modulus (E'', filled symbols) as a function of frequency from OSQ measurement at fixed strain amplitude 0.0026. Note that curves have been shifted vertically by the multiplier indicated by the ordinate.

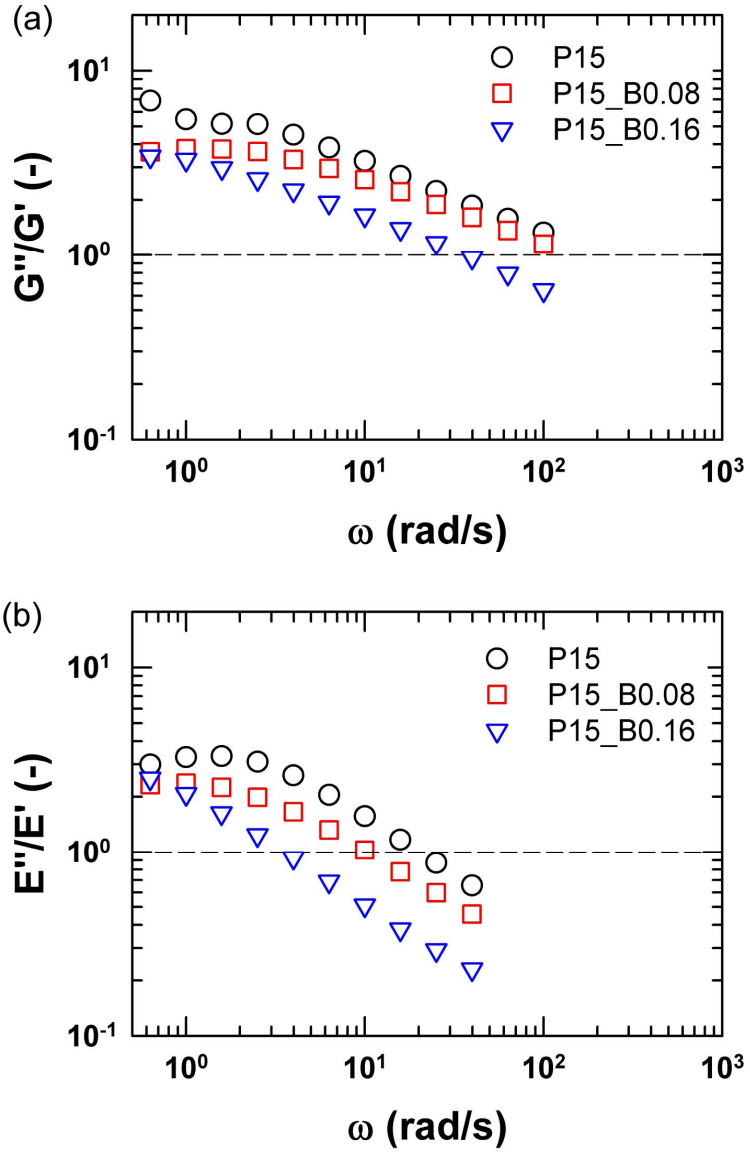

Fig. 4-16 Ratio (G''/G' , E''/E') of the loss over the storage modulus as a function of frequency with OS (a) and OSQ (b) measurements.

The strain sweep test was performed to classify the linear and nonlinear regime of P15, P15_B0.08 and P15_B0.16 as shown in Fig. 4-17 & 4-18. At small strain region, the storage and loss modulus are constant regardless of strain amplitude generally. In the nonlinear regime, however, the storage and loss modulus vary with strain amplitude. The storage and loss modulus show strain thinning or strain hardening behavior which is commonly observed in polymer solutions and melts. The samples display strain thinning behavior which arises from chain orientation or alignment of microstructure with the flow direction. The storage modulus decreases at large strain amplitude, but the loss modulus is nearly constant with strain amplitude. Even though the loss modulus was constant within overall strain amplitude imposed in this study, it will decrease at larger strain amplitude. In both OS and OSQ measurement, no strain hardening was observed for P15, P15_B0.08 and P15_B0.16.

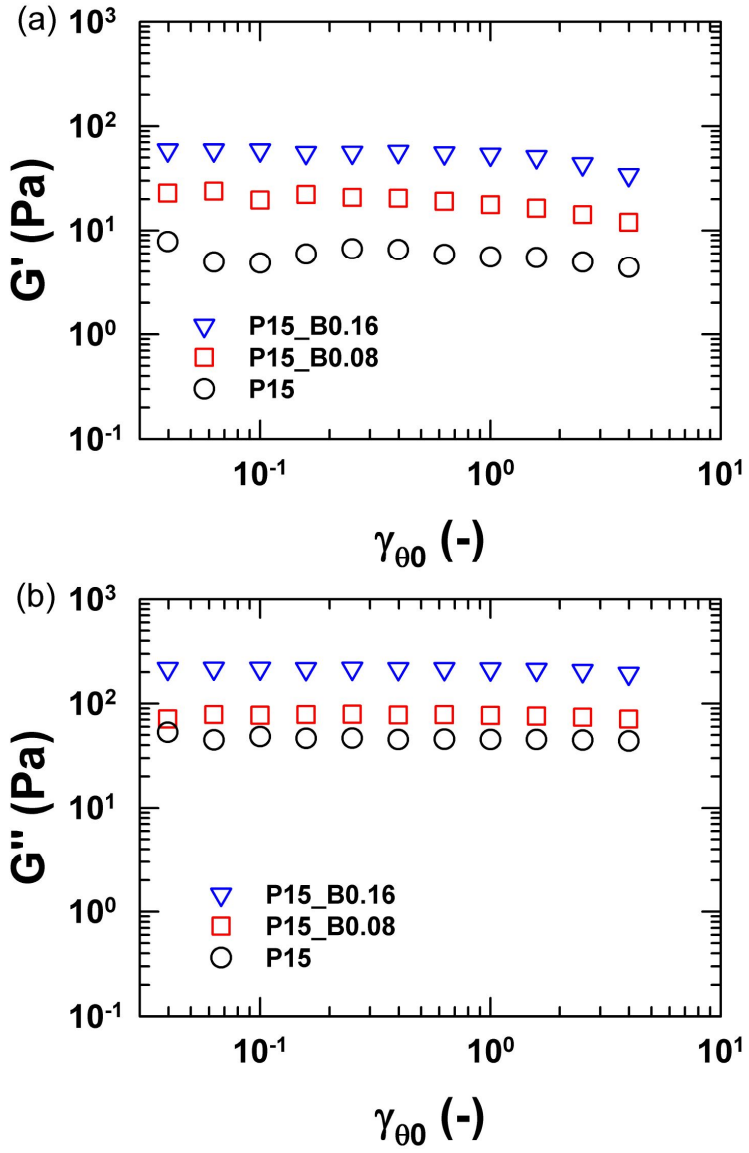

Fig. 4-17 (a) Storage modulus (G'), (b) loss modulus (G'') as a function of strain amplitude under OS at fixed frequency 1 rad/s.

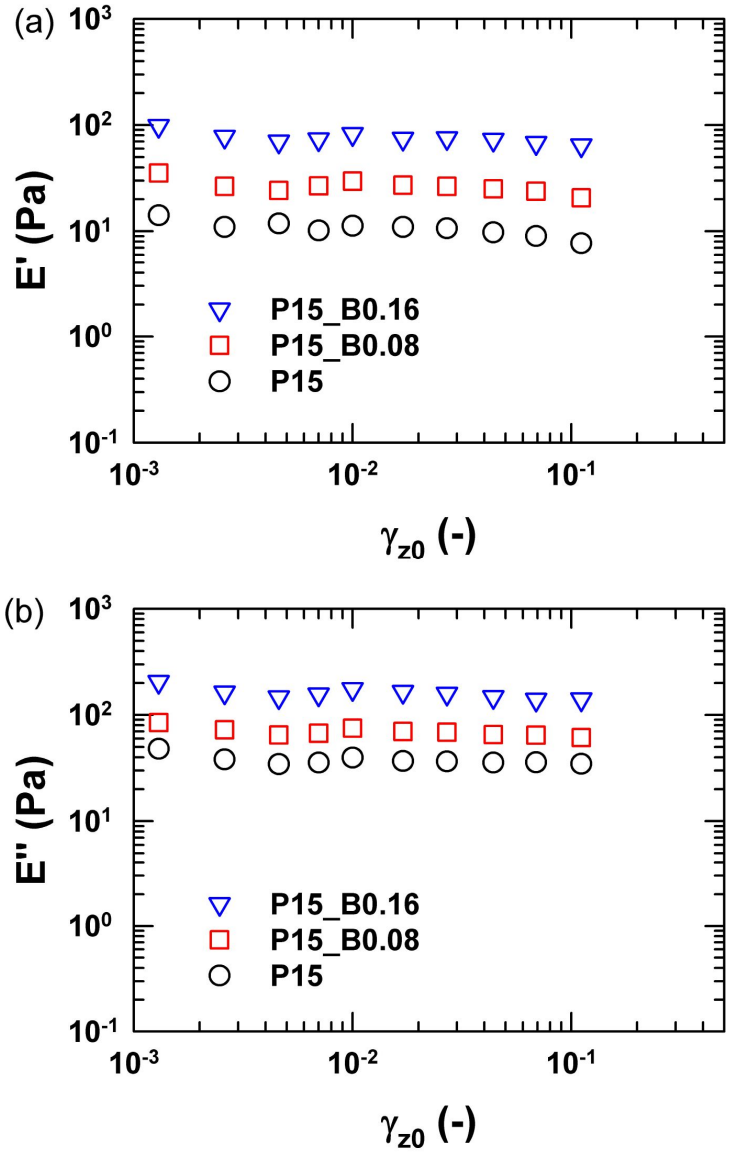

Fig. 4-18 (a) Storage modulus (E'), (b) loss modulus (E'') as a function of strain amplitude under OSQ at fixed frequency 1 rad/s.

No strain hardening was observed for PVA borate solutions used in previous section (see in Fig. 4-17 & 4-18). However, P2_B1 significantly showed the strain hardening as the strain amplitude increases. Fig. 4-19 displays storage (G', E') and loss (G'', E'') moduli as a function of strain amplitude at 1rad/s under OS and OSQ. The storage and loss moduli of OS show stronger strain hardening behavior than those of OSQ. When polymer chains are linked together by cross-links, they generally lose some of their ability to move as individual polymer chains. For example, a liquid polymer (where the chains are freely flowing) can be turned into a solid or gel by cross-linking the chains together. For this reason the moduli increase due to a strong interaction between some segments of the complex fluids. It can be more clear by the ratio (G'/G'', E'/E'') of the storage over the loss modulus as a function of strain amplitude (in Fig. 4-20).

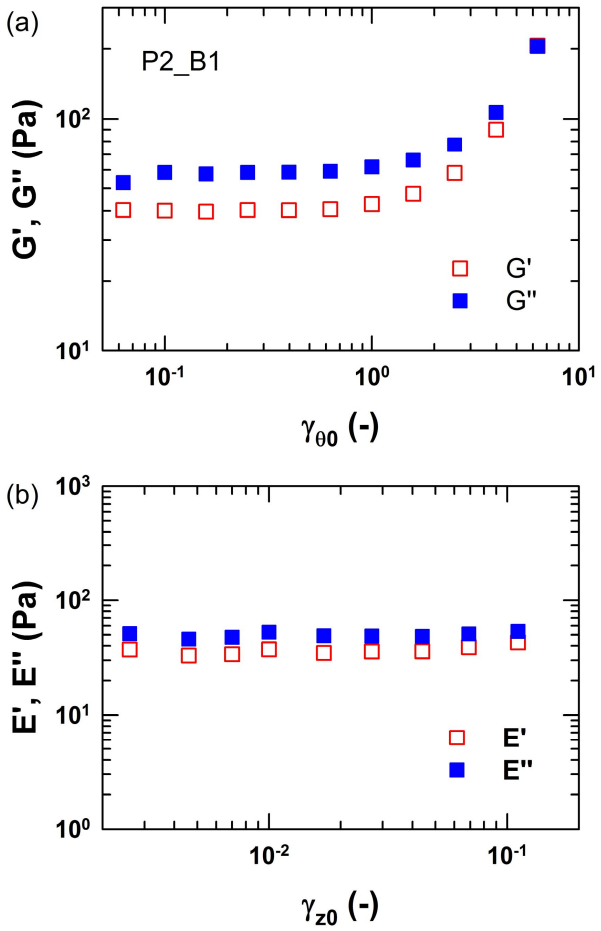

Fig. 4-19 Storage (G', E') and loss (G'', E'') moduli as a function of strain amplitude at 1rad/s; (a) OS and (b) OSQ.

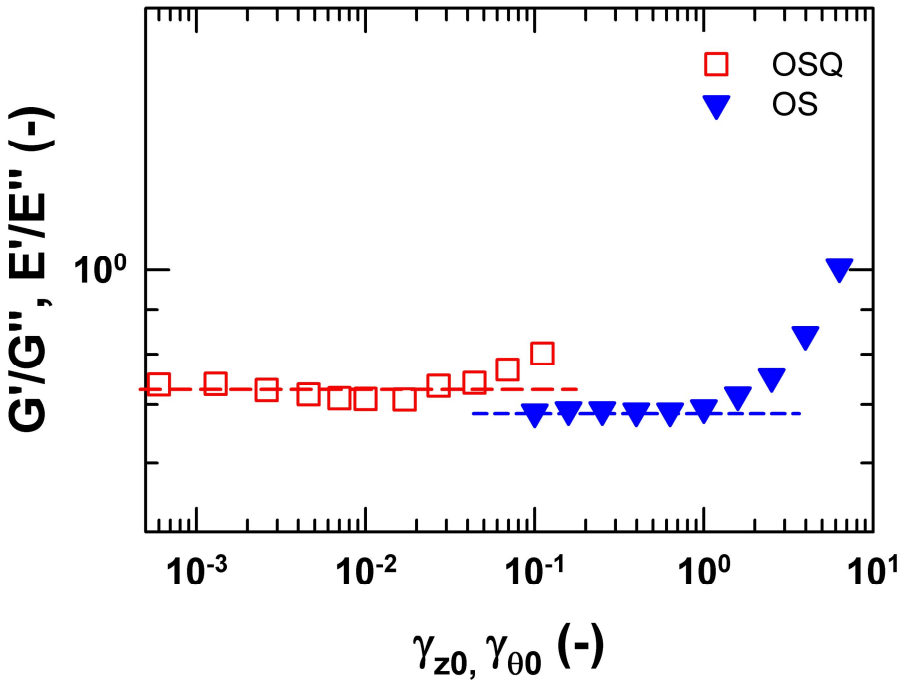

Fig. 4-20 Ratio (G'/G'', E'/E'') of the storage over the loss modulus as a function of strain amplitude with OS and OSQ measurements.

Chapter 5. Model prediction of normal stress under oscillatory squeeze flow

5.1 Constitutive equations

Three different constitutive equations of Maxwell type have been employed to predict the nonlinear responses of viscoelastic fluids under oscillatory squeeze flow: upper-convected Maxwell, Giesekus, and exponential Phan-Thien Tanner model with single mode. The simplest model, the upper-convected Maxwell (UCM) model is given by:

$$\boldsymbol{\tau} + \lambda \boldsymbol{\tau}_{(1)} = 2\lambda G \mathbf{D} \tag{5-1}$$

where $\boldsymbol{\tau}$ is the extra-stress tensor, λ and G are the relaxation time and the modulus of the fluid, **D** is the rate of deformation tensor. The subscript (1) denotes the upper convective time derivative, which is defined as follows:

$$\boldsymbol{\tau}_{(1)} = \frac{\partial \boldsymbol{\tau}}{\partial t} + \mathbf{v} \cdot \nabla \boldsymbol{\tau} - (\nabla \mathbf{v})^T \cdot \boldsymbol{\tau} - \boldsymbol{\tau} \cdot \nabla \mathbf{v} . \tag{5-2}$$

This simple constitutive equation is nonlinear because $\boldsymbol{\tau}_{(1)}$ contains products of the velocity gradient and the stress tensor $\boldsymbol{\tau}$.

It was also performed simulation with Giesekus model,

$$\boldsymbol{\tau} + \lambda \boldsymbol{\tau}_{(1)} + \frac{\alpha}{G} \boldsymbol{\tau} \cdot \boldsymbol{\tau} = 2\lambda G \mathbf{D}, \tag{5-3}$$

where λ and G are the relaxation time and the modulus, **D** is the rate of deformation tensor [Larson, 1988]. The Giesekus model is equivalent to a dumbbell model with anisotropic drag from the viewpoint of kinetic theory. α is the anisotropy parameter or mobility factor which is associated with anisotropic Brownian motion and anisotropic hydrodynamic drag, and typically ranges from 0 to 1. When α=0, this model becomes the upper-convected Maxwell (UCM) model. As α increases, the anisotropic drag becomes more pronounced.

The exponential Phan-Thien Tanner (EPTT) model is given as follows:

$$\boldsymbol{\tau} \exp\left(\frac{\varepsilon}{G} tr\boldsymbol{\tau} \right) + \lambda \boldsymbol{\tau}_{(1)} + \lambda \xi \left(\mathbf{D} \cdot \boldsymbol{\tau} + \boldsymbol{\tau} \cdot \mathbf{D} \right) = 2\lambda G \mathbf{D}. \tag{5-4}$$

Here, λ and G are the relaxation time and the modulus, **D** is the rate of deformation tensor. This model was derived based on a network theory which includes non-affine motion [Larson, 1988]. ξ and ε are the nonlinear parameters, which control the level of shear thinning. If $\xi \neq 0$, unphysical oscillation occurs in the prediction of steady shear viscosity and first normal stress coefficient during the start-up of shear flow. When ξ is set to zero, the motion is supposed to be affine; the unphysical oscillation disappears but shear thinning still exists due to the nonlinear parameter, ε. Thus it was

performed model simulations with ξ=0, and ε was varied from 0 to 1. As the nonlinear parameter ε increases, the level of shear-thinning becomes pronounced in shear flow.

5.2 Model parameters

Table 5-1 Description of the sample used. Zero-shear viscosity (η_0^*) was obtained by fitting the complex viscosity data to the Carreau model*. The relaxation time (λ) is the reciprocal of the cross-over frequency [ω_c, frequency at G′(ω)= G″(ω) in the frequency sweep test].

Sample	Molecular weight [g/mol]	Concentration (wt%)	η_0^* [Pa·s]	G [Pa]	λ (=1/ω_c) [s]
PEO4m2.5	4×10^6	2.5	114	104	1.1

*Carreau model: $\eta/\eta_0 = \left[1+(a\dot{\gamma})^b\right]^{(n-1)/b}$

The nonlinear parameters were selected by comparing model prediction to experimental data from the dynamic strain sweep test under simple shear flow. The relative viscosity (η^*/η_0^*) is plotted as a function of

strain amplitude at specified nonlinear parameters (α, ε) in Fig. 5-1. As the nonlinear parameter α for Giesekus model and ε for EPTT model increases, strain-thinning behavior becomes more pronounced. When α=0.15 for Giesekus model and ε=0.2 for EPTT model, the reduced viscosity best fits with experimental data. Although the nonlinear parameters were determined by fitting with viscosity in shear flow, it will be used in numerical simulations for oscillatory squeeze flow [Debbaut and Thomas, 2004]. Table 5-1 lists the characteristics of the samples used in this work.

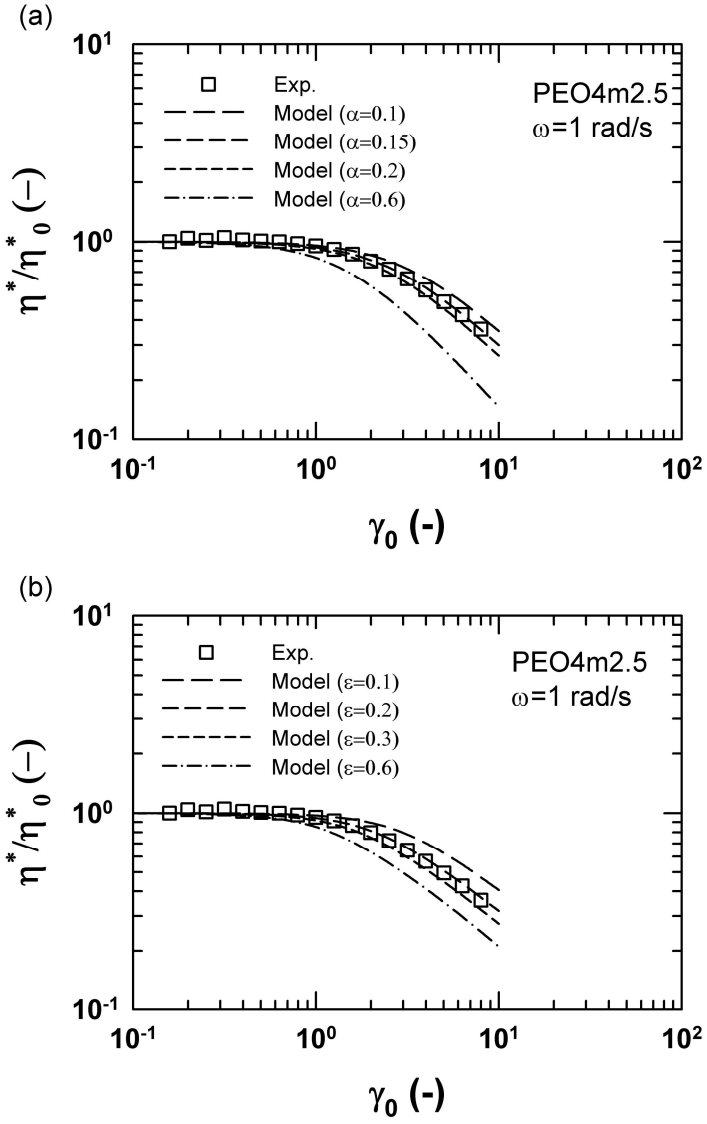

Fig. 5-1 Reduced shear viscosity from experiment (symbols) and simulation (dashed lines) at ω=1rad/s: (a) Giesekus model, (b) exponential PTT (EPTT) model, at various nonlinear parameters.

5.3 Stress curve and Lissajous plot

To investigate the nonlinear response of normal stresses under oscillatory squeeze flow, the model simulations were performed by employing UCM model, Giesekus model, and EPTT model. In order to analyze the normal stress signals, stress shape analysis and Lissajous plot analysis have been performed. Stress shape analysis shows the raw stress signal, which varies from sinusoidal to distorted wave as the strain amplitude increases. The stress shape provides insightful and visual information during structural changes of the material when the deformation becomes large. The Lissajous plot, which is plotted as [stress vs. strain] or [stress vs. strain rate], is useful in observing the transformation of nonlinear responses. The Lissajous plot is elliptical in the linear regime, but becomes distorted in the nonlinear regime. Fig. 5-2 shows the normal stress calculated from UCM model, Giesekus model with α=0.15, and EPTT model with ε=0.2, ξ=0 for G=104, λ=1.1. The normal stress was normalized by its amplitude. The normal stress changes from sinusoidal to distorted shape, and from symmetric to nonsymmetric shape with respect to zero mean value as the strain amplitude increases as shown in Fig. 5-2. This nonsymmetric response is one of the distinctive features of the normal stresses under oscillatory squeeze flow [Phan-Thien, 2000; Phan-Thien *et al*., 2000]. The constitutive equations show the nonlinear

and nonsymmetric response under oscillatory squeeze flow in the simple model prediction.

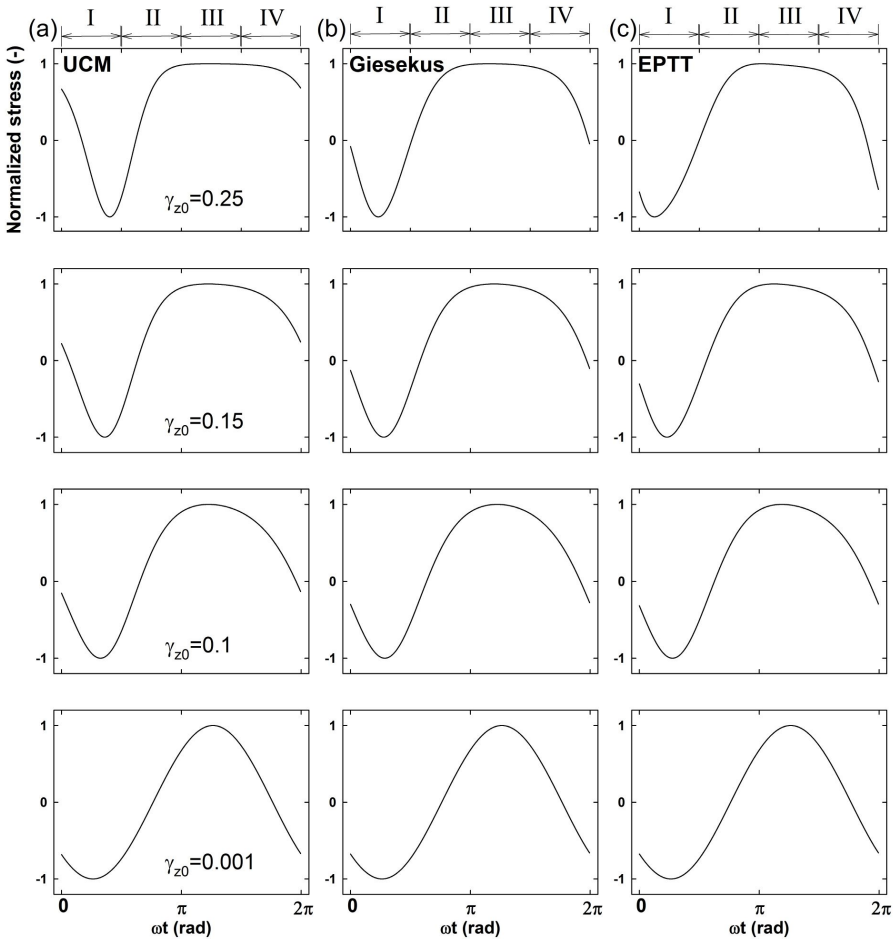

Fig. 5-2 Normal stress of model prediction; (a) UCM model (G=104, λ=1.1), (b) Giesekus model (α=0.15, G=104, λ=1.1), (c) EPTT model (ε=0.2, ξ=0, G=104, λ=1.1) at frequency 1 rad/s. The index I and IV indicate compression part; II and III indicate extension part during oscillation.

The Lissajous plots [stress vs. strain] is displayed in Fig. 5-3. The loop of [stress vs. strain] shows different shape at larger strain amplitude according to the constitutive equations. The loop of [stress vs. strain] varies from symmetric to nonsymmetric shape with respect to zero mean value as the strain amplitude increases. At low strain amplitude 0.001, the loop of [stress vs. strain] is symmetric, which is caused by the same response of the fluid during compression and extension. However, at higher strain amplitudes, the loops become nonsymmetric, which implies different response during the oscillation. As the strain amplitude increases, this nonsymmetric response becomes more pronounced in all predictions as shown in Fig. 5-3. The internal area of the loop corresponds to the mechanical energy dissipation, and normally increases with strain amplitude; that is, mechanical energy dissipation $\approx \frac{1}{\pi\gamma_{z0}^2}\left|\oint \sigma_{zz} d(\gamma_z)\right|$. The Giesekus and EPTT model show that the area increases with strain amplitude, while that of UCM model decreases with strain amplitude. In this sense, the UCM model exhibits poor prediction under oscillatory squeeze flow.

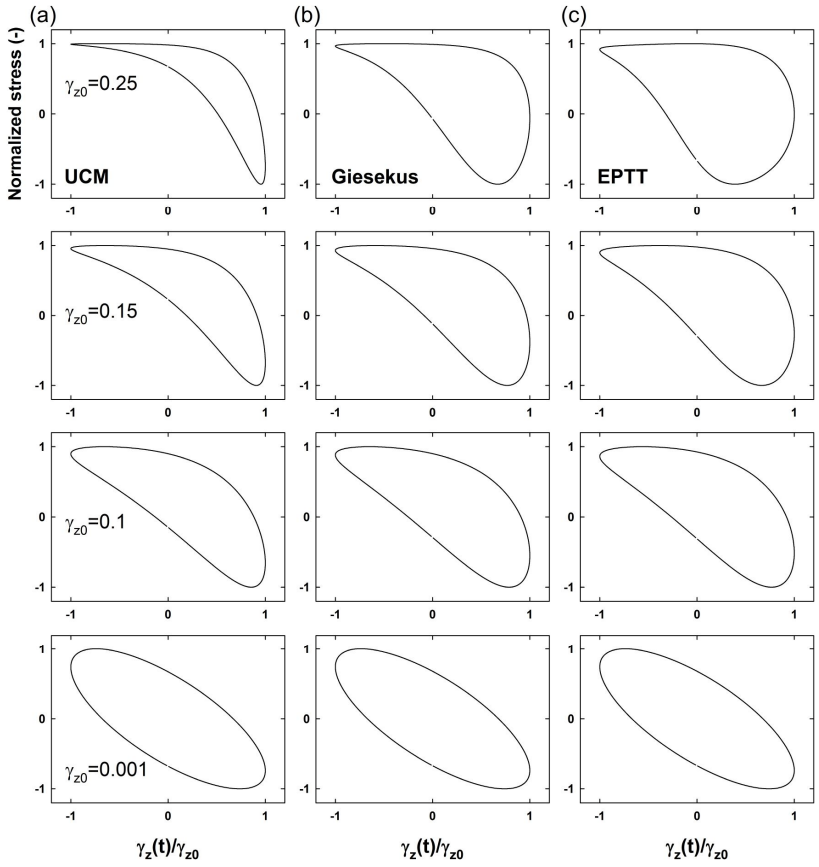

Fig. 5-3 Closed loops are normal stress vs. strain, [$\sigma_{zz}(t)/\sigma_0$ vs. $\gamma_z(t)/\gamma_{z0}$]; (a) UCM model (G=104, λ=1.1), (b) Giesekus model (α=0.15, G=104, λ=1.1), (c) EPTT model (ε=0.2, ξ=0, G=104, λ=1.1) at frequency 1 rad/s.

Fig. 5-4 shows the loops of both [stress vs. strain rate] at various strain amplitudes. The loop of [stress vs. strain rate] changes from elliptic to distorted shape and becomes nonsymmetric with the increase of strain amplitude. The elliptical and symmetric shape results from the same response during compression and extension. But, the distorted and nonsymmetric shape is caused by the different response during the oscillation. The constitutive equations show similar results in Lissajous plot at low strain amplitude, but exhibit different shape at larger strain amplitude. At large strain amplitude γ_{z0}=0.25, the UCM model shows unrealistic result, in which the area of the [stress vs. strain rate] loop is nearly constant independent of strain amplitude. The area of the loop [stress vs. strain rate] corresponds to the mechanical energy storage; that is, mechanical energy storage $\approx \frac{1}{\pi\gamma_{z0}^2}\left|\oint \sigma_{zz} d(\dot{\gamma}_z/\omega)\right|$. In general, the area of [stress vs. strain rate] loop decreases with strain amplitude. On the other hand, the Giesekus model and EPTT model show reasonable result, in which the area of the loop decreases as the strain amplitude increases.

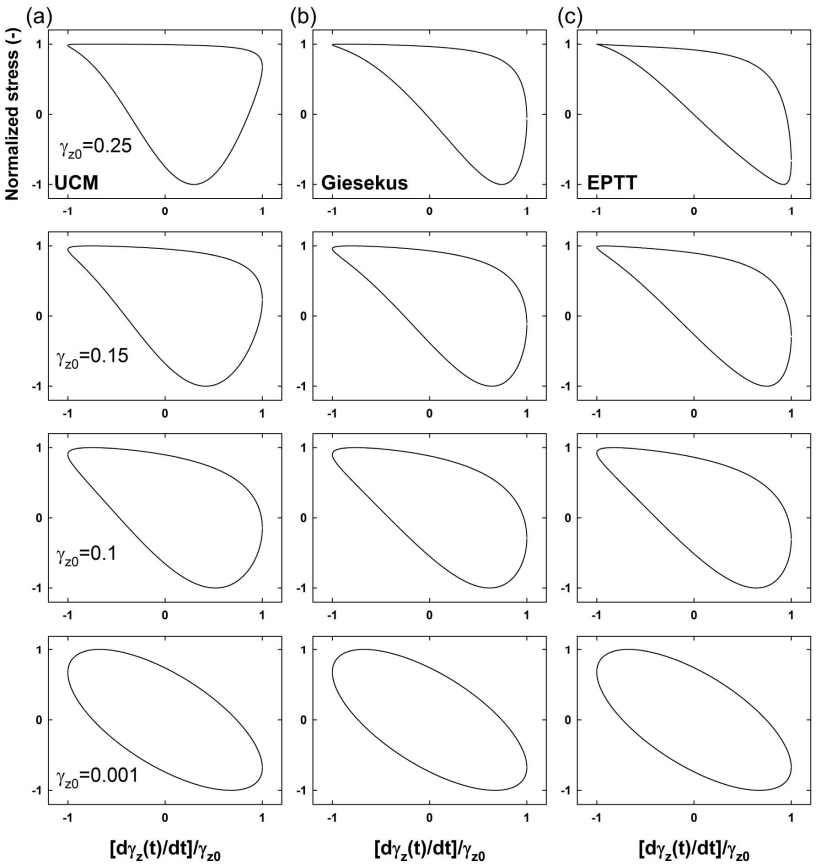

Fig. 5-4 Closed loops are normal stress vs. strain rate, [$\sigma_{zz}(t)/\sigma_0$ vs. $\dot{\gamma}_z(t)/\gamma_{z0}$]; (a) UCM model (G=104, λ=1.1), (b) Giesekus model (α=0.15, G=104, λ=1.1), (c) EPTT model (ε=0.2, ξ=0, G=104, λ=1.1) at frequency 1 rad/s.

It was compared experimental data of PEO solution (PEO4m2.5) with simulation results calculated by UCM model, Giesekus model (α=0.15), and EPTT model (ε=0.2, ξ=0). The normal stresses are plotted as a function of time in Fig. 5-5. The stress curve varies from sinusoidal to distorted shape, and changes from symmetric to nonsymmetric at both positive and negative region. At low strain amplitude, the predictions are good, while the predictions are poor at larger strain amplitude. The models predict the nonsymmetric stresses very well, but show a large deviation in a quantitative sense especially at positive region over the x-axis. The deviation of UCM model is larger than that of Giesekus and EPTT model. The discrepancy comes partly from the broad spectrum of relaxation modes in the polymer solution (the models are all single mode), but may originates from the incompleteness of the constitutive equations. In this sense, the oscillatory squeeze flow can be a good test flow to evaluate the performance of the constitutive equations.

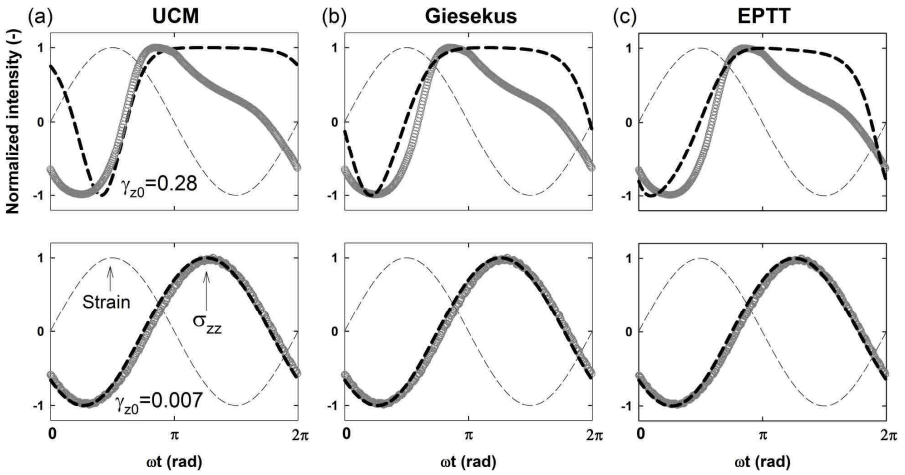

Fig. 5-5 Normal stress; (a) UCM model, (b) Giesekus model (α=0.15), (c) EPTT model (ε=0.2, ξ=0) for G=104, λ=1.1. The experimental data (PEO4m2.5, symbols) are compared with model predictions (thick lines) at frequency 1 rad/s. The strain (thin lines) is plotted together as a reference.

Fig. 5-6 shows the Lissajous plot of [stress vs. strain] at strain amplitudes, 0.007 and 0.28. At small strain amplitude 0.007, both the loop of [stress vs. strain] displays elliptical shape, which indicates linear viscoelasticity. However, the plot of [stress vs. strain] exhibits nonsymmetric loop at larger strain amplitude, in both experiment and model predictions. In this sense, the model equations qualitatively predict nonsymmetric characteristics of normal stress reasonably well. However, the predictions are far from realistic in the quantitative sense.

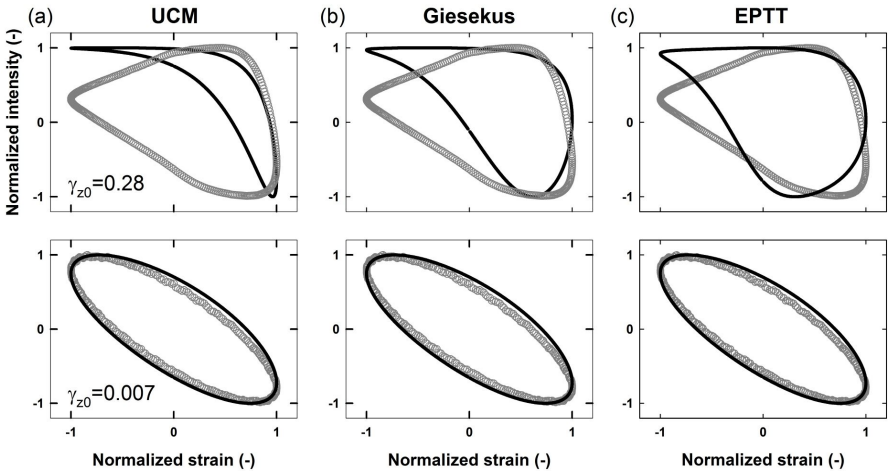

Fig. 5-6 Lissajous plot of normal stress vs. strain, [$\sigma_{zz}(t)/\sigma_0$ vs. $\gamma_z(t)/\gamma_{z0}$]; (a) UCM model, (b) Giesekus model (α=0.15), (c) EPTT model (ε=0.2, ξ=0) for G=104, λ=1.1. The experimental data (PEO4m2.5, symbols) are compared with model predictions (dashed lines) at frequency 1 rad/s.

It was also plotted [stress vs. strain rate] in Fig. 5-7. At strain amplitude 0.007, the curves of both [stress vs. strain rate] show elliptical shape, which means linear response. However at high strain amplitude 0.28, the loop of [stress vs. strain rate] shows one-fold nonsymmetry in experiment only. This one-fold nonsymmetric loop means the nonlinear response. However, all model predictions (dashed line) which show nonsymmetric loop do not predict one-fold nonsymmetric loop of [stress vs. strain rate] observed from experiment. Here again, it is clear that the oscillatory squeeze flow can be a good test flow to evaluate the performance of the constitutive equations.

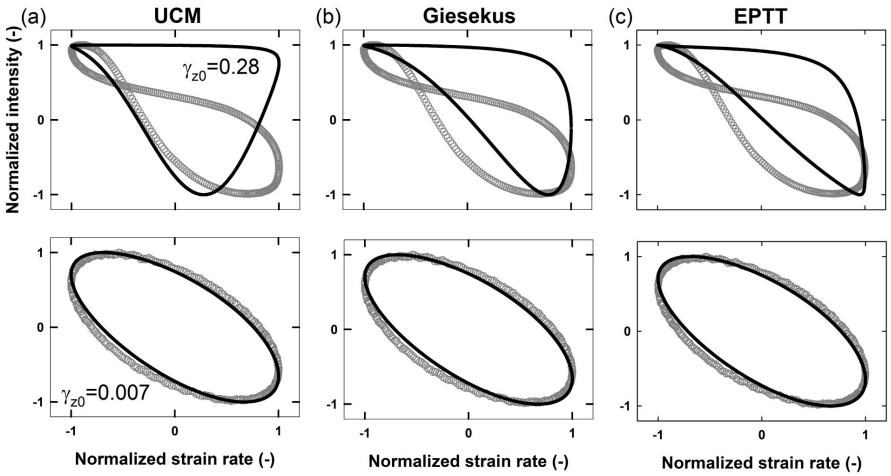

Fig. 5-7 Lissajous plot of normal stress vs. strain rate, [$\sigma_{zz}(t)/\sigma_0$ vs. $\dot{\gamma}_z(t)/\gamma_{z0}$]; (a) UCM model, (b) Giesekus model (α=0.15), (c) EPTT model (ε=0.2, ξ=0) for G=104, λ=1.1. The experimental data (PEO4m2.5, symbols) are compared with the model prediction (lines) at frequency 1 rad/s.

In comparison with experiment, the model simulation showed good prediction in terms of the nonsymmetric stress signal and corresponding Lissajous plot except UCM model. However the model predictions fail to describe the experimental data completely. A possible cause of the discrepancy lies in determining the set of nonlinear parameters (α, ε). The model prediction is very sensitive to the variation of the nonlinear parameters [Nam *et al*., 2008]. It may be that the best-fit to the shear viscosity (in Fig. 5-1) is not the best-fit to the normal stress. The discrepancy can also be explained in terms of the relaxation spectrum of the polymer solution. The polymer solution typically has the broad relaxation spectrum due to its broad molecular weight distribution, however it was considered only the models with single relaxation mode. If multi-mode is considered in model calculation, the discrepancy may be minimized between experiment and simulation. And lastly, it cannot be removed the possibility that the constitutive equations are not complete enough to predict the response of viscoelastic fluids under the oscillatory squeeze flow.

5.4 Fourier transform (FT)

Fourier transformation captures inherent periodic nature of time dependent signals and displays the corresponding amplitudes and phases as a function of frequency. FT is widely used to quantify the nonlinearity with high sensitivity. In both experiment and simulation, the normal stress reveals all high order harmonics, both odd and even. The Fourier intensity increases and higher order harmonics start to appear as the strain amplitude increases. The reason why there appear all higher harmonics is due to the nonsymmetric nature of the normal stresses in the oscillatory squeeze flow. The higher order harmonic intensity divided by the fundamental intensity, $I_{n/1}$, is plotted as a function of strain amplitude in Fig. 5-8. The relative intensity $I_{n/1}$ shows a scaling relationship with strain amplitude as follows:

$$\log(I_{n/1}) = a + b\log\gamma_{z0} \tag{5-5}$$

where a is an intercept and b is the slope in the log-log plot. In Fig. 5-8, the lines indicate linear regression with Eq. (5-5). $I_{n/1}$ obtained from model equations are almost proportional to the (n-1)th power of strain amplitude. This relationship is similar to that of large amplitude oscillatory shear, in both experiment and simulation [Nam *et al*., 2008; Hyun *et al*., 2011]. In the oscillatory squeeze flow, the relative intensity grows with both odd and even

power (b=1,2,3,…) of strain amplitude for normal stress. The relative intensity shows similar trend and slope (b) in both experiment and model predictions. The model predictions show good agreement with experiment in terms of FT rheology. It is also to be noted that the normal stresses calculated from the model equations as well as from experiment show all high order contributions.

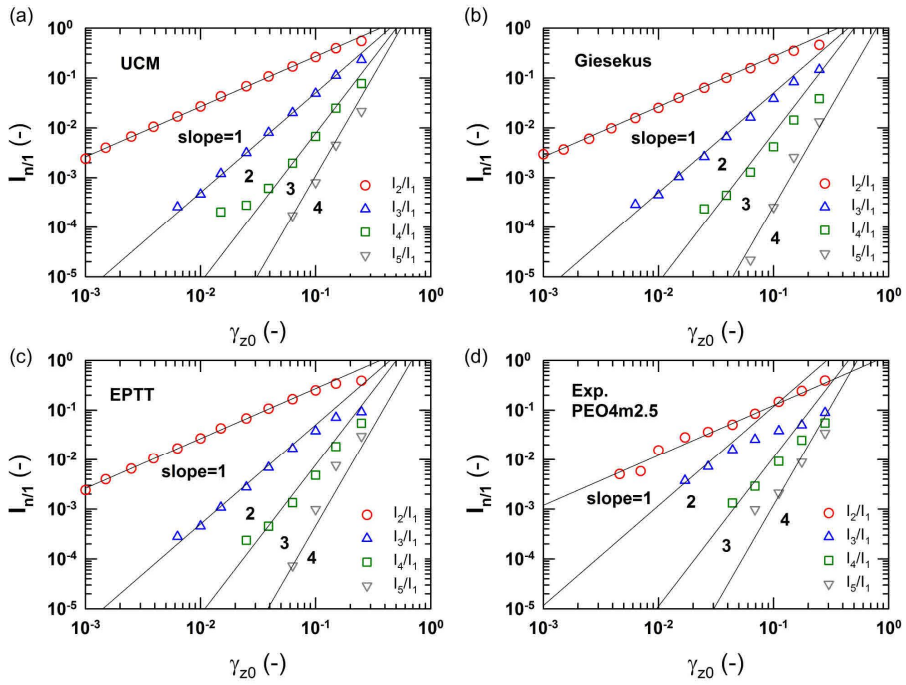

Fig. 5-8 Relative Fourier intensity ($I_{n/1}$) as a function of strain amplitude; (a) UCM model (G=104, λ=1.1), (b) Giesekus model (α=0.15, G=104, λ=1.1), (c) EPTT model (ε=0.2, ξ=0, G=104, λ=1.1), (d) experimental data of PEO4m2.5, at frequency 1 rad/s. The lines indicate linear fitting with Eq. (5-5).

From the FT results, it was found that the nonlinearity, $I_{2/1}$ and $I_{3/1}$, linearly and quadratically depends on the strain amplitude, respectively. Thus, the nonlinear coefficients, $K_{2/1}$ and $K_{3/1}$, can be defined as follows:

$$K_{2/1} \equiv I_{2/1} / \gamma_{z0} , \tag{5-6}$$

$$K_{3/1} \equiv I_{3/1} / \gamma_{z0}^2 . \tag{5-7}$$

These nonlinear coefficients from FT analysis are defined using the relationship between stress and deformation like other rheological properties from steady shear test: shear viscosity ($\eta \equiv \sigma_{12} / \dot{\gamma}$), first normal stress difference ($\psi_1 \equiv N_1 / \dot{\gamma}^2$) [Hyun and Wilhelm, 2008]. In this section, it was systematically investigated the nonlinear parameters $K_{2/1}$ and $K_{3/1}$ using the single mode UCM, Giesekus, and EPTT model. In Fig. 5-9 and 5-10, the nonlinear coefficients calculated from the constitutive equations are constant at low strain amplitude, but decreases as the strain amplitude increases like strain-thinning from dynamic shear test. These nonlinear coefficients show similar tendency as the constitutive equations used. The EPTT model presents most strain-thinning behavior as a function of strain amplitude in Fig. 5-9(c). On the other hand, in experimental observation, polymer solution of PEO4m2.5 does not show strain-thinning behavior with respect to the nonlinear coefficient $K_{2/1}$. This experimental result will display the strain-

thinning at higher strain amplitude than that of model prediction. However, we cannot measure the nonlinear characteristics at higher strain amplitudes over γ_{z0}=0.25 due to a limitation of the normal transducer on the rheometer, RMS800 (TA Instruments).

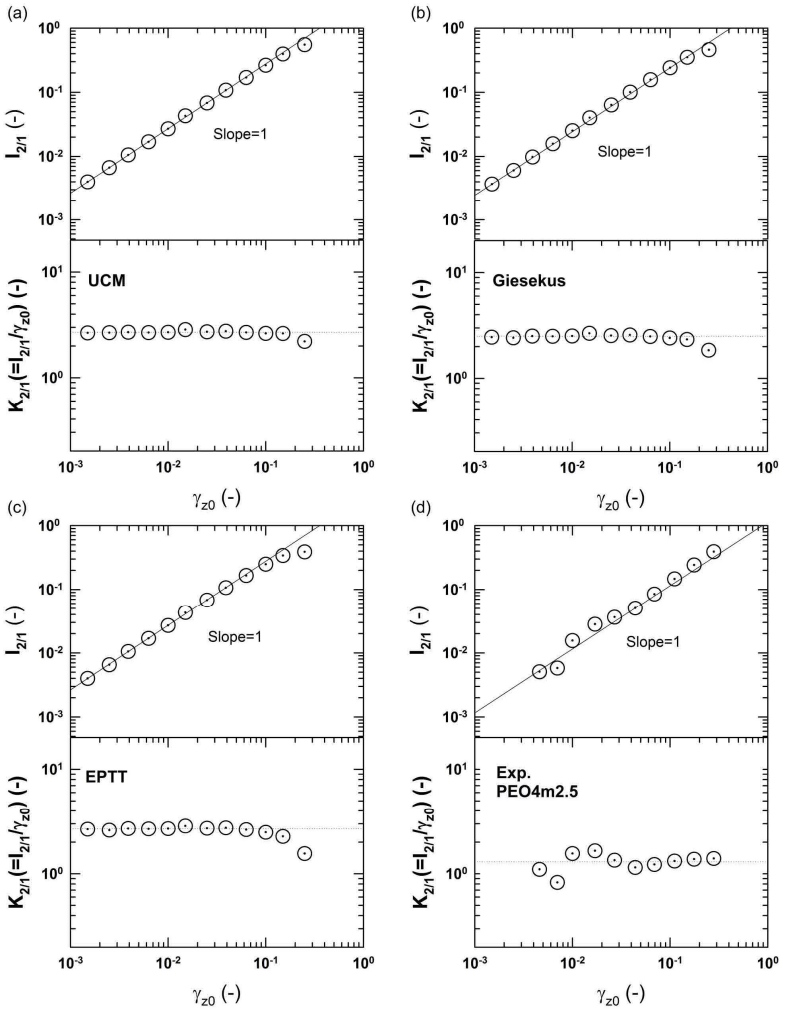

Fig. 5-9 $I_{2/1}$ and $K_{2/1}$ as a function of strain amplitude; (a) UCM model (G=104, λ=1.1), (b) Giesekus model (α=0.15, G=104, λ=1.1), (c) EPTT model (ε=0.2, ξ=0, G=104, λ=1.1), (d) experimental data with PEO4m2.5, at fixed frequency 1 rad/s.

Fig. 5-10 shows the nonlinear coefficients $K_{3/1}$ which is calculated from the relative intensity $I_{3/1}$ divided by squared strain amplitude. This nonlinear coefficient $K_{3/1}$ also presents strain-thinning as the strain amplitude increases in common with $K_{2/1}$. At the low strain amplitude, the nonlinear coefficient is constant regardless of strain amplitude, while $K_{3/1}$ shows the strain-thinning behavior at larger strain amplitudes in all constitutive equations. The EPTT model shows more pronounced strain-thinning than other models. In experimental investigation, $K_{3/1}$ exhibits stronger strain-thinning than that of model prediction. This could be due to decrease of the slope of $I_{3/1}$ with increasing strain amplitude. The slope of $I_{3/1}$ is nearly 2 within medium strain amplitude region, but the slope is less than 2 at larger strain amplitude region. From this result, we found that the model equations can predict the nonlinear coefficients reasonably compared with experimental data. Fig. 5-11 summarizes the nonlinear coefficients $K_{2/1}$ and $K_{3/1}$ as a function of strain amplitude. It was clearly confirmed that the EPTT model, which shows most strain thinning among constitutive equation, can predict the experimental result reasonably well in OSQ flow.

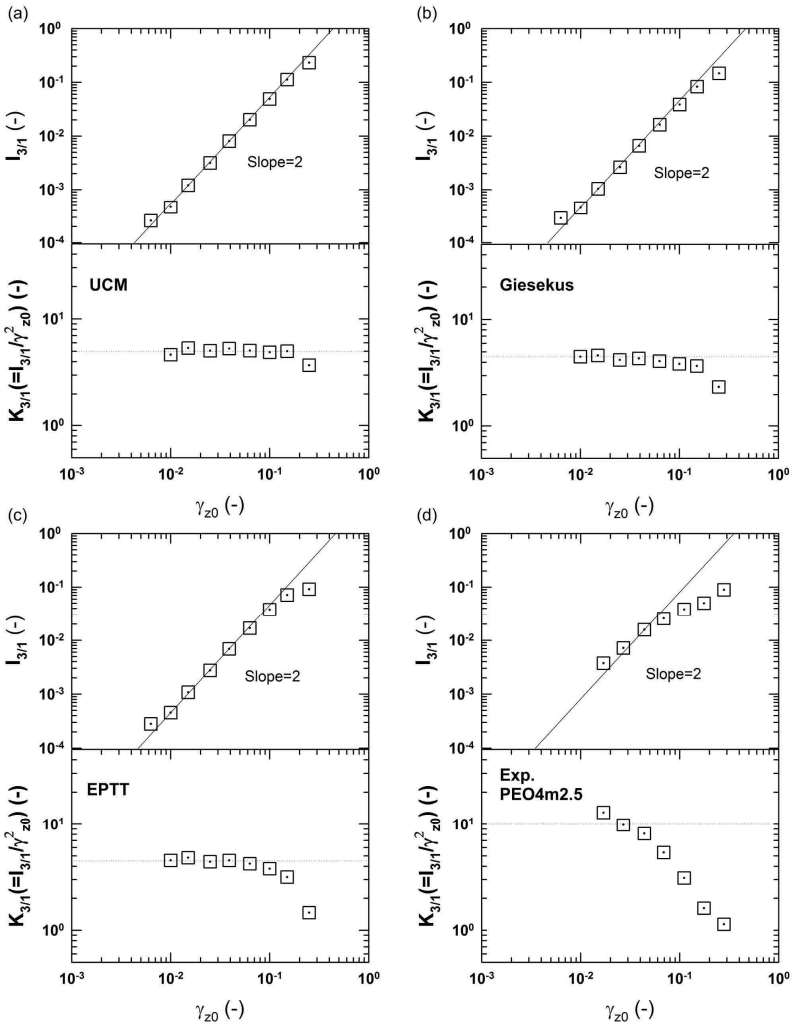

Fig. 5-10 $I_{3/1}$ and $K_{3/1}$ as a function of strain amplitude; (a) UCM model (G=104, λ=1.1), (b) Giesekus model (α=0.15, G=104, λ=1.1), (c) EPTT model (ε=0.2, ξ=0, G=104, λ=1.1), (d) experimental data with PEO4m2.5, at fixed frequency 1 rad/s.

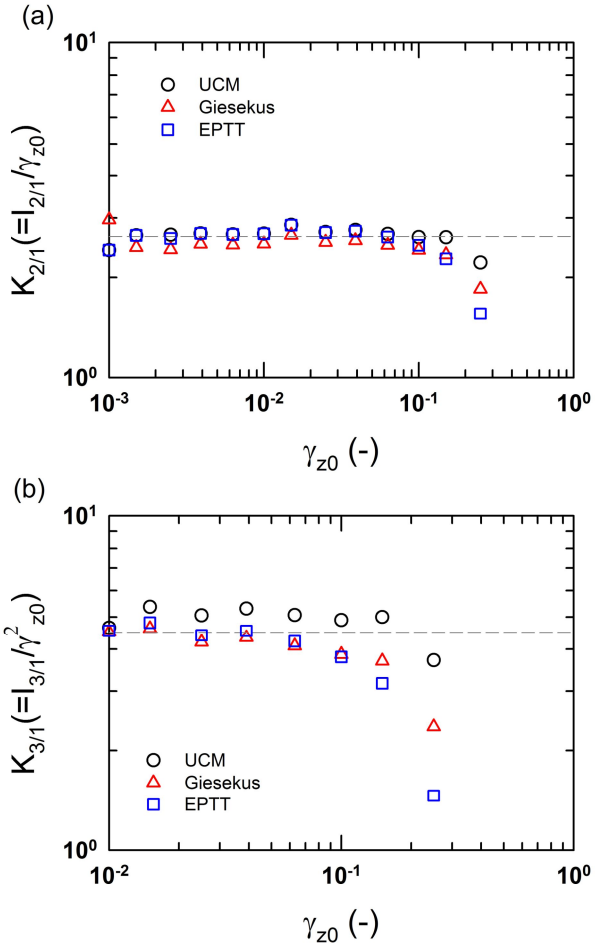

Fig. 5-11 $K_{2/1}$ and $K_{3/1}$ as a function of strain amplitude; (a) UCM model (G=104, λ=1.1), (b) Giesekus model (α=0.15, G=104, λ=1.1), (c) EPTT model (ε=0.2, ξ=0, G=104, λ=1.1).

5.5 Multi-mode prediction

The single mode predictions have been already studied above. The model simulation showed good prediction for the nonsymmetric stress signal. However, they showed the discrepancy which can also be explained in terms of the relaxation spectrum of viscoelastic fluids. In order to overcome the discrepancy, multi-mode simulation was performed with EPTT model. The EPTT model corresponded best with the experiment among the models. For this reason, the multi-mode model prediction of EPTT was performed with 5-mode of relaxation spectrum from linear viscoelastic data.

$$\boldsymbol{\tau} = \sum_{i=1}^{5} \boldsymbol{\tau}_i \tag{5-8}$$

$$\boldsymbol{\tau}_i \exp\left(\frac{\varepsilon_i}{G_i} tr\boldsymbol{\tau}_i \right) + \lambda_i \boldsymbol{\tau}_{i(1)} + \lambda_i \xi_i \left(\mathbf{D} \cdot \boldsymbol{\tau}_i + \boldsymbol{\tau}_i \cdot \mathbf{D} \right) = 2\lambda_i G_i \mathbf{D} \tag{5-9}$$

Here i denotes the number of relaxation mode.

The linear viscoelastic moduli (G', G'') were used to obtain a set of Maxwell parameters using nonlinear regression. The five sets of parameters (λ_i, G_i) satisfied the experimental moduli completely as shown in Fig. 5-12. The model curves shown are for a set of parameters with generalized Maxwell model as following,

$$G'(\omega) = \sum_{i=1}^{n} G_i \frac{(\omega\lambda_i)^2}{1+(\omega\lambda_i)^2} \tag{5-10}$$

$$G''(\omega) = \sum_{i=1}^{n} G_i \frac{\omega\lambda_i}{1+(\omega\lambda_i)^2} \tag{5-11}$$

Table 5-2 lists the set of Maxwell parameters for PEO4m2.5.

Table 5-2 Discrete relaxation spectra of five modes for PEO4m2.5. The Maxwell parameters (λ_i, G_i) were obtained from the linear viscoelastic data. The nonlinear parameter ε_i was determined by the best fit with the strain sweep data of the experiment.

i	λ_i (s)	G_i (Pa)	ε_i
1	0.010	52.170	0.2
2	0.056	21.320	0.2
3	0.316	19.350	0.2
4	1.778	11.120	0.2
5	11.000	4.220	0.2

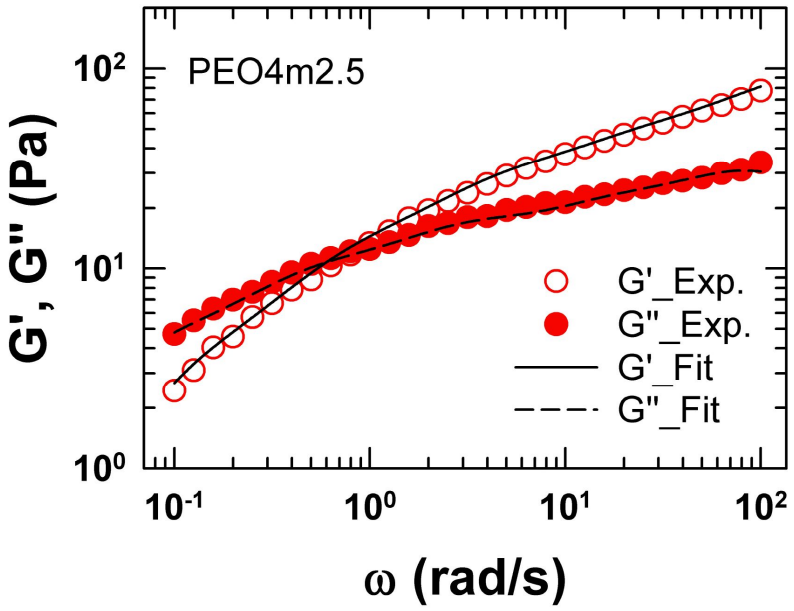

Fig. 5-12 The linear viscoelastic moduli as a function of frequency for PEO4m2.5. Fitting curves were plotted with the generalized Maxwell model with five modes.

Comparison of single- and multi-mode prediction was performed in terms of the stress curve and Lissajous plot analysis (in Fig. 5-13). The evaluation of multi-mode simulation shows good agreement in the nonsymmetric characteristics which is a distinct feature of normal stress in OSQ flow. The normal stress curve of model prediction displays nonsymmetric wave form which arises from the difference of response during compression and extension. The Lissajous plot of [stress vs. strain] and [stress vs. strain rate] also shows nonsymmetric loop for the origin (in Fig. 5-13(b)&(c)). From the numerical results, it can be proved that the multi-mode EPTT model is a reliable method predicting the nonsymmetric response of OSQ. Nonetheless, the multi-mode prediction did not show better performance than the single mode significantly. This numerical investigation certifies that the discrepancy between experiment and prediction may originate from the incompleteness of the constitutive equations or the determination a set of the nonlinear parameters. The further study in numerical prediction is left as future problems.

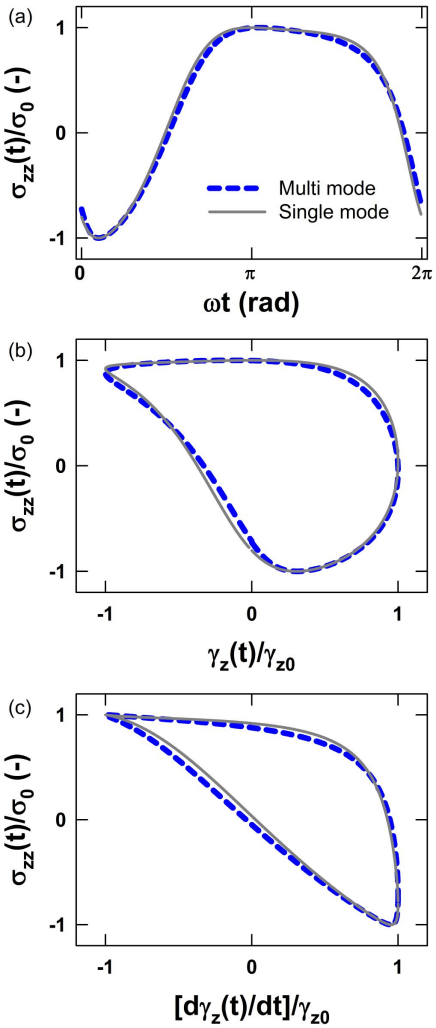

Fig. 5-13 (a) Normalized normal stress curve, (b) Lissajous plot of stress vs. strain, and (c) Lissajous plot of stress vs. strain rate of single (solid lines) and multi mode (dashed lines) prediction with EPTT model at strain amplitude 0.28.

Chapter 6. Nonlinear behavior of complex fluids under dynamic helical squeeze flow

6.1 Nonlinear response in DHSQ

In this study, the rheological measurement was carried out on a strain-controlled type rheometer (RMS800, TA Instruments) with the modified bottom fixture at room temperature. For raw data acquisition, a 16 bit analog digital converting (ADC) card (PCI-6052E; National Instruments) was used. The strain, torque and normal force signals were obtained simultaneously by the ADC card. Fig. 6-1(a) and 6-2(a) show the raw data of normal force and torque of the PEO4m4 from the strain sweep test γ_{z0} =0.027–0.11 ($\gamma_{\theta 0}$=0.016–0.064) at frequency ω=2 rad/s, respectively. The magnitude of torque and normal force increased with increasing strain amplitude as shown in Fig. 6-1(a) and 6-2(a). The strain $\gamma_z(t)$ and the normal stress are plotted in Fig. 6-1(b), the strain $\gamma_\theta(t)$ and the shear stress are displayed in Fig. 6-2(b). Both shear and normal stress signal show the nonsymmetric curve that means the difference in response of the material when the sample is compressed or extended. This nonsymmetric stress response was also reported in the first normal stress difference of polymer solution under LAOS [Nam *et al.*, 2008]. The stress curve shows distinct features in terms of stress shape

and the magnitude at both maximum and minimum.

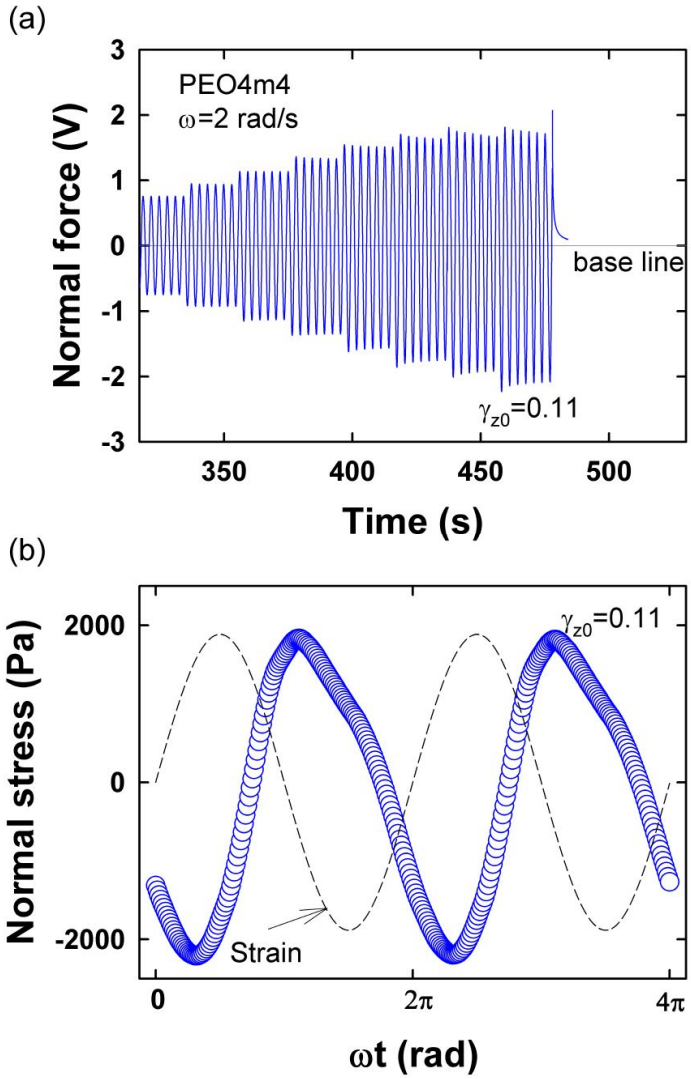

Fig. 6-1 (a) Normal force signal of PEO4m4 during the strain sweep test γ_{z0}=0.027-0.11, and (b) strain and normal stress σ_{zz} at the strain amplitude γ_{z0}= 0.11 ($\gamma_{\theta 0}$=0.06), at fixed frequency 2 rad/s.

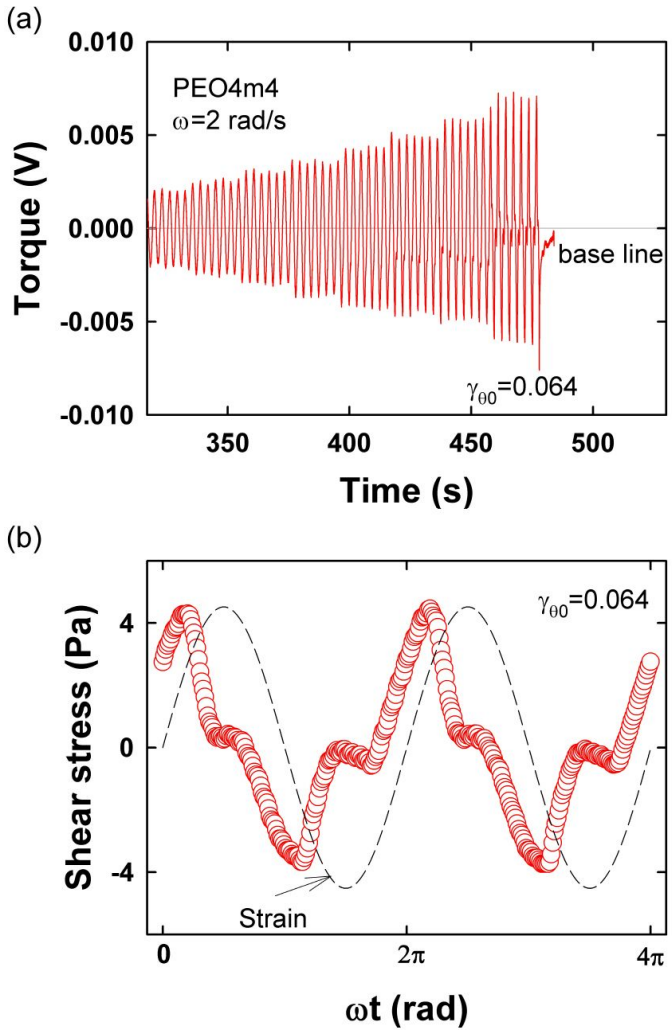

Fig. 6-2 (a) Torque signal of PEO4m4 during the strain sweep test $\gamma_{\theta 0}$=0.016-0.064, and (b) strain and shear stress $\sigma_{z\theta}$ at the strain amplitude $\gamma_{\theta 0}$=0.064 (γ_{z0}= 0.11), at fixed frequency 2 rad/s.

6.2 Normal stress curves and Lissajous plots

It was employed the stress shape analysis, and Lissajous loop analysis to characterize the raw stress signals of DHSQ. The stress shape analysis is to plot the stress curve as a function of time. This provides insightful and visual information during structural changes of the material when the deformation becomes large. The Lissajous loop of stress vs. strain or stress vs. strain rate is useful in observing the transformation of nonlinear responses. The Lissajous plot is elliptical in the linear regime, but become distorted in the nonlinear regime. Using the modified fixtures, it could be imposed the bi-directional deformations (γ_θ and γ_z) operating both oscillatory shear and oscillatory squeeze for DHSQ or the unidirectional deformation (γ_z) for OSQ. The DHSQ superposes the oscillatory squeeze flow on the oscillatory shear flow. The superposed flow provides the information on the coupling effect in the flow-induced microstructural changes [Vermant *et al.*, 1997]. The normal stress in OSQ was measured in order to compare with the normal stress in DHSQ. Here, the strain amplitude γ_{z0} in vertical direction was kept same in both DHSQ and OSQ.

Fig. 6-3 shows the normal stress of both dynamic helical squeeze flow (DHSQ) and oscillatory squeeze flow (OSQ) corresponding to the applied strain amplitude at frequency 2 rad/s. At strain amplitude γ_{z0}=0.0007

(corresponding $\gamma_{\theta 0}$=0.0004), the normal stresses are sinusoidal. As the strain amplitude increases, the normal stresses become distorted which means nonlinear response. The normal stress exhibits nonsymmetric response with respect to zero mean value of x-axis as the strain amplitude increases. This nonsymmetric response results from the different structural change of material during compression and extension. The nonsymmetric characteristics of normal stress were reported in experiments and simulations [Phan-Thien, 2000; Phan-Thien *et al*., 2000; Debbaut and Thomas, 2004; Jiang *et al*., 2004]. They also show forward-tilted shape as shown in most polymer solutions and melts in term of stress shape analysis. Within the measurable region, the stress curve of DHSQ is similar with that of OSQ as the strain amplitude increases. Although the bi-directional deformation was applied, the normal stress showed little difference compared with OSQ. It is inferred that the normal stress was not affected significantly by the deformation of oscillatory shear.

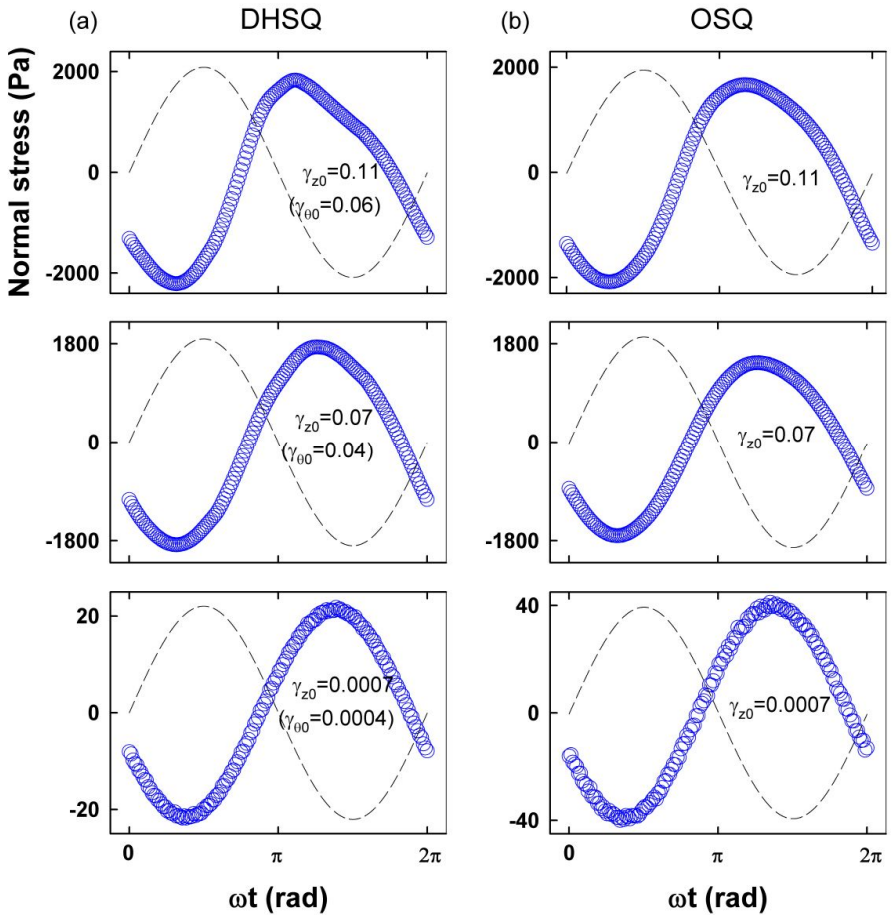

Fig. 6-3 The strain (dashed line) and the normal stress (solid line) signals of PEO4m4 at frequency ω=2rad/s; (a) dynamic helical squeeze flow (DHSQ), (b) oscillatory squeeze flow (OSQ).

Fig. 6-4 shows Lissajous plot of [$\sigma_{zz}(t)$ vs. $\gamma_z(t)$]. The area of the loop in [stress vs. strain] corresponds to the mechanical energy storage, and normally it increases with strain amplitude; that is, mechanical energy storage $\approx \frac{2H_0^2}{3R^2}\frac{1}{\pi\gamma_{z0}^2}\left|\oint\sigma_{zz}d(\dot{\gamma}_z/\omega)\right|$. At strain amplitude 0.0007, the Lissajous plot of [$\sigma_{zz}(t)$ vs. $\gamma_z(t)$] shows an ellipsoidal loop meaning the linear response in both DHSQ and OSQ. As the strain amplitude increases, the normal stress becomes nonsymmetric with respect to zero mean value of x-axis. This nonsymmetric response is a distinctive feature of normal stress at larger strain amplitude. When the strain is small, the Lissajous plot shows the symmetric loop which indicates the same response during compression and extension. However, at larger strain amplitude, the Lissajous plot exhibits nonsymmetry which implies the different response during compression and extension. In addition, the nonsymmetric normal stress also shows the difference in magnitude at both maximum and minimum, and the difference increases with the strain amplitude. This difference is negligible at low strain amplitude, but becomes pronounced at large strain amplitude. It is inferred as the result of the microstructural change when the viscoelastic fluid is compressed and extended.

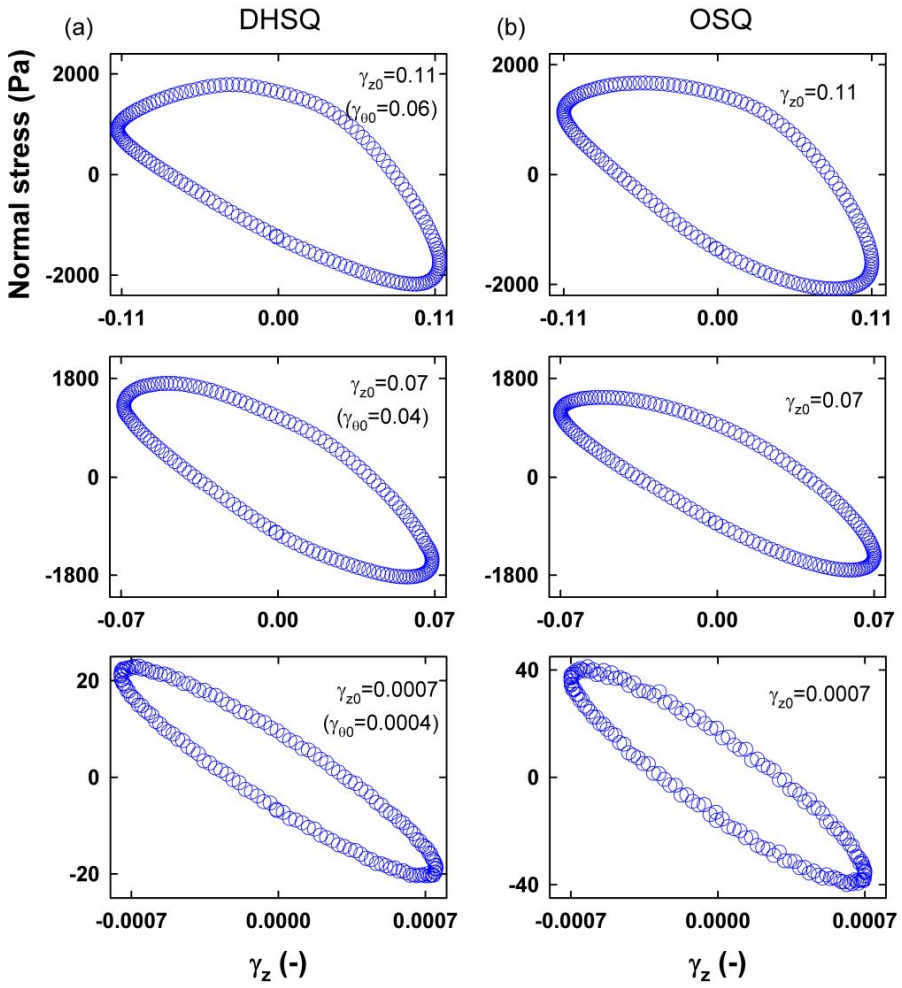

Fig. 6-4 Closed loops are normal stress vs. strain, [$\sigma_{zz}(t)$ vs. $\gamma_z(t)$] of PEO4m4 at frequency ω=2rad/s; (a) dynamic helical squeeze flow (DHSQ), (b) oscillatory squeeze flow (OSQ).

Fig. 6-5 shows the Lissajous plot of [$\sigma_{zz}(t)$ vs. $\dot{\gamma}_z(t)$]. The internal area of the loop in [stress vs. strain rate] corresponds to the mechanical energy dissipation, and normally decreases with strain amplitude; that is, mechanical energy dissipation $\approx \frac{2H_0^2}{3R^2}\frac{1}{\pi\gamma_{z0}^2}\left|\oint \sigma_{zz} d(\gamma_z)\right|$. At low strain amplitude, the Lissajous plot [$\sigma_{zz}(t)$ vs. $\dot{\gamma}_z(t)$] shows a slightly ellipsoidal loop close to the round loop which is observed in viscous fluid. However, the Lissajous plot shows nonsymmetric loop with respect to the zero mean value as the strain amplitude increases. This nonsymmetric loop indicates the different response during compression and extension in the same way as in [stress vs. strain]. The Lissajous plot shows similar shape between DHSQ and OSQ as the strain amplitude increases. It implies that the normal stress is rarely affected by the shear deformation within the measurable region.

Fig. 6-6 shows frequency dependence on the normal stress (symbol) signals and Lissajous plot for PEO4m4 at frequency ω=1, 2, 5rad/s and strain amplitude 0.07. There is no difference of stress curve with the applied frequency, but is of significance in Lissajous plot of [stress vs. strain] and [stress vs. strain rate]. As the imposed frequency increases, Lissajous plot displays the difference in both shape and area. The area of loop of [stress vs. strain rate] and [stress vs. strain] corresponds to energy storage and loss, respectively. The area of [stress vs. strain rate] increases with applied

frequency, but that of [stress vs. strain] decreases. In other words, the storage modulus was increased, but the loss modulus was decreased at higher frequency.

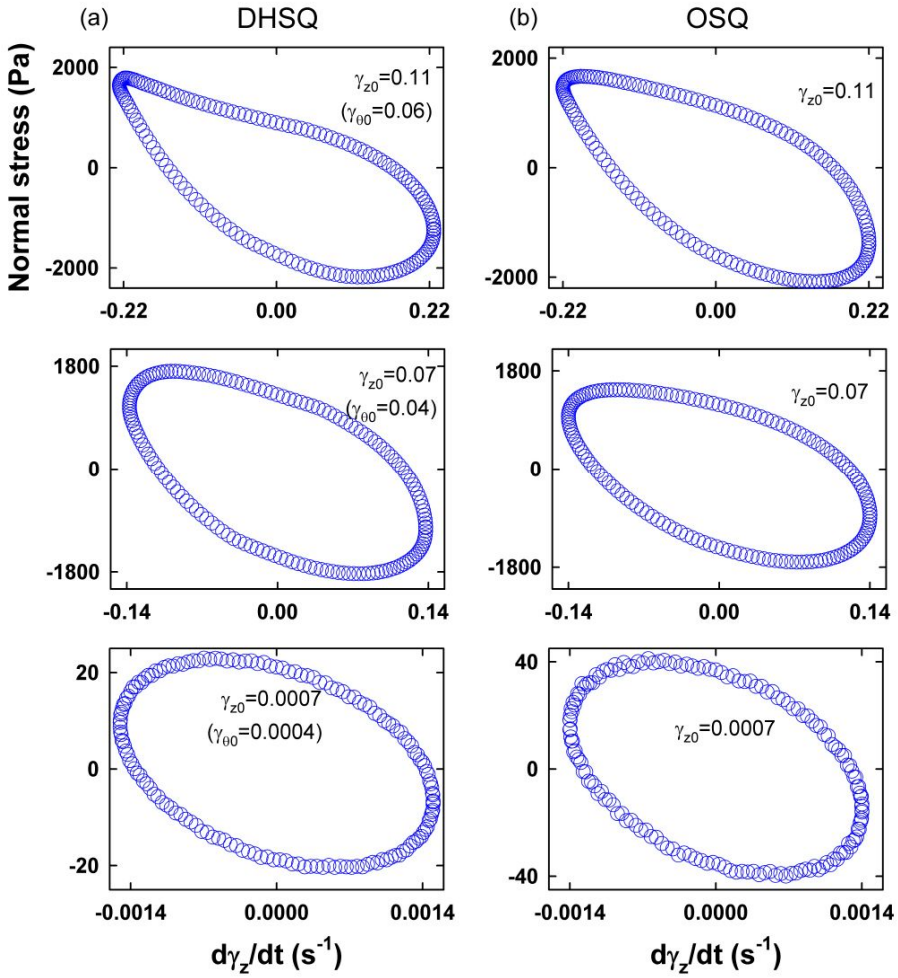

Fig. 6-5 Closed loops are normal stress vs strain rate, [$\sigma_{zz}(t)$ vs $\dot{\gamma}_z(t)$] of PEO4m4 at frequency ω=2rad/s; (a) dynamic helical squeeze flow (DHSQ), (b) oscillatory squeeze flow (OSQ).

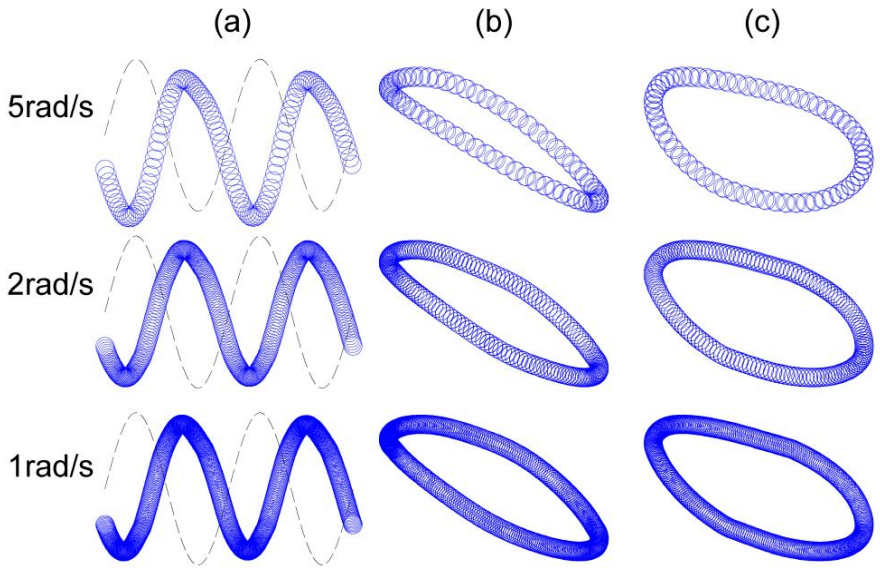

Fig. 6-6 (a) The strain (dashed line) and the normal stress (symbol) signals, (b) Normal stress vs. strain, [$\sigma_{zz}(t)$ vs. $\gamma_z(t)$], and (c) Normal stress vs. strain rate, [$\sigma_{zz}(t)$ vs $\dot{\gamma}_z(t)$] of PEO4m4 at frequency ω=1, 2, 5rad/s and strain amplitude 0.07.

As implied above, stress shape analysis, e.g. stress curve and Lissajous plot, was used to investigate the superposition effect of DHSQ by comparison with OSQ. Here, trigonometric polynomial is employed to analyze further for the superposition. The polynomial regression is introduced as follows;

$$F = A_0 + \sum_{n=odd}^{5}\left(A_n^1 \sin \omega t + A_n^2 \cos \omega t\right) + \sum_{n=even}^{4}\left(B_n^1 \sin \omega t + B_n^2 \cos \omega t\right) \quad (6\text{-}1)$$

where $A_n = \sqrt{\left(A_n^1\right)^2 + \left(A_n^2\right)^2}$ and $B_n = \sqrt{\left(B_n^1\right)^2 + \left(B_n^2\right)^2}$. The regression of normal force of periodic wave function was estimated up to n=5. Fig. 6-7 shows a comparison of coefficients (A_1, B_2) as a function of strain amplitude in OSQ and DHSQ. Coefficient A_1 corresponding to odd contribution was higher than B_2, and shows saturation curve with strain amplitude. Coefficient B_2 corresponding to even contribution displays exponential increase as the strain amplitude increase. This result means that the nonsymmetric characteristics of normal stress becomes more pronounced with the even contributions. On the other hand, the regression method has disadvantage that the coefficients cannot explain physical meaning of nonlinearity, exactly.

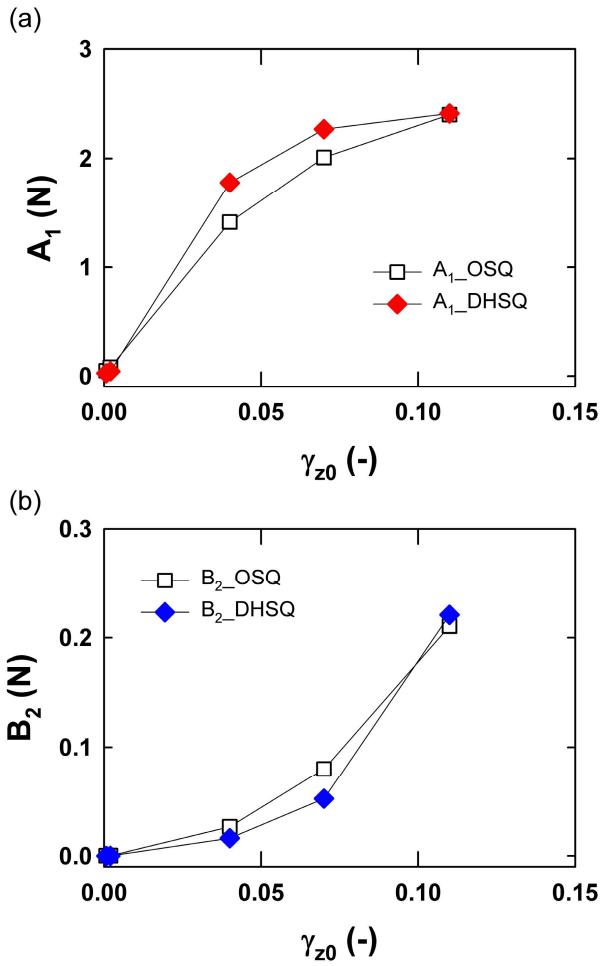

Fig. 6-7 Polynomial coefficients (A_1, B_2) as a function of strain amplitude in OSQ and DHSQ. The coefficients were obtained from the normal force signal using polynomial regression.

6.3 Shear stress curves and Lissajous plots

Fig. 6-8 shows the shear stress curves in dynamic helical squeeze flow (DHSQ) and oscillatory shear flow (OS). In both DHSQ and OS measurement, the shear stress signal was less clear than the normal stress due to relatively low intensity. Nevertheless, the shear stress shows a periodical response and a dramatic change even at small strain amplitude. At strain amplitude $\gamma_{\theta 0}$=0.02, the shear stress shows sinusoidal shape in both DHSQ and OS. As the strain amplitude increases, the stress signal keeps the sinusoidal shape under oscillatory shear flow. The shear stress in simple shear flow also exhibits symmetric response from low to large strain amplitude [Hyun *et al.,* 2003; 2006]. On the other hand, the shear stress in DHSQ becomes distorted and nonsymmetric as the strain amplitude increases. This shear stress shows nonsymmetric response at both positive and negative region with respect to zero mean value of x-axis. As shown in Fig. 6-8, the shear stress signal was first distorted at negative region where the sample is extended, and then become also distorted at positive region when the sample is compressed. It is clear that the shear stress exhibits nonlinear response earlier during extension than compression. From this stress analysis, it can be confirmed that shear stress of DHSQ is interrupted by extension and compression during oscillation.

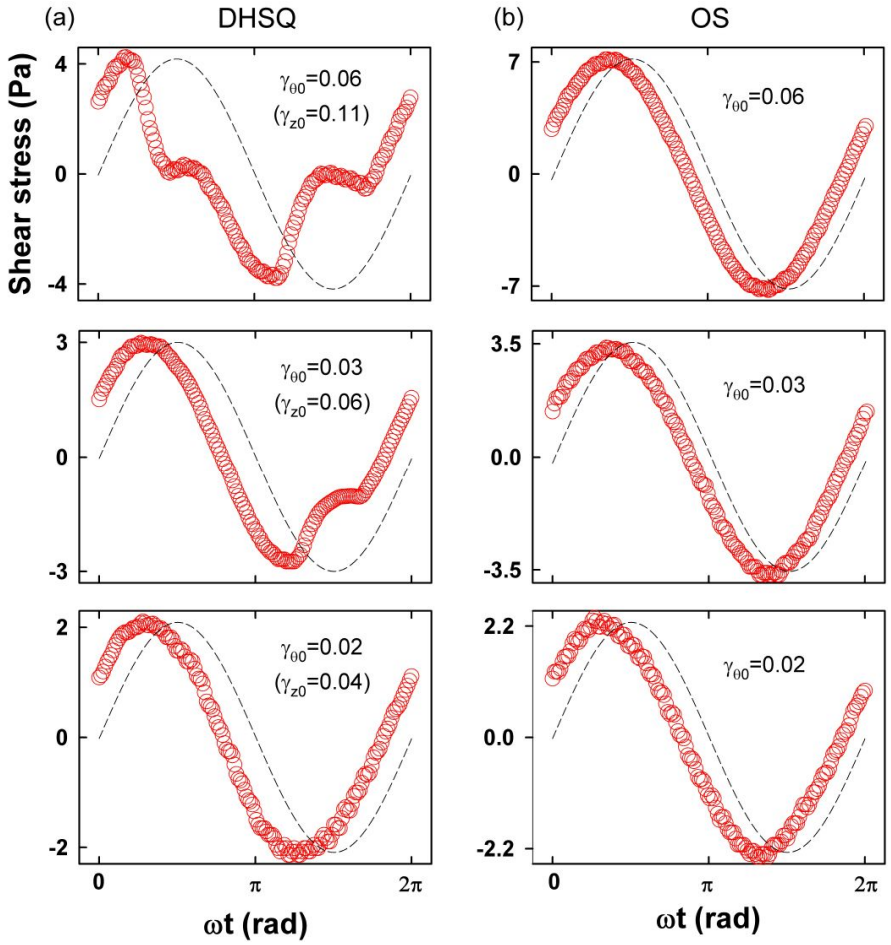

Fig. 6-8 The strain (dashed line) and the shear stress (solid line) signals of PEO4m4 at frequency ω=2rad/s; (a) dynamic helical squeeze flow (DHSQ), (b) oscillatory shear flow (OS).

Fig. 6-9 displays the Lissajous plot of both [$\sigma_{z\theta}(t)$ vs. $\gamma_{\theta}(t)$] at fixed frequency 2 rad/s. At strain amplitude $\gamma_{\theta 0}$=0.02 (γ_{z0}=0.04), the closed loop of [stress vs. strain] shows elliptical shape meaning linear response in both DHSQ and OS. As the strain amplitude increases, the loop of [$\sigma_{z\theta}(t)$ vs. $\gamma_{\theta}(t)$] in OS shows elliptical shape which means linear viscoelasticity, however the loop of [$\sigma_{z\theta}(t)$ vs. $\gamma_{\theta}(t)$] in DHSQ becomes distorted and nonsymmetric with respect to zero mean value. This nonsymmetric Lissajous pattern arises from nonsymmetric shear stress caused by the different response during compression and extension. Under DHSQ, the strong nonlinear response of shear stress is likely to occur by extension and compression during oscillation mainly.

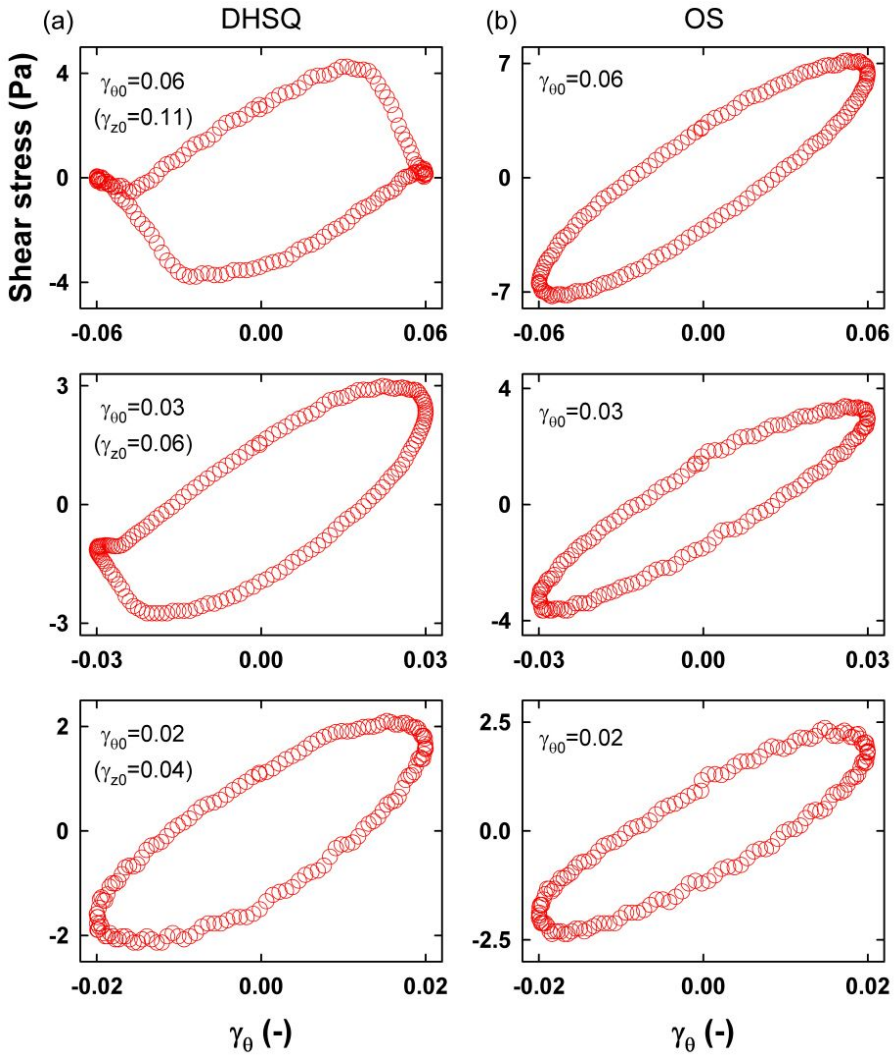

Fig. 6-9 Closed loops are shear stress vs. strain, [$\sigma_{z\theta}(t)$ vs. $\gamma_{\theta}(t)$] of PEO4m4 at frequency ω=2rad/s; (a) dynamic helical squeeze flow (DHSQ), (b) oscillatory shear flow (OS).

The Lissajous plot of [shear stress vs. strain rate] is plotted in Fig. 6-10. The Lissajous plots show different shape in DHSQ and OS at large strain amplitude. The Lissajous plot in OS keeps the round loop regardless of the strain amplitudes. However, the loop of DHSQ shows strong nonlinear and nonsymmetric response compared with that of OS at the same strain amplitude. This nonsymmetric loop is the result from the different response during compression and extension. The loop of DHSQ undergoes dramatic changes at large strain amplitude. The internal area of the loop which corresponds to the mechanical energy storage normally decreases with strain amplitude; that is, mechanical energy storage $\approx \frac{1}{\pi\gamma_{\theta 0}^2}\left|\oint \sigma_{z\theta} d\left(\dot{\gamma}_\theta/\omega\right)\right|$. At strain amplitude $\gamma_{\theta 0} = 0.06$, the area of the loop was very small compared to the one below $\gamma_{\theta 0} = 0.06$. It indicates that the energy storage decreased greatly due to the oscillatory squeeze flow at strain amplitude 0.06. It is supposed that the shear stress of DHSQ is interrupted by the oscillatory squeeze flow perpendicular to the shear flow. Fig. 6-11 displays frequency dependence on the shear stress and Lissajous plot of PEO4m4 at frequency ω=1, 2, 5rad/s and fixed strain amplitude 0.06. Unlike the normal stress and corresponding Lissajous plot in Section 6-2, the shear stress shows small deviation as the applied frequencies.

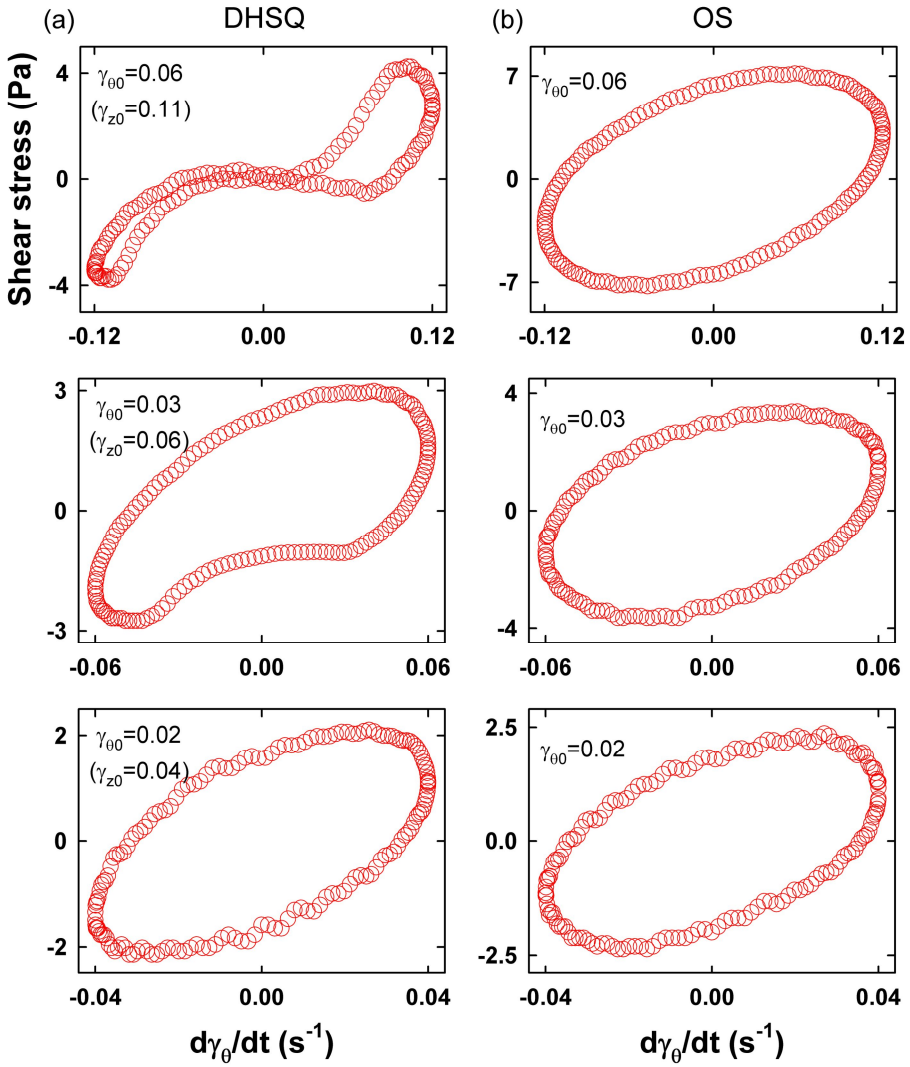

Fig. 6-10 Closed loops are shear stress vs strain rate, [$\sigma_{z\theta}(t)$ vs $\dot{\gamma}_{\theta}(t)$] of PEO4m4 at frequency ω=2rad/s; (a) dynamic helical squeeze flow (DHSQ), (b) oscillatory shear flow (OS).

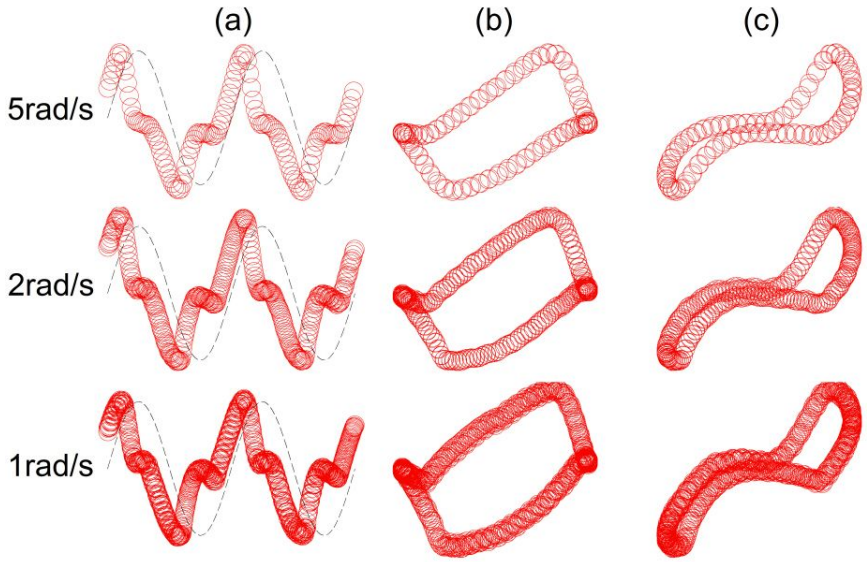

Fig. 6-11 (a) The strain (dashed line) and the shear stress (symbol) signals, (b) Shear stress vs. strain, [$\sigma_{z\theta}(t)$ vs. $\gamma_{\theta}(t)$], and (c) Shear stress vs. strain rate, [$\sigma_{z\theta}(t)$ vs $\dot{\gamma}_{\theta}(t)$] of PEO4m4 at frequency ω=1, 2, 5rad/s and strain amplitude 0.06.

It has been already proved that the stress and Lissajous plot with squared strain can be a useful method to verify the nonsymmetric response during compression and extension in section 4.6. Fig. 6-12 shows the Lissajous plot of the shear stress vs. squared strain, [$\sigma_{z\theta}(t)$ vs. $\gamma_{\theta}^{2}(t)$] and the shear stress and squared strain as a function of time at applied frequency 2rad/s. Here, solid line indicates compressive part and dashed line means the extensional part during oscillation. The Lissajous plot of the shear stress vs. squared strain, [$\sigma_{z\theta}(t)$ vs. $\gamma_{\theta}^{2}(t)$], shows the nonsymmetric characteristics of the response on the material with graphical presentation (in Fig. 6-12(a)). At strain amplitude 0.02, the one fold loop was symmetric for the stress=0. However, the symmetric loop became nonsymmetric at strain amplitude 0.06. This result clearly indicates that the shear stress of DHSQ is affected by OSQ flow perpendicular to OS flow. Fig. 6-12(b) decomposes the shear stress into extensional and compressive part. For the first time, the sinusoidal stress becomes distorted in negative region where the extensional deformation arises. Next, the distortion of stress signal also occurs in positive region where the compressive deformation take place.

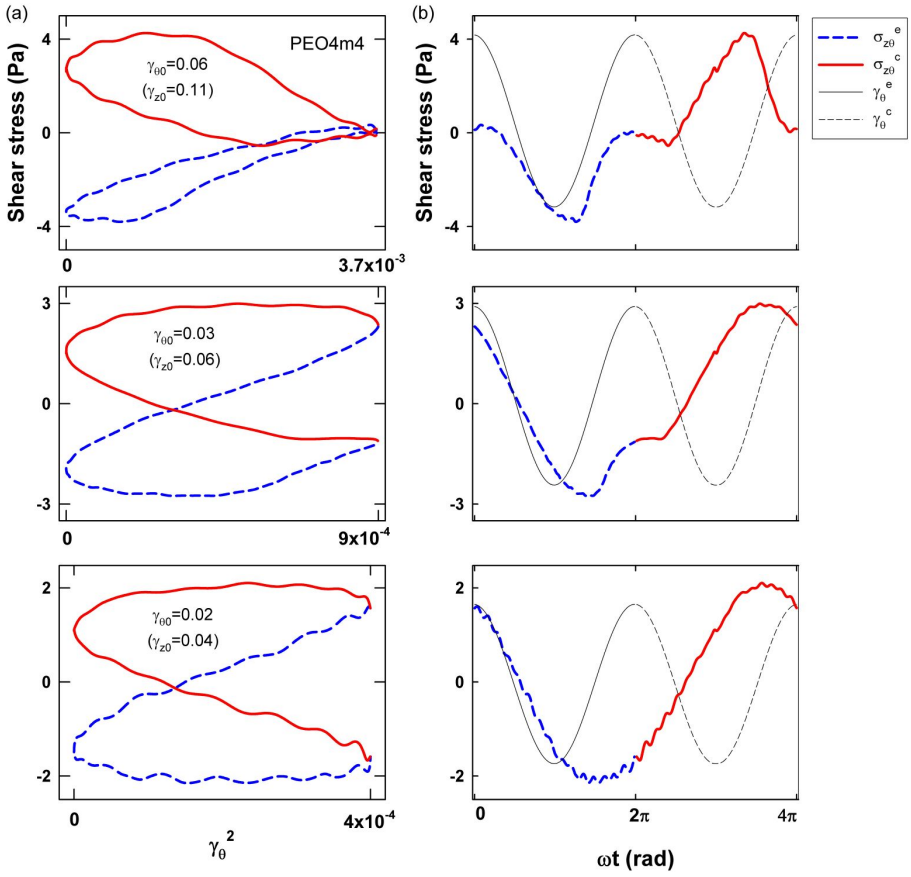

Fig. 6-12 (a) The Lissajous plot of the shear stress vs. squared strain, [$\sigma_{z\theta}(t)$ vs $\gamma_{\theta}^{2}(t)$]. (b) The shear stress and squared strain as a function of time at frequency 2rad/s. The solid line represents compressive part and dashed line indicates the extensional part of the shear stress of DHSQ.

As already mentioned in section 6.2, the polynomial regression was also performed with torque signal measured at strain amplitude 0.06. The torque signal can be fitted by trigonometric polynomial as given by

$$T = A_0 + \sum_{n=odd}^{5}\left(A_n^1 \sin \omega t + A_n^2 \cos \omega t\right) + \sum_{n=even}^{4}\left(B_n^1 \sin \omega t + B_n^2 \cos \omega t\right) \qquad (6\text{-}2)$$

where $A_n = \sqrt{\left(A_n^1\right)^2 + \left(A_n^2\right)^2}$ and $B_n = \sqrt{\left(B_n^1\right)^2 + \left(B_n^2\right)^2}$.

The polynomial regression up to n=5 has accurately modeled the experimental observation as shown in Fig. 6-13. Coefficients A_1 and B_2 present odd and even contribution of shear stress respectively. To explore the superposition effect of shear stress in DHSQ, coefficient A_1 of OS and DHSQ was plotted as a function of strain amplitude (in Fig 6-14(a)). The odd contribution of OS increases with constant slope linearly, but that of DHSQ becomes saturation curve with strain amplitude. The deviation of coefficient between OS and DHSQ was pronounced at larger strain region. Unlike coefficient A_1, however, coefficient B_2 of DHSQ increase with strain amplitude linearly as shown in Fig. 6-14(b). This result implies that the odd contribution becomes less dominant, while the even contribution becomes more dominant with strain amplitude by the superposition effect.

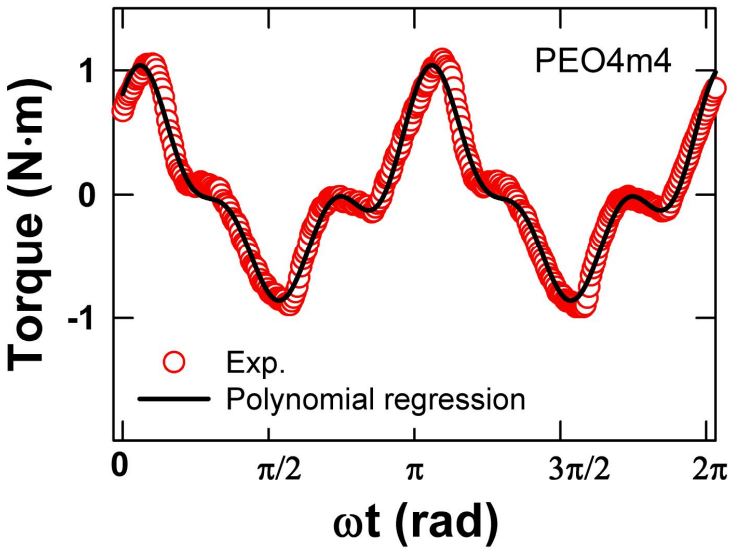

Fig. 6-13 The torque and regression curve using trigonometric polynomial for PEO4m4 at strain amplitude 0.06 and applied frequency 2 rad/s.

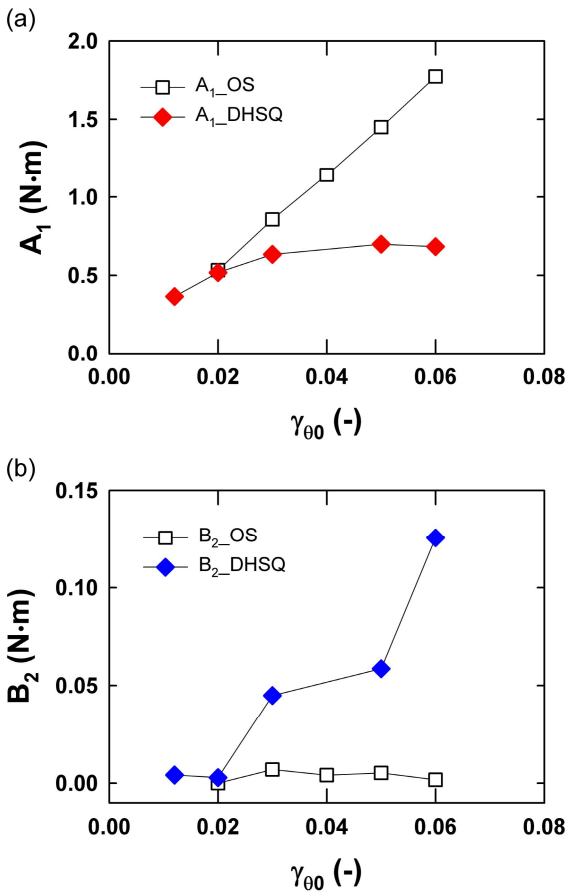

Fig. 6-14 Coefficients A_1 (a) and B_2 (b) as a function of strain amplitude in OS and DHSQ. The coefficients were obtained from the torque signal using polynomial regression.

6.4 Superposition effect

In the commercial software of a rheometer, the dynamic strain sweep produces the average viscoelastic properties even when the stress is non-sinusoidal at large strain amplitude. This non-sinusoidal stress includes higher order harmonics from Fourier transform analysis. This method has the limitation which the dynamic moduli use only the phase angle of fundamental harmonic and averaged magnitude from nonsinusoidal stress even under the nonlinear regime. Furthermore, they cannot consider nonsymmetric stress signal. For this reason, it is needed the measurement via the internal area of closed loop, [stress vs. strain] or [stress vs. strain rate]. Using the internal area, the moduli from shear and normal stress can be defined as follows:

$$E' \equiv \frac{2H_0^2}{3R^2}\frac{1}{\pi\gamma_{z0}^2}\left|\oint \sigma_{zz} d\left(\dot{\gamma}_z/\omega\right)\right|, E'' \equiv \frac{2H_0^2}{3R^2}\frac{1}{\pi\gamma_{z0}^2}\left|\oint \sigma_{zz} d\gamma_z\right|, \tag{6-1}$$

$$G' \equiv \frac{1}{\pi\gamma_{\theta 0}^2}\left|\oint \sigma_{z\theta} d\left(\dot{\gamma}_\theta/\omega\right)\right|, \quad G'' \equiv \frac{1}{\pi\gamma_{\theta 0}^2}\left|\oint \sigma_{z\theta} d\gamma_\theta\right|, \tag{6-2}$$

where $2H_0^2/3R^2$ is the additional geometrical factor for the moduli of normal stress [Cho *et al.*, 2005; Bell *et al*., 2006].

Fig. 6-15 shows the storage (E') and loss modulus (E'') obtained from the normal stresses of both DHSQ and OSQ. In the linear regime, the storage modulus (E') is nearly constant irrespective of strain amplitude as shown in

Fig. 6-15(a). However, in the nonlinear regime, the storage modulus decreases as the strain amplitude increases. For storage modulus, it shows strain-thinning behavior which is often observed in polymer solution and melt. The storage modulus shows no deviation between DHSQ and OSQ measurement. The loss modulus (E'') is nearly constant regardless of strain amplitude in the measurable region. This result means that the energy dissipation is maintained during the oscillation without reduction. The loss modulus which is related to energy dissipation is proportional to Lissajous area of [$\sigma_{zz}(t)$ vs. $\gamma_z(t)$]. In the simple shear flow, the loss modulus for PEO aqueous solution decreases with increasing strain amplitude in nonlinear regime after linear regime. In the DHSQ measurement, the moduli (E' , E'') are hardly affected by the oscillatory shear flow perpendicular to the oscillatory squeeze flow.

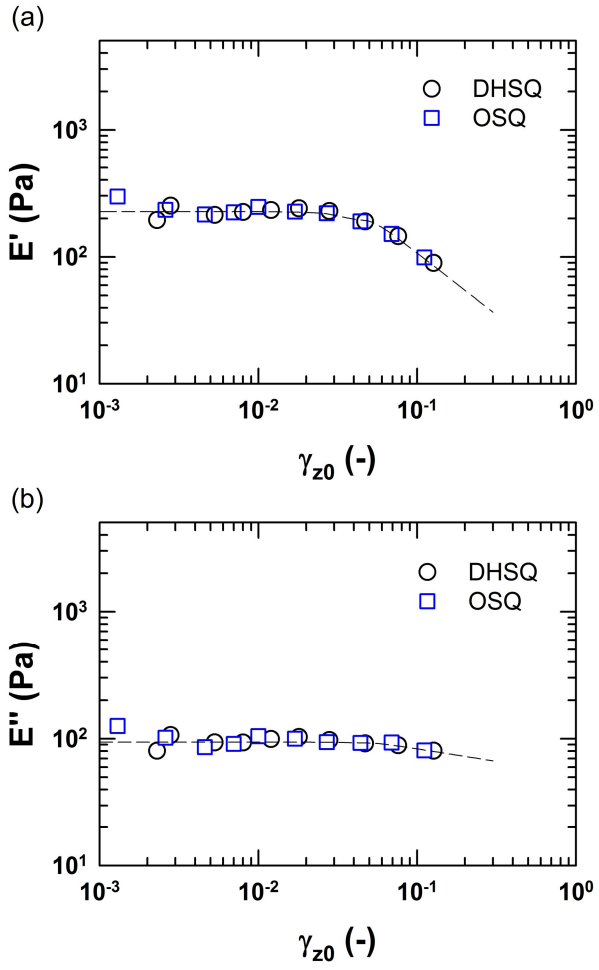

Fig. 6-15 (a) Storage modulus (E'), (b) loss modulus (E'') as a function of strain amplitude under DHSQ and OSQ at frequency 2 rad/s.

Fig. 6-16 shows storage (G') and loss modulus (G'') obtained by shear stress in DHSQ and OS. The storage modulus in DHSQ starts to decrease at much lower strain amplitude compared to OS as shown in Fig. 6-16(a). The modulus G' also shows very narrow linear regime compared with the oscillatory shear flow (OS). This storage modulus exhibits strain-thinning behavior over strain amplitude $\gamma_{\theta 0}$=0.01 in DHSQ. In the DHSQ measurement, the storage modulus was strongly affected by the oscillatory squeeze flow perpendicular to the oscillatory shear flow. But, simple shear flow shows strain-thinning behavior over strain amplitude $\gamma_{\theta 0}$=1. It is clear that the complex flow in DHSQ move toward low strain region the onset of nonlinear behavior of shear stress. On the other hand, as the strain amplitude increases, the loss modulus in DHSQ shows nearly constant value as the same manner with linear regime in OS. The loss modulus related with energy dissipation is not influenced by the oscillatory squeeze flow unlike the storage modulus. This result is easily confirmed through visual inspection of Lissajous plot, [shear stress vs. strain], as shown in Fig. 6-16(a). In the Lissajous plot of [shear stress vs. strain], the area of Lissajous loop keeps nearly constant value with increasing strain amplitude. Although the loss modulus is unvaried in the strain sweep test, the Lissajous plot shows strong nonlinear behavior compared to OS even under low strain amplitude as shown

in Fig. 6-16(a). From these facts, it can be concluded that DHSQ shifts the onset of nonlinear behavior to low strain region by coupling effect in the complex flow.

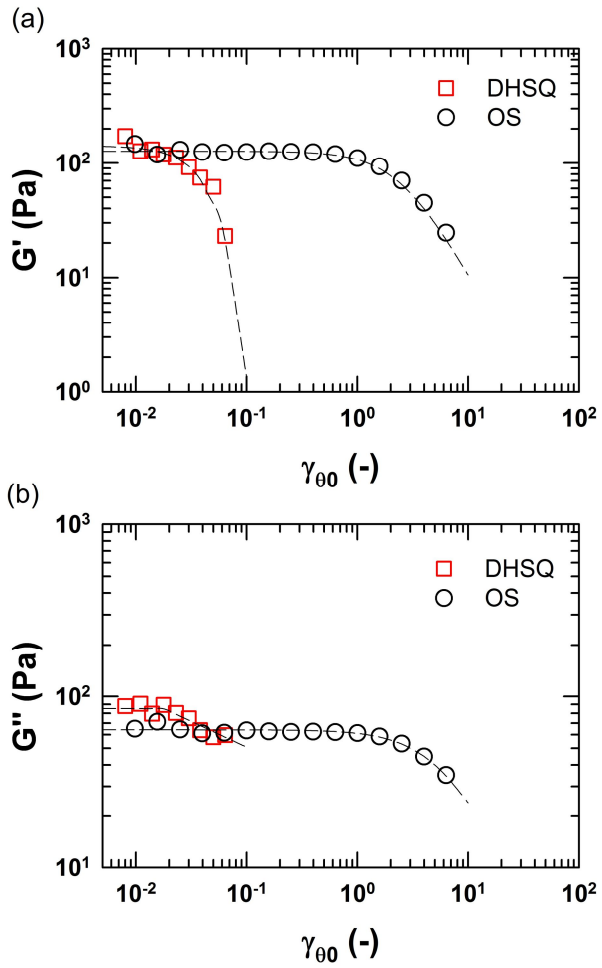

Fig. 6-16 (a) Storage modulus (G′), (b) loss modulus (G″) as a function of strain amplitude under DHSQ and OS at frequency 2 rad/s.

6.5 Model prediction

Model prediction was performed with five modes relaxation spectrum using EPTT model. It was well-known that EPTT model can predict rheological phenomena under a variety of different types of deformation reasonably well [Macosko, 1994]. For this reason, multi-mode EPTT model was employed to predict the normal and shear stress under DHSQ. Total stress and EPTT model are given by

$$\boldsymbol{\tau} = \sum_{i=1}^{6} \boldsymbol{\tau}_i \tag{6-3}$$

$$\boldsymbol{\tau}_i \exp\left(\frac{\varepsilon_i}{G_i} tr\boldsymbol{\tau}_i \right) + \lambda_i \boldsymbol{\tau}_{i(1)} + \lambda_i \xi_i \left(\mathbf{D} \cdot \boldsymbol{\tau}_i + \boldsymbol{\tau}_i \cdot \mathbf{D} \right) = 2\lambda_i G_i \mathbf{D} \tag{6-4}$$

Here, i denotes the number of relaxation mode.

Nonlinear parameter ε_i was obtained from the best fit on the reduced viscosity of strain sweep test in comparison of experiment and prediction (see in Fig. 6-17). Maxwell parameters (λ_i, G_i) was set through the linear viscoelastic moduli using nonlinear regression. The sets of parameters (λ_i, G_i) satisfied the experimental moduli completely (in Fig. 6-18). Table 6-1 lists the set of Maxwell parameters for PEO4m4.

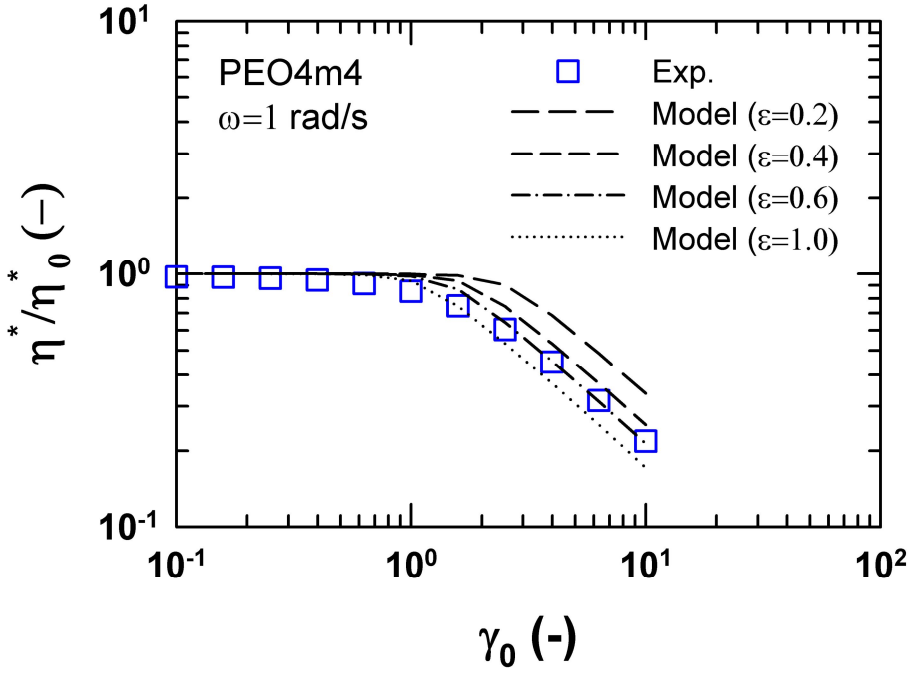

Fig. 6-17 Reduced shear viscosity from experiment (symbols) and EPTT model (dashed lines) at ω=1rad/s.

Table 6-1 Discrete relaxation spectra of five modes for PEO4m4. The linear viscoelastic data were used to determine the Maxwell parameters (λ_i, G_i). The nonlinear parameter ε_i was determined by the best fit with the strain sweep data of the experiment.

i	λ_i (s)	G_i (Pa)	ε_i
1	0.010	133.799	0.6
2	0.056	68.359	0.6
3	0.316	70.125	0.6
4	1.778	45.214	0.6
5	11.000	30.147	0.6

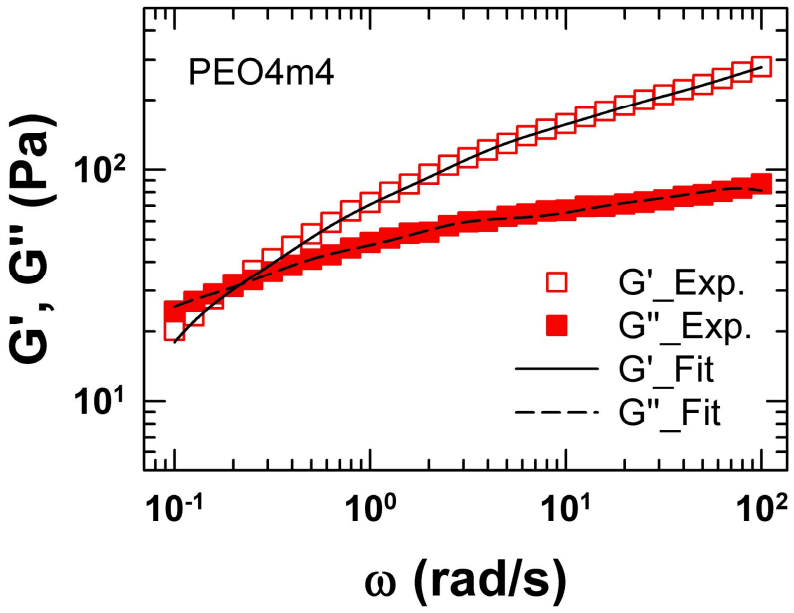

Fig. 6-18 The linear viscoelastic moduli as a function of frequency for PEO4m4. Fitting curves were plotted with the generalized Maxwell model with five modes.

Numerical simulation was examined to predict the experimental observation under DHSQ. Experimental data of PEO solution (PEO4m4) was compared with simulation results calculated by EPTT model (ε=0.6, ξ=0). First, prediction for normal stress which shows nonsymmetry has been performed with strain amplitude 0.11 (see in Fig. 6-19). The stress shape analysis, e.g. stress curve and Lissajous plot, was used to compare experiment to prediction. In spite of the high complexity of DHSQ flow, model prediction was in good agreement with that obtained by the experiment in DHSQ.

On the other hand, prediction of the shear stress shows larger deviation as compared with experimental data as shown in Fig. 6-20. There are no agreement in comparison of experiment and prediction in terms of stress curve and Lissajous plot. A practicable explanation of the discrepancy lies in determining the set of nonlinear parameters (ε_i, ξ_i). The model prediction can be very sensitive to the adaptation of the non-linear parameters as implied above. It may be supposed that the best-fit to the shear viscosity (in Fig. 6-17) is not the best-fit to the shear stress in DHSQ. Furthermore, there is another possibility that the constitutive equation is not enough to predict the nonlinear response of viscoelastic fluids under DHSQ flow.

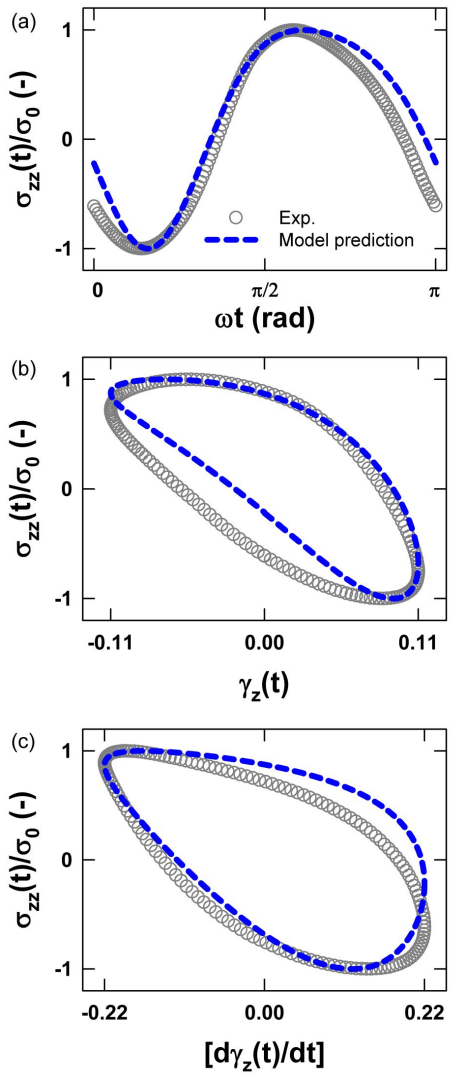

Fig. 6-19 (a) Normalized normal stress curves, (b) Lissajous plot of stress vs. strain, and (c) Lissajous plot of stress vs. strain rate of single (solid lines) and multi mode (dashed lines) prediction with EPTT model at strain amplitude 0.11.

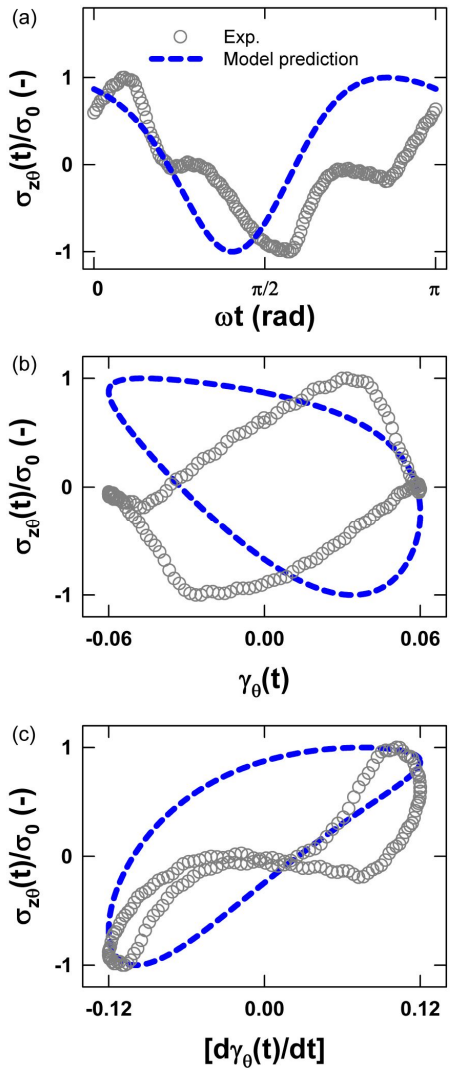

Fig. 6-20 (a) Normalized shear stress curves, (b) Lissajous plot of stress vs. strain, and (c) Lissajous plot of stress vs. strain rate of single (solid lines) and multi mode (dashed lines) prediction with EPTT model at strain amplitude 0.06.

6.6 Non-colloidal hard sphere

The rheology of colloidal dispersions has received the spotlight by scientists and engineers working in academy and industry. Colloidal dispersion refers to the dispersed phase of a two-component or more system. The type of colloidal dispersion can be often classified as follows: suspension, emulsion, and foam. They can be liquid or solid particles dispersed in a gaseous, liquid, or solid medium. Suspension comprise of solid particles suspended in a liquid medium and shows totally different behavior as the volume fraction of solid particles. Emulsion whose the dispersed and the continuous phase are liquid is a mixture of two or more liquids that are normally immiscible each other. Examples of emulsions include ice cream, butter, vinaigrettes, milk, mayonnaise, and so on. Lastly, foam is a matter which is formed by entrapping gas in a liquid or solid.

In this thesis, suspension of non-colloidal hard sphere was investigated under DHSQ. The non-colloidal suspension with particle size of a few micrometer or more can neglect the contributions from Brownian motion, interparticle force, and so on. For this reason, hydrodynamic force dominates the rheological behavior of the non-colloidal suspension. Concentrated suspension of non-colloidal particles gives rise to a very complex

hydrodynamic phenomena, which leads to the possibility of mutual effects, coupling between flow and microstructure, and many body interactions between the solid particles [Coussot and Wagner, 2009]. Furthermore, industrial suspensions often have both a wide range of particle size distribution and many complex interactions which arise from a variety of different chemical surfaces, solvent mixtures, added surfactants, polymers, and salts [Coussot and Wagner, 2009]. They also take into account the nonlinear effects such as normal force, shear migration, shear banding, sedimentation, thixotropy, aging, shear thickening, and jamming which cause unexpected bad situation in materials processing industry.

Shear thickening or strain stiffening behavior of non-colloidal suspension has been highly studied for several decades. The shear thickening points out that apparent viscosity increases with applied strain or rate. Further increasing the volume fraction of solid particle leads to a more rapid rise in apparent viscosity of rheological property. Possible demonstration is order-disorder transition and hydro-cluster formation which have been heated controversy for explaining the shear thickening behavior [d'Haene *et al.*, 1993; Hoffman, 1998]. Even though concentrated suspension shows interesting response in previous literatures, they have been studied in simple shear flow only. In this thesis, dynamic helical squeeze flow was introduced to

investigate on nonlinear characteristic of the non-colloidal hard sphere suspension. The nonlinear behavior of DHSQ can provide more information on the suspension than that of simple shear flow.

Fig. 6-21 displays strain stiffening behavior of the moduli obtained from normal stress of PMMA20 dispersed in PB with the volume fraction ϕ=0.5 at frequency 2, 5, 10 rad/s. The strain stiffening is observed over the critical strain amplitude where the moduli start to increase after strain thinning. The elastic modulus E' shows different critical strain amplitude as the applied frequencies, 2, 5, and 10 rad/s. Critical strain amplitude increased with frequency in DHSQ: 0.013 for ω=2 rad/s, 0.024 for ω=5 rad/s, and 0.055 for ω=10 rad/s. On the other hand, viscous modulus E'' begins to increase at consistent strain amplitude regardless of applied frequency. This tendency corresponded with that reported for highly concentrated suspension under LAOS (large amplitude oscillatory shear) flow [Nam *et al.*, 2010]. It concludes that the storage modulus from normal stress was affected by characteristic flow time ($t \sim 1/\omega$) under DHSQ flow. Fig. 6-22 shows comparison of storage and loss moduli of PMMA20 dispersed in PB under OSQ and DHSQ with the volume fraction ϕ=0.5 at frequency 10 rad/s. The storage modulus of OSQ and DHSQ produces strain stiffening behavior as the strain amplitude increases. At low strain amplitudes, OSQ and DHSQ have no

difference in the storage modulus, but they exhibit a difference at higher strain amplitude. Critical strain amplitude of storage modulus was lower in OSQ than in DHSQ. The storage modulus of OSQ increased with a gentle slope gradually, but that of DHSQ increased with a steep slope abruptly over the critical strain amplitude. This result means that normal stress in DHSQ is affected by the superposition of oscillatory shear flow and oscillatory squeeze flow which act perpendicular to each other. The effect of superimposed flow became pronounced at larger strain amplitude. On the other hand, loss modulus of both OSQ and DHSQ did not show any significant difference as the strain amplitude increases. Unlike the energy storage, the energy loss was hardly affected by the complex flow field induced by DHSQ compared with that of OSQ.

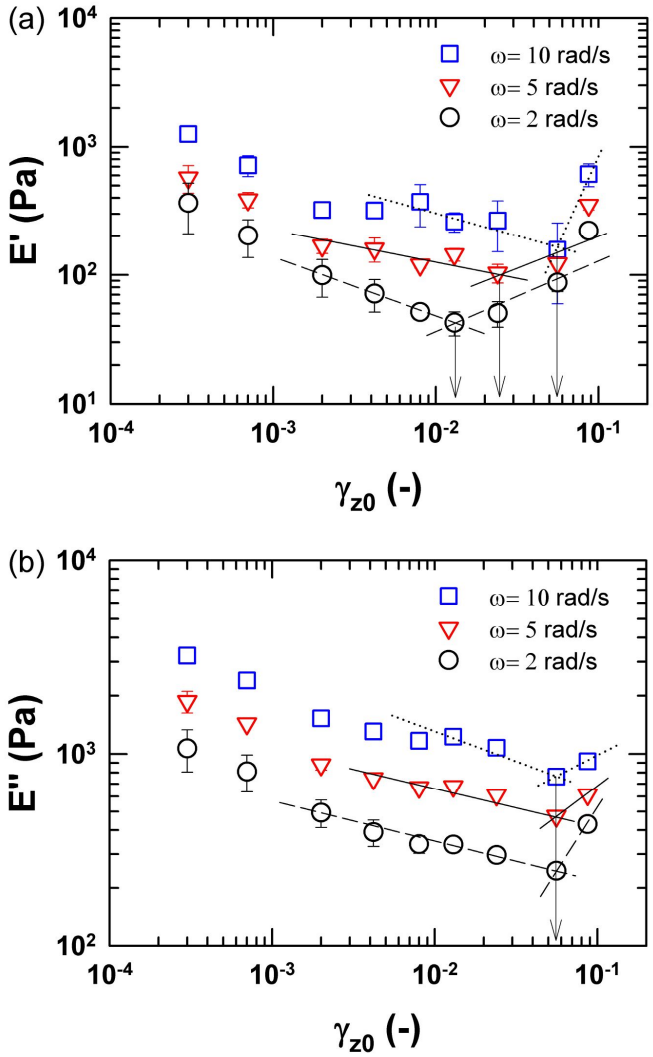

Fig. 6-21 Strain stiffening behavior of storage (a) and loss (b) moduli from the normal stress of PMMA20 dispersed in PB with the volume fraction ϕ=0.5 at frequency 2, 5, 10 rad/s. The arrows indicate the critical strain amplitude where the modulus begins to increase.

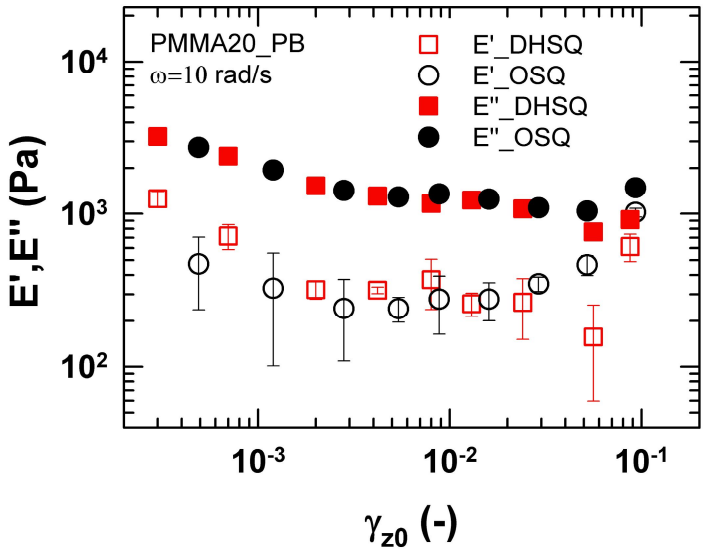

Fig. 6-22 Comparison of storage and loss moduli in DHSQ and OSQ of PMMA20 dispersed in PB with the volume fraction ϕ=0.5 at frequency 10 rad/s.

The moduli from shear stress also shows strain stiffening behavior as shown in Fig. 6-23., however, the moduli calculated by shear stress presents an opposite tendency compared with those from normal stress. All of storage and loss modulus show that onset point of critical strain amplitude decreased at higher frequency in DHSQ flow. The critical strain amplitude was smaller in loss modulus than in storage modulus at consistent frequency. This result emphasizes the significance that non-colloidal suspension in DHSQ can be strongly affected by the characteristic flow time, unlike in simple shear flow. Fig. 6-24 displays comparison of storage and loss modulus from shear stress obtained by OS and DHSQ of PMMA20 dispersed in PB with the volume fraction ϕ=0.5 at applied frequency 10 rad/s. The critical strain amplitude of both G' and G'' was lower in DHSQ than in OS: 0.05 for DHSQ and 0.2 for OS in storage modulus, 0.009 for DHSQ and 0.6 for OS in loss modulus. This showed similar tendency with polymer solutions which the moduli begin to decrease with strain amplitude (see in section 6.4). It intimates that the shear stress of non-colloidal suspension start to energy dissipation even at very small deformation under DHSQ flow.

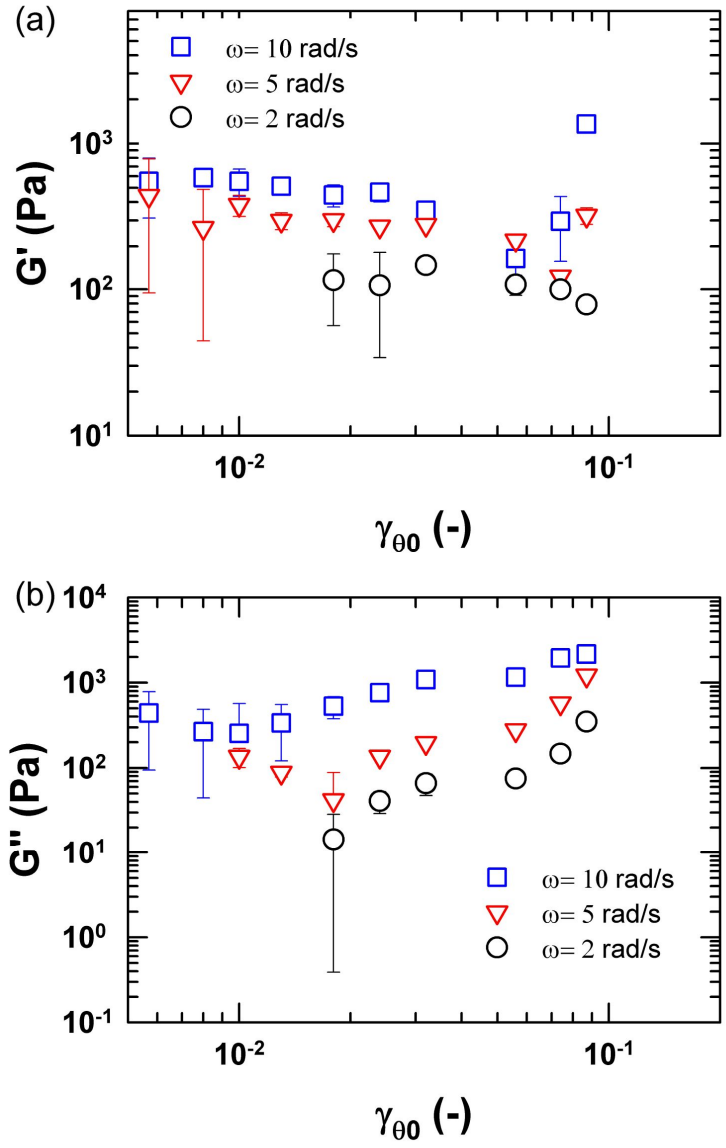

Fig. 6-23 Strain stiffening behavior of storage (a) and loss (b) moduli from shear stress of PMMA20 dispersed in PB with the volume fraction ϕ=0.5 at frequency 2, 5, 10 rad/s.

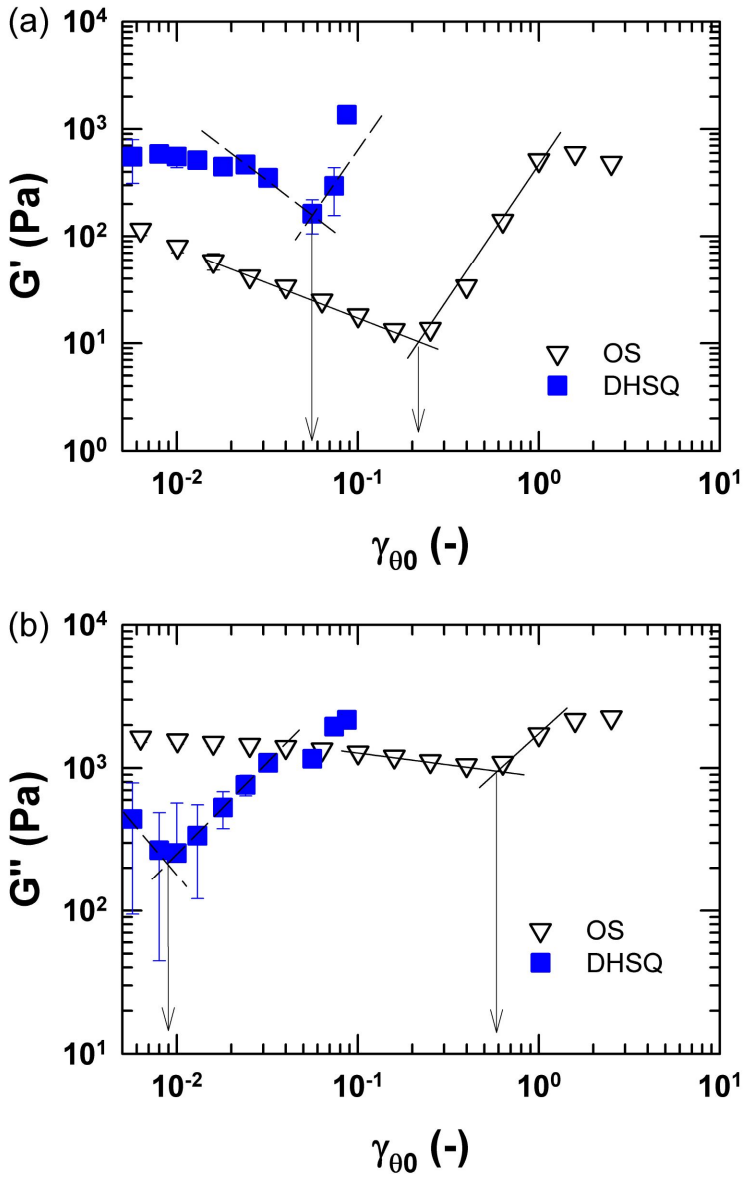

Fig. 6-24 Comparison of storage (a) and loss (b) modulus from shear stress obtained by OS and DHSQ of PMMA20 dispersed in PB with the volume fraction ϕ=0.5 at frequency 10 rad/s.

The onset point of strain stiffening was started in lower strain amplitude as the volume fraction increases under large amplitude oscillatory shear flow [Nam *et al*., 2010]. This tendency was observed in steady rate test for concentrated suspension with non-colloidal hard sphere [Barnes, 1989]. Even though the previous literatures show significant difference as volume fraction under simple flow, DHSQ flow does not display serious difference. As shown in Fig. 6-25, critical strain amplitude of storage and loss moduli was similar with the volume fraction 0.3, 0.4, and 0.5. It means that the onset of strain stiffening behavior may be almost not affected by the volume fraction of solid particles suspended in continuous medium under DHSQ flow. Unlike the normal stress, the shear stress shows substantial difference as the volume fraction under DHSQ flow. As the volume fraction increases, the strain stiffening behavior becomes more pronounced with increasing strain amplitude as shown in Fig. 6-26. From the results, it was confirmed that the superimposed flow can enhance strain stiffening in shear stress of complex fluids by adding solid particle.

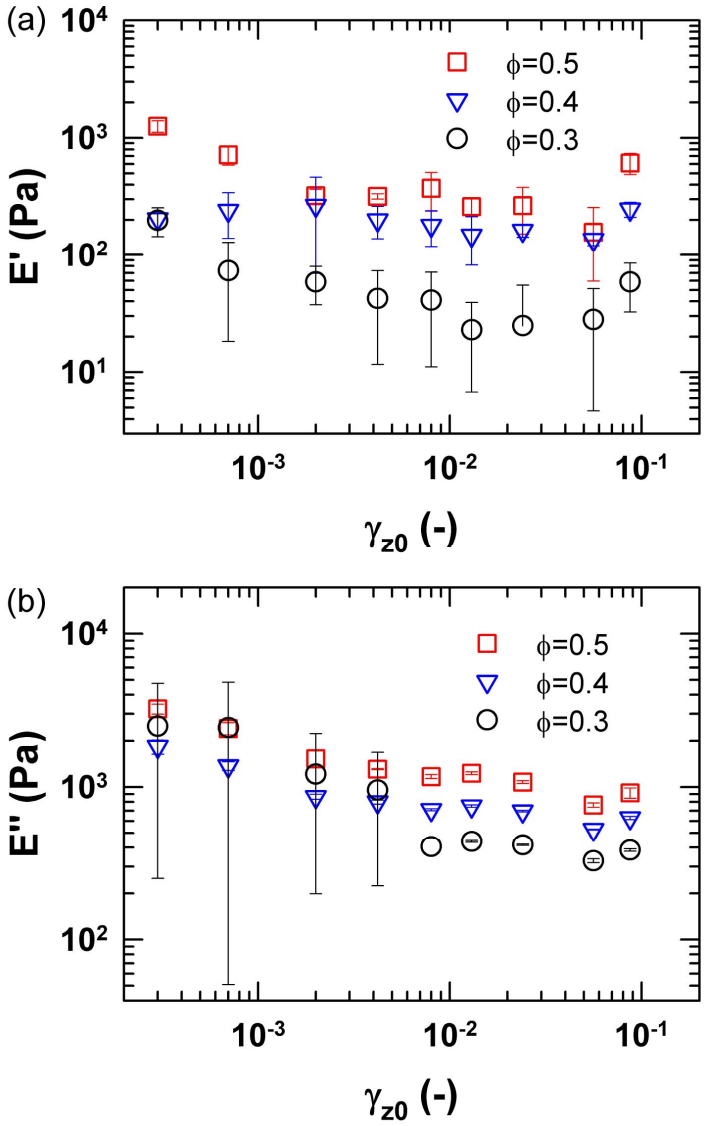

Fig. 6-25 Storage (a) and loss (b) moduli from normal stress of PMMA20 dispersed in PB under DHSQ with the volume fraction ϕ=0.3, 0.4, 0.5 at frequency 10 rad/s.

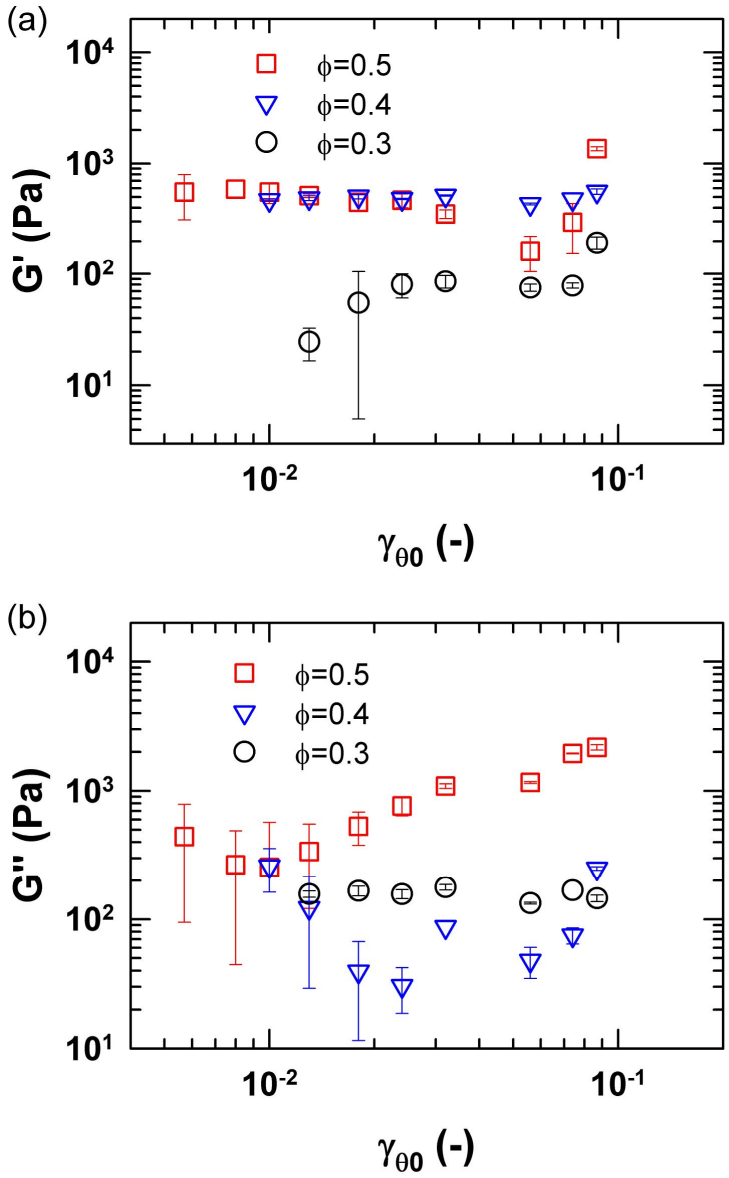

Fig. 6-26 Storage (a) and loss (b) moduli from shear stress of PMMA20 dispersed in PB under DHSQ with the volume fraction ϕ=0.3, 0.4, 0.5 at frequency 10 rad/s.

Two different kinds of hard particle, PMMA20 and PMMA50, were used to investigate an effect of particle size under DHSQ. Fig. 6-27 shows storage and loss moduli obtained from normal stress of PMMA20 and PMMA50 dispersed in PB under DHSQ with the volume fraction ϕ=0.5. Under large amplitude oscillatory shear flow, the onset of strain stiffening has no concern with particle size a [μm] (or diameter) [Nam *et al*., 2010]. However, the shear thickening in steady shear flow was delayed with decreasing the average particle size [Barnes, 1989]. The strain stiffening of normal stress for DHSQ was not influenced by the average particle size like the result for non-colloidal suspension under LAOS. Fig. 6-28 displays storage and loss moduli from shear stress of PMMA20 and PMMA50 dispersed in PB with the volume fraction ϕ=0.5 under DHSQ. Strain stiffening behavior of shear stress in DHSQ was significantly influenced by the particle size. The storage and loss moduli started the onset of strain stiffening at lower for PMMA20 than for PMMA50. Possible answer is that the contact between particles occurs more frequently on smaller average particles during DHSQ flow. In summary, non-colloidal hard sphere suspensions under DHSQ are dependent of the parameters: applied frequency, particle size, volume fraction. The DHSQ proposed in this thesis may provide useful information for understanding the responses of concentrated

suspensions in more complicated flow field than simple flow

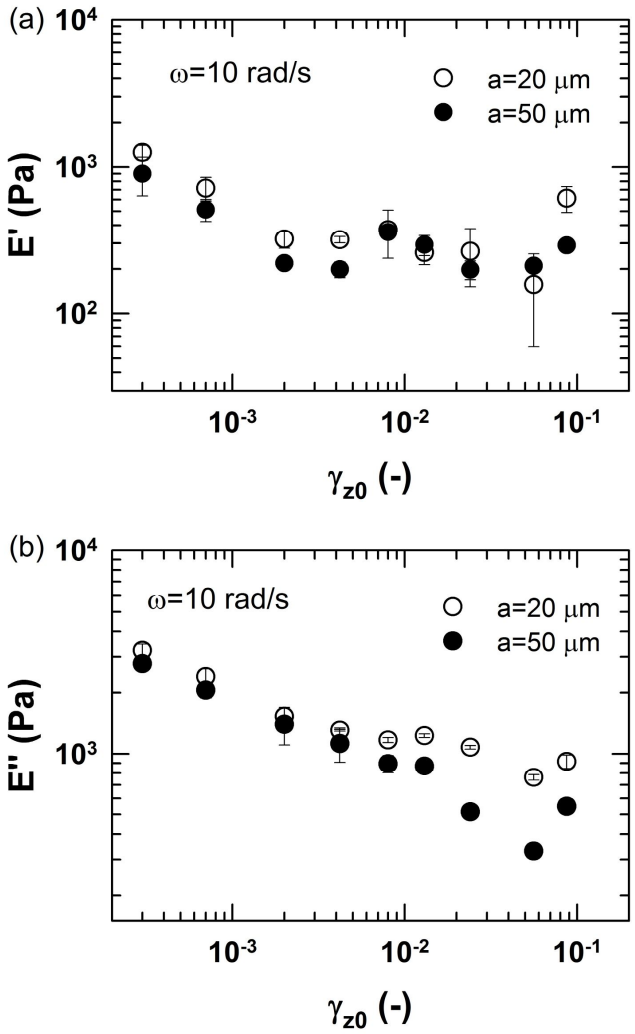

Fig. 6-27 Storage (a) and loss (b) moduli from normal stress of PMMA20 and PMMA50 dispersed in PB under DHSQ with the volume fraction ϕ=0.5 at frequency 10 rad/s.

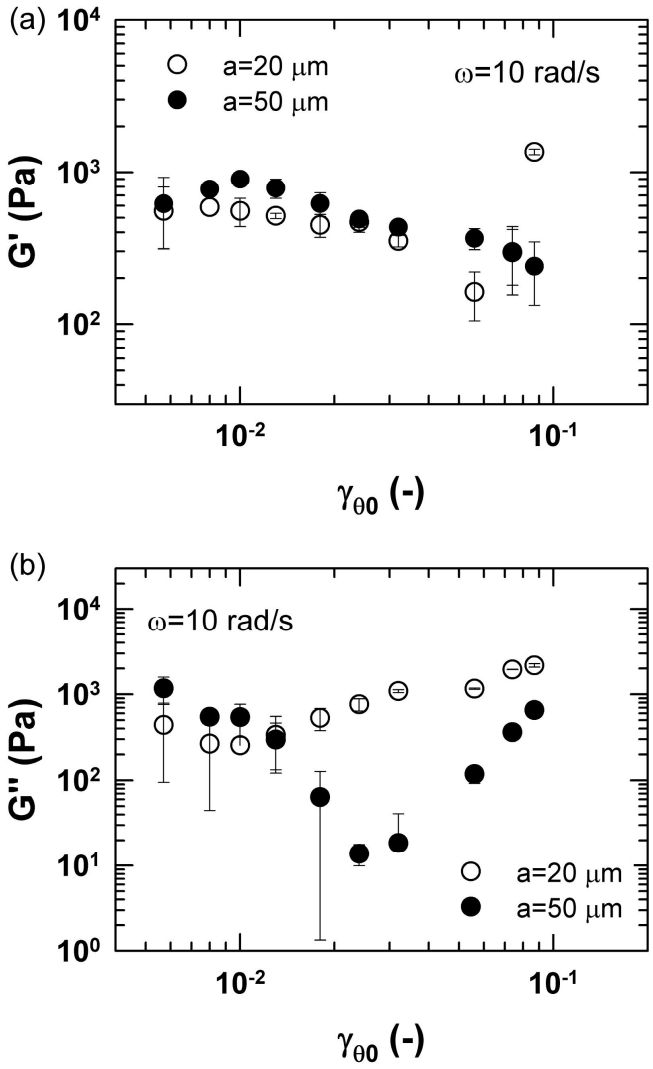

Fig. 6-28 Storage (a) and loss (b) moduli from shear stress of PMMA20 and PMMA50 dispersed in PB under DHSQ with the volume fraction ϕ=0.5 at frequency 10 rad/s.

Chapter 7. Conclusions and outlook

The rheological behavior of complex fluids under oscillatory squeeze flow and dynamic helical squeeze flow was investigated. The normal stress showed more complicated responses than in simple shear flow; such as the appearance of all higher harmonics and nonsymmetric stress signals. As the strain amplitude increases, the normal stress became nonsymmetric in terms of both magnitude and shape in positive and negative region of oscillation. This unique feature may be considered as the result of the microstructural change when the viscoelastic fluid is compressed and extended. In the loop of the Lissajous plot, normal stress vs. strain or normal stress vs. strain rate, the trace follows different paths as the sample is compressed or extended. The loop of the elastic Lissajous plot becomes nonsymmetric curvilinear, while the loop of viscous Lissajous plot keeps symmetry even at large strain amplitude. The loop of normal stress vs. squared strain showed a dramatic change, from one-fold symmetry to two-fold nonsymmetry with increasing strain amplitude. From the Fourier transform analysis, it was confirmed that the nonsymmetric stress originates from the contribution of even harmonics. This platform will be useful in characterizing the rheological responses of complex fluids in

oscillatory squeeze flow, which is a little bit more complex flow field than simple shear flow but still well-defined and controllable.

It was also predicted the nonsymmetric response of normal stresses under oscillatory squeeze flow by model calculation. The UCM, Giesekus, and EPTT model were employed to predict the nonsymmetric stress which is one of the distinctive features of the oscillatory squeeze flow. The model prediction was compared with experimental results in terms of stress shape, Lissajous plot, and Fourier transformation. Furthermore, it was examined and compared the performance of the constitutive equations in terms of nonlinear and nonsymmetric response under oscillatory squeeze flow. All the constitutive equations predicted the nonsymmetric characteristics of normal stresses in nonlinear regime under oscillatory squeeze flow. However, the UCM model displayed unrealistic result such that the mechanical energy storage is nearly constant and the mechanical energy loss decreases with strain amplitude. In both experiment and simulation, the normal stress changed from sinusoidal to distorted shape, and varied from symmetric to nonsymmetric shape with respect to zero mean value as the strain amplitude increases. In comparison with experiment, the models predicted the nonsymmetric stresses and corresponding nonsymmetric Lissajous loop

except for UCM model, but there existed fairly large deviation between model prediction and experiment. They could not predict the one-fold nonsymmetric loop in [stress vs. strain rate] at large strain amplitude. A possible cause of the discrepancy lies in determining the set of nonlinear parameters and in considering the relaxation spectrum. In FT analysis, the model prediction showed all high harmonic contributions of both odd and even harmonics, and the relative intensity ($I_{n/1}$) was proportional to the (n-1)th power of strain amplitude in accordance with the experimental data.

Finally, the design and methodology for rheological measurements on materials under dynamic helical squeeze flow (DHSQ) are suggested. The rheological behavior of complex fluids was investigated under DHSQ of both oscillatory shear (OS) and oscillatory squeeze flow (OSQ), and then also established the theoretical platform for the interpretation of experimental data. Within the measurable region, the normal stress curve of DHSQ is similar with that of OSQ as the strain amplitude increases. It means that the normal stress is not significantly affected by the deformation of oscillatory shear. In the DHSQ, the stress shape and Lissajous plot of shear and normal stress showed dramatic change and nonsymmetric signal as the strain amplitude increases. This nonsymmetric response may be considered as the result of the

microstructural change when the viscoelastic fluid is compressed and extended. The onset of nonlinear response in shear stress was faster in dynamic helical squeeze flow than in simple shear flow. It is inferred that the shear stress is strongly influenced by the oscillatory squeeze flow perpendicular to the oscillatory shear flow. It is concluded that the rheological behavior under dynamic helical squeeze flow provides useful information for the materials in more complicated flow-induced environment compared with a simple flow.

Nomenclature

a: Particle diameter [μm]

a : Deformation amplitude in vertical direction (or z-direction) [mm]

α : Inclined angle [°]

A_n , B_n : nth coefficient from polynomial regression

β : Compressibility [Pa^{-1}]

D : Deformation rate tensor

E' : Elastic or storage modulus [Pa] from normal stress (σ_{zz})

E'' : Viscous or loss modulus [Pa] from normal stress (σ_{zz})

δ_θ : Phase angle [rad or °] of shear stress ($\sigma_{z\theta}$)

δ_z : Phase angle [rad or °] of normal stress (σ_{zz})

F : Normal force [N]

$F_{inertia}$: Inertia force [N]

F_{sur} : Surface force [N]

ϕ : Particle volume fraction

G' : Elastic or storage modulus [Pa] from shear stress ($\sigma_{z\theta}$)

G'' : Viscous or loss modulus [Pa] from shear stress ($\sigma_{z\theta}$)

γ_θ : Shear strain

$\gamma_{\theta 0}$: Shear strain amplitude

γ_z : Normal strain (or vertical strain)

γ_{z0} : Normal strain amplitude

Γ : Surface tension [N/m]

$\dot{h}$: Axial velocity [mm/s]

η : Shear viscosity [Pa·s]

η_0 : Zero shear viscosity [Pa·s]

η_θ^*: Complex viscosity [Pa·s] from shear stress in DHSQ (dynamic helical squeeze) flow

η_z^*: Complex viscosity [Pa·s] from normal stress in DHSQ (dynamic helical squeeze) flow

H_0 : Initial gap height [mm]

I_n : nth harmonic intensity from Fourier transform

λ : Relaxation time [s]

Ω : Angular velocity [rad/s]

P : Pressure [Pa]

θ : Angular displacement [rad]

ρ : Density [kg/m^3 or g/cm^3]

R : Radius

$R_{c,1}$: Radius of curvature of the sample in $r\theta$ plane

$R_{c,2}$: Radius of curvature of the sample in rz plane

T : Torque [N·m]

$\sigma_{z\theta}$: Shear stress [Pa]

σ_{zz} : Normal stress [Pa]

$\sigma_{z\theta 0}$: Magnitude of shear stress

σ_{zz0} : Magnitude of normal stress

v_r : Velocity field of r-direction in cylindrical coordinate (r,θ,z)

v_θ : Velocity field of θ-direction in cylindrical coordinate (r,θ,z)

v_z : Velocity field of z-direction in cylindrical coordinate (r,θ,z)

V : Volume [cm^3 or m^3]

ω : Angular frequency [rad/s]

Bibliography

In alphabetical order by first author,

Anderson, V., Pearson, J. and Sherwood, J., Oscillation superimposed on steady shearing: measurements and predictions for wormlike micellar solutions, Journal of Rheology, 50, 771, 2006.

Barnes, H., Shear-thickening ("Dilatancy") in suspensions of nonaggregating solid particles dispersed in Newtonian liquids, Journal of Rheology, 33, 329, 1989.

Bell, D., Binding, D. and Walters, K., The oscillatory squeeze flow rheometer: comprehensive theory and a new experimental facility, Rheologica Acta, 46, 111, 2006.

Bernstein, B., A rheological relation between parallel and transverse superposed complex dynamic shear moduli, Rheologica Acta, 11, 210, 1972.

Booij, H.C., Influence of superimposed steady shear flow on the dynamic properties of non-Newtonian fluids I. Measurements on Non-Newtonian solutions, Rheologica Acta, 5, 215, 1966.

Booij, H.C., Influence of superimposed steady shear flow on the dynamic properties of non-newtonian fluids III. Measurements on oscillatory

normal stress components, Rheologica Acta, 7, 202, 1968.

Boukany, P. and Wang, S., Nature of steady flow in entangled fluids revealed by superimposed small amplitude oscillatory shear, Journal of Rheology, 53, 1425, 2009.

Cho, K.S., Hyun, K., Ahn, K.H. and Lee, S.J., A geometrical interpretation of large amplitude oscillatory shear response, Journal of Rheology, 49, 747, 2005.

Cho, K.S., Song, K.W. and Chang, G.S., Scaling relations in nonlinear viscoelastic behavior of aqueous PEO solutions under large amplitude oscillatory shear flow, Journal of Rheology, 54, 27, 2010.

Coussot, P. and Wagner, N.J., The future of suspension rheophysics: comments on the 2008 workshop, Rheologica Acta, 48, 827, 2009.

d'Haene, P., Mewis, J. and Fuller, G., Scattering dichroism measurements of flow-induced structure of a shear thickening suspension, Journal of colloid and interface science, 156, 350, 1993.

Dasgupta, B.R., Tee, S.Y., Crocker, J.C., Frisken, B. and Weitz, D., Microrheology of polyethylene oxide using diffusing wave spectroscopy and single scattering, Physical Review E, 65, 51505, 2002.

De Cleyn, G. and Mewis, J., Constitutive equation for polymer liquids:

application to shear flow, Journal of Non-Newtonian Fluid Mechanics, 9, 91, 1987.

Debbaut, B. and Thomas, K., Simulation and analysis of oscillatory squeeze flow, Journal of Non-Newtonian Fluid Mechanics, 124, 77, 2004.

Dinser, S., Haeusler, K. and Dual, J., Novel Rheometer for Superposed Constant and Oscillatory Shear Rate, Key Engineering Materials, 345, 1605, 2007.

Ewoldt, R.H., Hosoi, A.E. and McKinley, G.H., New measures for characterizing nonlinear viscoelasticity in large amplitude oscillatory shear, Journal of Rheology, 52, 1427, 2008.

Field, J.S., Swain, M.V. and Phan-Thien, N., An experimental investigation of the use of random squeezing to determine the complex modulus of viscoelastic fluids, Journal of Non-Newtonian Fluid Mechanics, 65, 177, 1996.

Haward, R., Compressibility of polymers, Journal of Polymer Science Part A-2: Polymer Physics, 7, 219, 1969.

Hoffman, R.L., Explanations for the cause of shear thickening in concentrated colloidal suspensions, Journal of Rheology, 42, 111, 1998.

Hyun, K., Kim, S.H., Ahn, K.H. and Lee, S.J., Large amplitude oscillatory shear as a way to classify the complex fluids, Journal of Non-

Newtonian Fluid Mechanics, 107, 51, 2002.

Hyun, K., Nam, J.G., Wilhellm, M., Ahn, K.H. and Lee, S.J., Large amplitude oscillatory shear behavior of PEO-PPO-PEO triblock copolymer solutions, Rheologica Acta, 45, 239, 2006.

Hyun, K., Nam, J.G., Wilhelm, M., Ahn, K.H. and Lee, S.J., Nonlinear response of complex fluids under LAOS (large amplitude oscillatory shear) flow, Korea-Australia Rheology Journal, 15, 97, 2003.

Hyun, K., Wilhellm, M., Klein, C.O., Cho, K.S., Nam, J.G., Ahn, K.H., Lee, S.J., Ewoldt, R.H. and Mckinley, G.H., A review of nonlinear oscillatory shear tests Analysis and application of large amplitude oscillatory shear (LAOS), Progress in Polymer Science, 36, 1697, 2011.

Hyun, K. and Wilhelm, M., Establishing a New Mechanical Nonlinear Coefficient Q from FT-Rheology: First Investigation of Entangled Linear and Comb Polymer Model Systems, Macromolecules, 42, 411, 2008.

Isayev, A. and Wong, C., Parallel superposition of small and large amplitude oscillations upon steady shear flow of polymer fluids, Journal of Polymer Science Part B: Polymer Physics, 26, 2303, 1988.

Jiang, P., See, H., Swain, M. and Phan-Thien, N., Using oscillatory squeezing

flow to measure the viscoelastic properties of dental composite resin cements during curing, Rheologica Acta, 42, 118, 2004.

Kataoka, T. and Ueda, S., Influence of superimposed steady shear flow on the dynamic properties of polyethylene melts, Journal of Polymer Science Part A 2: Polymer Physics, 7, 475, 1969.

Kim, J.H., Ahn, K.H. and Lee, S.J., Mixed-Flow Rheometer, Korea Patent, #10-0877494, 2008.

Kramer, J., Large deformations of viscoelastic squeeze films, Applied Scientific Research, 30, 1, 1974.

Kwon, Y. and Leonov, A., Remarks on orthogonal superposition of small amplitude oscillations on steady shear flow, Rheologica Acta, 32, 108, 1993.

Larson, R.G., Constitutive equations for polymer melts and solutions, Butterworths, Boston, 1988.

Laufer, Z., Jalink, H. and Staverman, A., Dynamic properties of some polymer solutions subjected to a steady shear superimposed on an oscillatory shear flow, Rheologica Acta, 14, 641, 1975.

Macdonald, I., Parallel Superposition of Simple Shearing and Small Amplitude Oscillatory Motions, Journal of Rheology, 17, 537, 1973.

Macosko, C.W., Rheology: Principles, measurements, and applications, VCH,

New York, 1994.

Mewis, J., Kaffashi, B., Vermant, J. and Butera, R., Determining relaxation modes in flowing associative polymers using superposition flows, Macromolecules, 34, 1376, 2001.

Mobuchon, C., Carreau, P.J., Heuzey, M.-C., Reddy, N.K. and Vermant, J., Anisotropy of nonaqueous layered silicate suspensions subjected to shear flow, Journal of Rheology, 53, 517, 2009.

Nam, J., Ahn, K., Lee, S. and Hyun, K., Strain stiffening of non-colloidal hard sphere suspensions dispersed in Newtonian fluid near liquid-and-crystal coexistence region, Rheologica Acta, 1, 2010.

Nam, J.G., Ahn, K.H., Lee, S.J. and Hyun, K., First normal stress difference of entangled polymer solutions in large amplitude oscillatory shear flow, Journal of Rheology, 54, 1243, 2010.

Nam, J.G., Hyun, K., Ahn, K.H. and Lee, S.J., Prediction of normal stresses under large amplitude oscillatory shear flow, Journal of Non-Newtonian Fluid Mechanics, 150, 1, 2008.

Osaki, K., Tamura, M., Kurata, M. and Kotaka, T., Complex Modulus of Concentrated Polymer Solutions in Steady Shear, The Journal of Physical Chemistry, 69, 4183, 1965.

Ovarlez, G., Barral, Q. and Coussot, P., Three-dimensional jamming and flows

of soft glassy materials, Nature Materials, 9, 115, 2010.

Phan-Thien, N., Small strain oscillatory squeeze film flow of simple fluids, Journal of the Australian Mathematical Society, 22(Series B), 22, 1980.

Phan-Thien, N., Squeezing flow of a viscoelastic solid, Journal of Non-Newtonian Fluid Mechanics, 95, 343, 2000.

Phan-Thien, N., Nasseri, S. and Bilston, L.E., Oscillatory squeezing flow of a biological material, Rheologica Acta, 39, 409, 2000.

Powell, R. and Schwarz, W., Rheological properties of aqueous poly (ethylene oxide) solutions in parallel superposed flows, Journal of Rheology, 19, 617, 1975.

Renou, F., Stellbrink, J. and Petekidis, G., Yielding processes in a colloidal glass of soft star-like micelles under large amplitude oscillatory shear (LAOS), Journal of Rheology, 54, 1219, 2010.

Roe, R.-J., Surface tension of polymer liquids, The Journal of Physical Chemistry, 72, 2013, 1968.

See, H. and Nguyen, P., Using oscillatory squeeze flow to monitor the change in viscoelastic properties of curing materials, Journal of the Society of Rheology, Japan, 32, 33, 2004.

Simmons, J., Dynamic modulus of polyisobutylene solutions in superposed

steady shear flow, Rheologica Acta, 7, 184, 1968.

Somma, E., Valentino, O., Titomanlio, G. and Ianniruberto, G., Parallel superposition in entangled polydisperse polymer melts: Experiments and theory, Journal of Rheology, 51, 987, 2007.

Tanner, R., Comparative studies of some simple viscoelastic theories, Journal of Rheology, 12, 155, 1968.

Tanner, R. and Simmons, J., Combined simple and sinusoidal shearing in elastic liquids, Chemical Engineering Science, 22, 1803, 1967.

Tirtaatmadja, V., Tam, K. and Jenkins, R., Superposition of oscillations on steady shear flow as a technique for investigating the structure of associative polymers, Macromolecules, 30, 1426, 1997.

Vermant, J., Moldenaers, P., Mewis, J., Ellis, M. and Garritano, R., Orthogonal superposition measurements using a rheometer equipped with a force rebalanced transducer, Review of Scientific Instruments, 68, 4090, 1997.

Vermant, J., Walker, L., Moldenaers, P. and Mewis, J., Orthogonal versus parallel superposition measurements, Journal of Non-Newtonian Fluid Mechanics, 79, 173, 1998.

Vlastos, G., Lerche, D., Koch, B., Samba, O. and Pohl, M., The effect of parallel combined steady and oscillatory shear flows on blood and

polymer solutions, Rheologica Acta, 36, 160, 1997.

Walberer, J.A. and McHugh, A.J., The linear viscoelastic behavior of highly filled polydimethylsiloxane measured in shear and compression, Journal of Rheology, 45, 187, 2001.

Walker, L., Vermant, J., Moldenaers, P. and Mewis, J., Orthogonal and parallel superposition measurements on lyotropic liquid crystalline polymers, Rheologica Acta, 39, 26, 2000.

Wilhelm, M., Fourier Transform Rheology, Macromolecular Materials and Engineering, 287, 83, 2002.

Wilhelm, M., Maring, D. and Spiess, H.W., Fourier-transform rheology, Rheologica Acta, 37, 399, 1998.

Wong, C. and Isayev, A., Orthogonal superposition of small and large amplitude oscillations upon steady shear flow of polymer fluids, Rheologica Acta, 28, 176, 1989.

Yamamoto, M., Rate-dependent relaxation spectra and their determination, Journal of Rheology, 15, 331, 1971.

Yosick, J.A., Giacomin, A.J. and Moldenaers, P., A kinetic network model for nonlinear flow behavior of molten plastics in both shear and extension, Journal of Non-Newtonian Fluid Mechanics, 70, 103, 1997.

Yu, W., Wang, P. and Zhou, C., General stress decomposition in nonlinear

oscillatory shear flow, Journal of Rheology, 53, 215, 2009.

Zeegers, J., Ende, D., Blom, C., Altena, E., Beukema, G. and Mellema, J., A sensitive dynamic viscometer for measuring the complex shear modulus in a steady shear flow using the method of orthogonal superposition, Rheologica Acta, 34, 606, 1995.

국문 초록

김재희

학번: 2005-30274

유변 물성 측정은 선형 그리고 비선형 전단 유동 하에서 수행되어 왔다. 비록 이러한 방법이 복잡 유체에 대한 유용한 정보를 제공하더라도, 전단 유동은 실제 유동에 비해서 극단적으로 단순하다는 한계점이 있다. 따라서 우리는 단순 전단 유동보다 더 복잡한 유동에서 유변물성을 측정하는 것이 필요하다. 복잡 유동 하에서 유변물성을 측정하는 것은 어렵기 때문에 이 분야에서 매우 도전적인 과제로 여겨지고 있다. 이 논문의 목적은 단순 전단 유동보다 더 복잡한 동적 압착 유동 및 동적 나선 유동 하에서 복잡 유체의 유변학적 거동을 이해하는 것이다.

동적 압착 유동 하에서 유체는 비대칭 응력을 보여준다. 이러한 비대칭 응력은 단순 전단 유동의 독특한 성질 중 하나이며 거의 연구되지 않았다. 본 논문은 동적 압착 유동 하에서 진폭이 클 경우에 나타나는 비선형 그리고 비대칭 응력을 해석하기 위한 유용한 방법을 제공한다. 수직 응력은 대변형 하에서 크기와 형태 모두에서 비대칭을 보였으며, 이러한 비대칭 응력은 푸리에 변환을 통해서 짝수 고조파의 영향으로부터 기인됨을 알 수 있었다.

동적 나선 유동은 동적 전단 유동과 동적 압착 유동이 중첩된 유동장 하에서 물질의 미세 구조 변화에 대한 유용한 정보를 제공한다. 비록 산업 현장에서 관찰되는 실제 유동은 동적 나선 유동 보다 훨씬 더 복잡하지만, 동적 나선 유동은 복잡 유체의 거동을 이해하기 위한 유용하게 사용될 것이다. 또한 동적 나선 유동은 단순 전단 유동으로 제한된 기존 유변물성 측정 방법의 한계를 극복하게 될 것이다. 유동의 진폭이 증가함에 따라 응력 분석(응력 파형과 라자쥬 곡선)은 인상적인 결과를 보여주었다. 전단 응력과 수직 응력 모두 압착과 신장이 반복되는 변형 하에서 서로 다른 거동을 의미하는 비대칭 특성을 보였다. 중첩의 효과에 의해서 동적 나선 유동의 전단응력의 비선형의 시작은 단순 전단 유동과 비교하여 매우 작은 변형 진폭에서 시작되었다.

본 연구는 동적 전단 유동에서 전단 응력과 수직 응력의 비선형 거동과 중첩의 효과에 대한 연구에 좋은 방법이 될 수 있다는 것을 보였다. 더 나아가 좀 더 복잡한 유동에서 복잡유체들의 비선형 거동 연구를 위한 플랫폼을 마련해 줄 수 있을 것이라고 생각한다.

주요어: 동적 나선 유동, 동적 압착 유동, 동적 전단 유동, 복잡유체, 비대칭 응력, 라자쥬 곡선, 푸리에 변환